

Ph.D. DISSERTATION

**JÓZSEF CZIRÁKI DOCTORAL SCHOOL OF WOOD SCIENCES
AND TECHNOLOGIES**

**SIMONYI KÁROLY FACULTY OF ENGINEERING, WOOD
SCIENCES & APPLIED ARTS**

UNIVERSITY OF SOPRON

by

CHARU AGARWAL



SOPRON, HUNGARY

MAY 2019

**ULTRASONIC EXTRACTION OF BIOACTIVE COMPOUNDS
FROM *CANNABIS SATIVA* L. FOR THE GREEN REDUCTION OF
GRAPHENE OXIDE ON CELLULOSE FIBRES**

A DISSERTATION

*submitted in partial fulfilment of the
requirements for the award of the degree of*
DOCTOR OF PHILOSOPHY

by

CHARU AGARWAL

under the supervision of

PROF. DR. LEVENTE CSÓKA



**JÓZSEF CZIRÁKI DOCTORAL SCHOOL OF WOOD SCIENCES AND
TECHNOLOGIES**
**SIMONYI KÁROLY FACULTY OF ENGINEERING, WOOD SCIENCES &
APPLIED ARTS**
UNIVERSITY OF SOPRON
SOPRON, HUNGARY

MAY 2019

Ultrasonic Extraction of Bioactive Compounds from *Cannabis sativa* L. for the Green Reduction of Graphene Oxide on Cellulose Fibres

Értekezés doktori (Ph.D.) fokozat elnyerése érdekében

a Soproni Egyetem Cziráki József Faanyagtudomány és Technológiák Doktori Iskolája
Rosttechnikai és nanotechnológiai tudományok programja

Írta:
Charu Agarwal

Készült a Soproni Egyetem Cziráki József Faanyagtudomány és Technológiák Doktori Iskola Rosttechnikai és nanotechnológiai tudományok programja keretében

Témavezető: Prof. Dr. Csóka Levente DSc.

Elfogadásra javaslom (igen / nem)

(aláírás)

A jelölt a doktori szigorlaton93..... % -ot ért el,

Sopron, 2018.06.07.

.....

a Szigorlati Bizottság elnöke

Az értekezést bírálóként elfogadásra javaslom (igen /nem)

Első bíráló (Dr.) igen /nem

(aláírás)

Második bíráló (Dr.) igen /nem

(aláírás)

(Esetleg harmadik bíráló (Dr.) igen /nem

(aláírás)

A jelölt az értekezés nyilvános vitáján.....% - ot ért el

Sopron,

.....
a Bírálóbizottság elnöke

A doktori (PhD) oklevél minősítése.....

.....
Az EDHT elnöke



UNIVERSITY OF SOPRON

DECLARATIONS

I hereby certify that the work presented in this dissertation titled “**Ultrasonic Extraction of Bioactive Compounds from *Cannabis sativa* L. for the Green Reduction of Graphene Oxide on Cellulose Fibres**” in partial fulfilment of the requirements for the award of the degree of *Doctor of Philosophy in Material Science & Technology* and submitted in the Simonyi Károly Faculty of Engineering, Wood Sciences & Applied Arts of the University of Sopron, is an authentic record of my own work carried out at Institute of Wood Based Products and Technologies during a period from *September 2016* to *May 2019* under the guidance and supervision of *Prof. Dr. Levente Csóka* (Head of *József Cziráki Doctoral School of Wood Sciences and Technologies*, University of Sopron).

The matter presented in this dissertation has not been submitted by me for the award of any other degree of this or any other Institute.

May, 2019

Charu Agarwal

This is to certify that the above statement made by the candidate is correct to the best of my knowledge.

May, 2019

Prof. Dr. Levente Csóka

*This work is dedicated to my parents and
sister for always being there...*

©UNIVERSITY OF SOPRON, SOPRON-2019

ALL RIGHTS RESERVED

ACKNOWLEDGEMENTS

A dissertation is not only an accomplishment but also one of the achievements in life. The satisfaction and satiety of overcoming the hurdles faced during the research work cannot be attained without expressing sincere gratitude to all those who guided and supported me during the entire course of the PhD work.

I take this opportunity to bequeath my humble salutation and deep gratitude towards my supervisor, **Prof. Dr. Levente Csóka**, under whose invaluable guidance I have carried out this PhD study. I was very fortunate to have worked under his excellent guidance and thank him from the depth of my heart for having led me up the right path. With an eye of perfection, strong sense of dignity and integrity, he has set an example.

I am extremely grateful to the *Tempus Public Foundation* for providing financial assistance under the *Stipendium Hungaricum* scholarship programme. I also acknowledge the financial support received within framework of the programme “*EFOP-3.6.1-16-2016-00018 – Improving the role of research+development+innovation in the higher education through institutional developments assisting intelligent specialization in Sopron and Szombathely.*”

I convey my sincere thanks to all the faculty members of University of Sopron, especially *Dr. Tamás Hofmann* for their kind support cooperation and extending all possible assistance to carry out this work. I also wish to thank Dr. Katalin Halász, Dr. Ádám Makk, and Dr. Éva Papp and administrative staff for their kindness and cooperation during the course of this study. I cannot forget to express sincere appreciation to all my lab colleagues and peers- Annamária, Boris, *Chenar*, Fatima, Shadabeh, Worakan, Yanin for their support and motivation towards this work.

I express my gratitude to RRCAT, India for extending the facilities for XRD and XPS measurements at the synchrotron radiation source. I am also highly obliged to all the authors whose work has provided a significant contribution in this work.

Finally, I also thank Lord Almighty and my family for preparing me for everything that I desire to be through the good times and bad. Without their moral support, this work would not have seen the dawn of the day.

Charu Agarwal

TABLE OF CONTENTS

DECLARATIONS	IV
TABLE OF CONTENTS	VIII
LIST OF FIGURES	XII
LIST OF TABLES	XV
LIST OF ABBREVIATIONS	XVI
ABSTRACT	18
CHAPTER I- INTRODUCTION	20
1.1. Chapter synopsis	21
1.2. Problem statement	21
1.3. Cannabis sativa L. & its extract	22
1.3.1. Bioactive compounds in Cannabis sativa L.	22
1.3.1.1. Terpenes in Cannabis	23
1.3.1.2. Flavonoids in Cannabis	24
1.3.2. Phytocannabinoids.....	24
1.3.2.1. Biosynthesis and pharmacology of cannabinoids	24
1.3.2.2. Chemotypes in Cannabis	26
1.3.2.3. Therapeutic potential of cannabinoids	26
1.3.3. Extraction of phytoconstituents.....	27
1.3.3.1. Using conventional methods	27
1.3.3.2. Using modern methods	28
1.3.4. Plant extract as a green reducing agent.....	30
1.4. Cellulose as a substrate for functionalization of materials	31
1.4.1. Cellulose background.....	31
1.4.1.1. Structure	31
1.4.1.2. Polymorphs	33
1.4.1.3. Sources	33
1.4.1.4. Properties.....	34
1.4.2. Cellulose chemistry	34
1.4.2.1. Functionalization via physical adsorption	35
1.4.2.2. Functionalization via chemical bonding	35
1.4.3. Functionalization of cellulose.....	36
1.4.4. Functionalization of cellulose with carbonaceous materials	38

1.4.4.1.	<i>Carbon nanotubes</i>	38
1.4.4.2.	<i>Graphene/reduced-GO</i>	39
1.5.	Green reduction of GO	43
1.6.	Research rationale & objectives	44
1.7.	Dissertation outline	45
1.8.	Summary	46
	References	47
CHAPTER II- MATERIALS & METHODS		60
2.1.	Chapter synopsis	61
2.2.	Materials	61
2.2.1.	<i>Chemicals</i>	61
2.2.2.	<i>Plant material</i>	62
2.2.3.	<i>Instrumentation</i>	62
2.2.3.1.	<i>Probe sonicator</i>	62
2.2.3.2.	<i>Spectrophotometer</i>	62
2.3.	Methods	63
2.3.1.	<i>Ultrasonic extraction</i>	63
2.3.2.	<i>Control extraction without ultrasound treatment</i>	64
2.3.3.	<i>Determination of total phenolic content (TPC)</i>	64
2.3.4.	<i>Determination of total flavonoids (TF)</i>	64
2.3.5.	<i>Determination of ferric reducing ability of plasma (FRAP) antioxidant capacity</i>	64
2.3.6.	<i>Determination of extraction yield</i>	65
2.3.7.	<i>Experimental design of & statistical analysis</i>	65
2.3.8.	<i>Synthesis of GO</i>	66
2.3.9.	<i>Green reduction of GO and preparation of composites</i>	67
2.3.10.	<i>Handsheet-making</i>	68
2.4.	Characterization	69
2.4.1.	<i>High pressure liquid chromatography/mass spectrometry (HPLC-DAD-MS/MS)</i>	69
2.4.2.	<i>Gas chromatography/mass spectrometry (GC-MS)</i>	71
2.4.3.	<i>Fourier transform infrared spectroscopy (FTIR)</i>	72
2.4.4.	<i>Scanning electron microscopy (SEM)</i>	72
2.4.5.	<i>Synchrotron X-ray diffraction (XRD)</i>	73
2.4.6.	<i>Synchrotron X-ray photoelectron spectroscopy (XPS)</i>	74
2.5.	Electrical measurements	75
2.6.	Summary	75
	References	76

CHAPTER III- ULTRASONIC EXTRACTION OF BIOACTIVE COMPOUNDS FROM CANNABIS SATIVA L. OPTIMIZED BY RESPONSE SURFACE METHODOLOGY..... 79

3.1. Chapter synopsis.....	80
3.2. Extraction process and factor selection.....	80
3.3. Modelling and regression analysis.....	81
3.4. Influence of ultrasonic parameters (design factors) on the responses.....	84
3.4.1. <i>Influence of design factors on TPC.....</i>	84
3.4.2. <i>Influence of design factors on TF.....</i>	86
3.4.3. <i>Influence of design factors on FRAP.....</i>	88
3.4.4. <i>Influence of design factors on yield.....</i>	90
3.5. Optimization of extraction conditions.....	92
3.6. Ultrasonic vs control extraction.....	92
3.7. Summary and inferences.....	94
References.....	94

CHAPTER IV- IDENTIFICATION OF CANNABINOIDS IN CANNABIS SATIVA L. & THEIR ENTOURAGE EFFECTS WITH OTHER BIOACTIVE CONSTITUENTS..... 98

4.1. Chapter synopsis.....	99
4.2. Synthesis, pharmacological and therapeutic effects of cannabinoids.....	99
4.3. Administration of cannabinoids.....	100
4.4. Entourage effects of cannabinoids.....	100
4.5. Identification of compounds in the Cannabis extract.....	101
4.5.1. <i>Identification of cannabinoids using HPLC-DAD-MS/MS.....</i>	101
4.5.2. <i>Identification of other bioactive compounds using GC-MS.....</i>	108
4.6. Adverse events and safety concerns.....	109
4.7. Summary and inferences.....	109
References.....	110

CHAPTER V- IN SITU GREEN SYNTHESIS AND FUNCTIONALIZATION OF REDUCED GRAPHENE OXIDE ON CELLULOSE FIBERS BY CANNABIS SATIVA L. EXTRACT..... 113

5.1. Chapter synopsis.....	114
5.2. Morphology and structure analysis.....	114
5.2.1. <i>SEM analysis.....</i>	114
5.2.2. <i>FTIR analysis.....</i>	115
5.3. X-ray diffraction and photoelectron spectroscopy analysis.....	116
5.3.1. <i>XRD analysis.....</i>	116
5.3.2. <i>XPS analysis.....</i>	118
5.4. Electrical performance study.....	119

5.5. Summary and inferences	122
References.....	123
CHAPTER VI- CONCLUSIONS & FUTURE OUTLOOK.....	127
6.1. Chapter synopsis.....	128
6.2. Main conclusions and achievements of the research.....	128
6.3. Scope for further research.....	129
LIST OF PUBLICATIONS	130

LIST OF FIGURES

Figure no.	Figure caption	Page no.
Figure 1.1	Biosynthetic pathways for bioactive compounds in <i>Cannabis</i>	25
Figure 1.2	Therapeutic effects of cannabinoids for some diseases	27
Figure 1.3	Conventional and modern methods of extraction for phytoconstituents	28
Figure 1.4	Formation and collapse of cavitation bubble	29
Figure 1.5	Diffusion in a plant tissue surrounded by a solvent layer during ultrasonic extraction	30
Figure 1.6	Plants used for the green reduction of materials such as nanoparticles	31
Figure 1.7	(a) Two glucose rings in cellulose chain connected by $\beta(1-4)$ glycosidic linkage; dotted line indicates the intra-chain hydrogen bonding, (b) amorphous and crystalline regions in a cellulose chain, (c) hydrogen bonding in cellulose, the thin dotted lines indicate the intrachain bonding, while the thick dotted line represents the interchain bonding	32
Figure 1.8	(a) Directional asymmetry of cellulose, (b) chemical reactions for modification of cellulose	35
Figure 1.9	Common functionalization chemistries of cellulose surfaces: (clockwise from top-right) sulphuric acid treatment provides sulphate esters, carboxylic acid halides create ester linkages, acid anhydrides create ester linkages, epoxides create ether linkages, isocyanates create urethane linkages, TEMPO mediated hypochlorite oxidation creates carboxylic acids, halogenated acetic acids create carboxymethyl surfaces, and chlorosilanes create an oligomeric silylated layer	36
Figure 1.10	Applications of cellulose fibres modified with nanomaterials	37
Figure 1.11	(a) Schematic depicting transfer of graphene on to paper, (b) Graphene paper strip in action as a gas sensor may glow an LED bulb	40
Figure 1.12	(a) Increase in resistance change with pressure for graphene-based pressure sensor for different number of layers of tissue paper, (b) Sensor application for detection of wrist pulse, (c) Pulse waveform of the sensor	41
Figure 1.13	a) SEM and b) TEM images of a cellulose fibre in a GCP membrane showing GNSs anchored on the fibre surface, c) cellulose-GNSs binding in GCP	42
Figure 1.14	(a) GNS/cellulose composite paper (black) against pure cellulose paper (white), (b) the bent composite paper, showing flexibility of	43

	the paper and (c) composite paper adhered to conducting copper foil to make a flexible supercapacitor	
Figure 1.15	Mechanism for the reduction of GO with plant extracts	44
Figure 2.1	Inflorescence of fibre-type <i>Cannabis</i>	62
Figure 2.2	Photographs of (a) Probe-type ultrasonicator used for the extraction of phytoconstituents from <i>Cannabis</i> , (b) UV/vis spectrophotometer for the measurement of absorbance	63
Figure 2.3	Schematic illustration for the fabrication of RGO/cellulose composites	68
Figure 2.4	Photograph of laboratory sheet former with vacuum press-drying	68
Figure 2.5	RGO/cellulose composites with various loadings of RGO- (a) 0 m/m %, (b) 0.1 m/m %, (c) 1 m/m %, (d) 2 m/m %, (e) 5 m/m % and (f) 10 m/m %	69
Figure 2.6	Photograph of HPLC-DAD-MS/MS	70
Figure 2.7	Photograph of GC-MS	71
Figure 2.8	Photographs of (a) FTIR and (b) ATR probe	72
Figure 2.9	Photograph of SEM	73
Figure 2.10	Schematic layout of XRD beamline (BL-12) at Indus 2 synchrotron, RRCAT (India)	73
Figure 2.11	Schematic layout of XPS beamline (BL-14) at Indus 2 synchrotron, RRCAT (India)	74
Figure 2.12	Photographs of (a) Keithley resistivity test fixture and (b) Keithley electrometer	75
Figure 3.1	Response surface plots depicting the influence of design factors on TPC	85
Figure 3.2	Fig. 21 Response surface plots depicting the influence of design factors on TF	87
Figure 3.3	Response surface plots depicting the influence of design factors on FRAP	89
Figure 3.4	Response surface plots depicting the influence of design factors on extraction yield	91
Figure 3.5	Comparison between ultrasonic (green) and control (blue) extractions for the responses (The error bars indicate percentage error)	92
Figure 3.6	Qualitative HPLC chromatograms for ultrasonic (black represents optimal conditions & red represents central values) and control (blue) extracts of <i>Cannabis</i>	93
Figure 4.1	HPLC chromatogram showing various cannabinoids in the <i>Cannabis</i> extract	103
Figure 4.2	Mass spectrum of CBDVA	103

Figure 4.3	Mass spectrum of CBD	104
Figure 4.4	Mass spectrum of CBDA	104
Figure 4.5	Mass spectrum of CBGA	105
Figure 4.6	Mass spectrum of THCA-A	105
Figure 4.7	Mass spectrum of THC	106
Figure 4.8	Mass spectrum of THCVA	106
Figure 4.9	Mass spectrum of CBNA	107
Figure 4.10	Mass spectrum of CBLA	107
Figure 4.11	Mass spectrum of CBCA	108
Figure 4.12	GC-MS chromatogram of non-cannabinoid bioactive compounds in the <i>Cannabis</i> extract	109
Figure 5.1	SEM images of RGO/cellulose composites at various RGO loadings: (a) 0 m/m %, (b) 0.1 m/m %, (c) 1 m/m %, (d) 2 m/m %, (e) 5 m/m % and (f) 10 m/m % (the arrows indicate the dispersion of RGO on the cellulose fibre surface)	115
Figure 5.2	FTIR spectra of (a) GO & RGO powders and (b) RGO/cellulose composites with various RGO loadings	116
Figure 5.3	XRD spectra of (a) GO & RGO powders and (b) RGO/cellulose composites with various RGO loadings	117
Figure 5.4	XPS spectra of GO and RGO powders (a, b) C 1s region and (c, d) O 1s region	119
Figure 5.5	Surface resistivity of RGO/cellulose composites with increasing RGO loading from 0-10 m/m % at 40 V	120
Figure 5.6	Surface charging capacity of RGO/cellulose composites with increasing RGO loading from 0.1-10 m/m % on log scale at 40 V	122

LIST OF TABLES

Table no.	Table caption	Page no.
Table 1.1	Constituents of <i>Cannabis</i>	23
Table 1.2	Classes of cannabinoids with their pharmacological attributes	25
Table 2.1	Design space factors and levels	66
Table 2.2	Different weight fractions of RGO functionalized on cellulose fibres	67
Table 3.1	Central composite design factors in coded and actual forms along with the investigated responses of TPC, TF, FRAP and yield for various experimental run	81
Table 3.2	Regression coefficient estimates for second order polynomial model for TPC, TF, FRAP and yield along with their ANOVA parameter	83
Table 4.1	Major cannabinoids identified in the <i>Cannabis</i> extract using HPLC-DAD-MS/MS	102
Table 4.2	Bioactive compounds identified in the <i>Cannabis</i> extract using GC-MS	108
Table 5.1	Surface charging capacity of RGO/cellulose composites with different RGO loadings at 40 V	121

LIST OF ABBREVIATIONS

11-OH-THC	11-hydroxy- Δ^9 -tetrahydrocannabinol
11-OH-THCA	11-hydroxy- Δ^9 -tetrahydrocannabinolic acid A
5-HT1A	serotonin 1A receptor
ADXRD	angle dispersive X-ray diffraction
AgNWs	silver nanowires
ANOVA	analysis of variance
ATR	attenuated total reflection
CB ₁	cannabinoid-one receptor
CB ₂	cannabinoid-two receptor
CBC	cannabichromene
CBCA	cannabichromenic acid
CBD	cannabinoid
CBDA	cannabidiolic acid
CBDV	cannabidivarin
CBDVA	cannabidivarinic acid
CBG	cannabigerol
CBGA	cannabigerolic acid
CBLA	cannabicyclolic acid
CBN	cannabinol
CBNA	cannabinolic acid
CBND	cannabinodiol
CBNDA	cannabinodiolic acid
CNTs	carbon nanotubes
DMAPP	dimethylallyl diphosphate
FPP	farnesyl diphosphate
FTIR	Fourier transform infrared spectroscopy
GC-MS	gas chromatography/mass spectrometry
GPP	geranyl diphosphate
HPLC-DAD-MS/MS	high pressure liquid chromatography/mass spectrometry

IDA	information dependent analysis
IPP	isopentenyl diphosphate
LFIA	lateral flow immunoassays
MEP	methylethanol phosphate
MVA	mevalonate
PMMA	poly- (methyl methacrylate)
POC	point-of-care
PPAR- γ	peroxisome proliferator-activated receptor gamma
SEM	scanning electron microscopy
THC	tetrahydrocannabinol
THCA-A	tetrahydrocannabinolic acid A
THCV	tetrahydrocannabivarin
THCVA	tetrahydrocannabivarinic acid
TPTZ	2,4,6-tri(2-pyridyl)-1,3,5-triazine
TRPA1	transient receptor potential ankyrin-1
TRPV1	transient receptor potential cation channel vanilloid sub-family receptor 1
WHO	World Health Organization
XPS	X-ray photoelectron spectroscopy
XRD	X-ray diffraction

ABSTRACT

Ultrasonication was used to extract bioactive compounds from *Cannabis sativa* L. such as polyphenols, flavonoids and cannabinoids. The influence of three independent factors (time, input power and methanol concentration) was evaluated on the extraction of total phenols, flavonoids, ferric reducing ability of plasma (FRAP) assay and the overall yield. A face-centred central composite design was used for statistical modelling of the response data, followed by regression and analysis of variance in order to determine the significance of the model and factors. Both the solvent composition and the time significantly affected the extraction while the sonication power had no significant impact on the responses. The response predictions obtained at optimum extraction conditions of 15 min time, 130 W power and 80% methanol were 314.822 mg GAE/g DW of TPC, 28.173 mg QE/g DW of TF, 18.79 mM AAE/g DW of FRAP and 10.86% of yield. A good correlation was observed between the predicted and experimental values of the responses, which validated the mathematical model. On comparing the ultrasonic process with the control extraction, noticeably higher values were obtained for each of the responses. Additionally, ultrasound treatment considerably improved the extraction of cannabinoids such as THC, CBD, CBGA, CBDA, THCVA, CBLA, CBNA, CBCA, etc.

The last decade has seen an enormous rise in the use of green reducing agents such as plant extracts for the chemical synthesis of several of materials in view of the limitations of the conventional reducing agents such as their toxicity and instability. This study reports the green reduction and simultaneous functionalization of graphene oxide on cellulose fibres using the aqueous extract from the inflorescences of *Cannabis sativa* L. The graphene oxide, synthesized using the modified Hummer's method, was reduced in situ on the cellulose matrix in presence of the extract at elevated temperatures without external stabilizers in order to functionalize the fibres with reduced-graphene oxide (RGO). The cellulose fibres not only acted as a flexible, biodegradable and cost-effective matrix for the anchorage of RGO but also supported its in situ reduction on the fibre surface. Different weight fractions of RGO from 0.1 to 10 m/m % were used to fabricate RGO/cellulose composites by paper-making technique, which were characterized using Fourier transform infrared spectroscopy, scanning electron microscopy, X-ray diffraction and X-ray photoelectron spectroscopy techniques. The RGO sheets uniformly covered the surface of cellulose fibres and dispersed well within the fibre matrix. The surface resistivity at 40 V

decreased with increasing RGO content from $1.81 \times 10^{11} \Omega$ for 0.1 m/m % RGO to $0.15 \times 10^{11} \Omega$ for 10 m/m % RGO loading. The presence of air voids between the fibres hindered the physical contact between the RGO layers, thereby preventing the formation of an effective conductive network and significantly affecting the performance of the composites. Likewise, the surface charging capacity of the composites at 40 V dropped from $1.21 \times 10^{-3} \Delta\text{mAh}$ for 0.1 m/m % RGO to $0.05 \times 10^{-3} \Delta\text{mAh}$ for 10 m/m % RGO content indicating a rise in conductivity with RGO loading. These composites show immense potential as sustainable materials for portable energy storage devices such as capacitors.

CHAPTER I-
INTRODUCTION

1.1. Chapter synopsis

This chapter presents an in-depth review of literature on the phytoconstituents in *Cannabis sativa* L., which include the cannabinoids as well as the other non-cannabinoid bioactive compounds such as the terpenes and flavonoids. Extraction of the phytoconstituents using both the conventional and modern techniques with emphasis on ultrasonication has also been discussed. Further, the potential of the phytoextracts as an eco-friendly reducing agent for the synthesis of materials has been reviewed. This is followed by a discussion on cellulose chemistry and the functionalization of cellulose with special focus on carbon materials such as carbon nanotubes and graphene along with the functionalization strategies. Finally, the chapter throws light on the reduction of graphene oxide (GO) using phytoextracts. The problem statement and the research objectives have been formulated based on the review. An outline for the dissertation has been presented in the end.

1.2. Problem statement

Nanomaterials have become an inseparable part in the present times, playing a dominant role in various sectors such as biomedicine, catalysis and biosensing [1-3]. The two major pathways for the synthesis of nanomaterials are the bottom-up and top down approaches [4]. Both approaches rely on physico-chemical methods, which employ chemical agents for the reduction and stabilization of the nanomaterials. Most of these chemical agents are toxic or corrosive in nature and lead to hazardous by-products [4-6]. This is especially undesirable in case of biomedical healthcare and diagnostic applications. Moreover, they require an energy-intensive reaction environment and are expensive [4, 7]. Thus, there is an intense need for eco-friendly agents for the synthesis of nanomaterials having non-toxic reaction products.

In view of this, a number of eco-friendly agents have garnered the attention of the scientific community, which include entities of biological origin such as microorganisms, enzymes, plant extracts, etc. [8-10]. Of these, the plant extracts are particularly advantageous due to their wide availability and cost-effectiveness. Plant extracts have proven potential to act not only as natural reducing agents for the synthesis of nanomaterials but also as capping agents for the stabilization of the synthesized nanomaterials [11-13]. They need a much less energy-intensive environment and can react in ambient conditions of temperature and pressure [4]. Further, they can be used to synthesize nanomaterials in

large quantities free of chemical contaminants and hence, hold potential for industrial scale-up [4].

Having stated that, it is of utmost significance to select the appropriate extraction technique for the preparation of plant extracts. The conventional techniques used for extraction are laborious, time-consuming, energy-intensive and need large amounts of solvents [14]. These drawbacks can be overcome by employing the modern extraction techniques such as those assisted by ultrasound and microwaves [15, 16]. For instance, ultrasound allows the target compounds to dissolve in the solvent by disrupting the cell wall, thus enhancing the extraction yield in much lesser time [17, 18].

Another aspect to be considered is pertaining to the anchoring of the nanomaterials onto a matrix in order to prevent their dispersal and aid their recovery from the environment. Paper, polymer, glass, wood, ceramic and metal are some of the commonly used matrices (or substrates) for embedding of the nanomaterials. Paper is a principally attractive choice for a substrate owing to its innumerable advantages such as biodegradability, biocompatibility, porosity, flexibility and hydrophilicity [1, 19].

1.3. *Cannabis sativa* L. & its extract

1.3.1. Bioactive compounds in Cannabis sativa L.

Plants have since long been exploited for their medicinal value apart from their nutritional value. Herodotus referred to the use of *Leonurus cardiaca* by those living to the north of the Danube river in as early as 5th century BC [14]. A number of bioactive compounds are responsible for imparting different medicinal properties to the plants. These compounds are synthesized as secondary metabolites, which aid in the overall survival in plants by allowing their interaction with the surrounding environment. In other words, the bioactive compounds exert pharmacological or toxicological effects in humans and animals. They have been broadly classified as: a) terpenes and terpenoids, b) alkaloids and c) phenolic compounds [14]. Of these, the phenolic compounds constitute one of the most widely distributed groups of secondary metabolites in the plant kingdom and are well known for their antioxidant behaviour. The natural phenolic antioxidants present in fruits such as guavas, grapes and strawberries have been greatly explored for their defensive effects and therapeutic potential [20-22]. Flavonoids represent another class of low molecular weight phenolic compounds, which are also very effective antioxidants and less toxic than their synthetic counterparts such as BHT and BHA [23].

Cannabis sativa L. (hereinafter: *Cannabis*) has been around since ages and cultivated as an annual crop plant for its commercial value. It belongs to the family of *Cannabaceae* and has long been used in traditional Asian medicine, particularly in India [24]. Reportedly, the first successful attempt to extract active compounds from the flowers and leaves of *Cannabis* was made by Schlesinger in 1840 [25]. The phenolic compounds are comprised of phenolic acids such benzoic and hydroxycinnamic acids, flavonoids such as flavones and flavonols, lignans and stilbenes [26]. About 34 phenols and 23 flavonoids have been identified in *Cannabis* [27]. **Table 1.1** lists the different constituents commonly found in *Cannabis* as taken from literature [27].

Table 1.1 Constituents of *Cannabis*

Sr. No.	<i>Cannabis</i> constituents	Number
1.	Terpenoids	140
2.	Hydrocarbons	50
3.	Nitrogen compounds	>70
4.	Carbohydrates	34
5.	Flavonoids	23
6.	Fatty acids	33
7.	Phenols	34
8.	Alcohols	7
9.	Aldehydes	12
10.	Ketones	13
11.	Acids	21
12.	Esters and lactones	-

1.3.1.1. Terpenes in *Cannabis*

Terpenes are basic hydrocarbons as against terpenoids, which contain functional groups of a number of chemical elements; however, these terms are often used interchangeably in the literature. Terpenes form the largest group of phytochemicals; *Cannabis* contains up to 200 different terpenes. The most common primary terpenes found in *Cannabis* are β -caryophyllene, myrcene, α -pinene, humulene, linalool, limonene, terpinolene, terpineol, ocimene, valencene, and geraniol. Some of the common secondary terpenes in *Cannabis* include α -bisabolol, nerolidol, caryophyllene oxide, phytol, borneol, δ -3-carene, terpinene, camphene, sabinene, cineole (eucalyptol), phellandrene, guaiol,

isoborneol, cedrene, geranyl acetate, fenchol, camphor, menthol, isopulegol, cymene, citral, and citronellol [27, 28]. Preclinical studies using animal models have associated terpenes with a plethora of medicinal benefits including analgesia, anti-inflammatory, antidepressant, anxiolytic, anti-insomnia, cancer chemoprevention, antibacterial, antiviral, antifungal, anti-parasitic, and anti-hyperglycemic effects [28].

1.3.1.2. Flavonoids in Cannabis

Cannabis contains phenylpropanoid phenolic compounds, one of which is called the flavonoids. The flavonoids in plants act as antioxidants protecting them against the oxidative stress. They include apigenin, luteolin, quercetin, kaempferol, cannflavin A, cannflavin B (unique to *Cannabis*), β -sitosterol, vitexin, isovitexin, kaempferol, and orientin. The flavonoids have been associated with neuroprotective, anti-inflammatory and anti-cancer effects. For instance, apigenin exerts anxiolytic effects to inhibit TNF- α , which is involved in many inflammatory conditions. Cannflavin A and B also have potent anti-inflammatory effects, with cannflavin A shown to inhibit PGE-2 30 times more potently than aspirin. β -sitosterol was shown potential to reduce topical inflammation by 65% and chronic edema by 41% in skin models [28].

1.3.2. Phytocannabinoids

1.3.2.1. Biosynthesis and pharmacology of cannabinoids

Besides the common phenolic compounds, *Cannabis* has been widely explored for phytocannabinoids (or simply cannabinoids) which are unique to the plant. Cannabinoids represent a group of C₂₁ terpenophenolic compounds and are usually concentrated in the female inflorescence, the plant being dioecious. Among the 483 compounds unique to *Cannabis*, about 66 have been identified as cannabinoids, the most important of them being Δ 9-THC with psychoactive properties [27].

The cannabinoids are biosynthesized in acidic form as cannabinoid acids in the female inflorescences of *Cannabis*, which get decarboxylated into their respective neutral cannabinoids by heat, UV exposure and prolonged storage (**Figure 1.1**). The predominant cannabinoid acids are THCA, CBDA and CBNA followed by CBGA, CBCA, CBNDA, THCVA and CBDVA, which are converted to their free forms viz. THC, CBD and CBN, CBG, CBC, CBND, THCV and CBDV, respectively [28, 29]. The numerous health benefits linked to cannabinoids, which are an outcome of the interactions of the cannabinoids with the endocannabinoid system in humans, are already well documented

[29]. THC, the primary psychoactive component of *Cannabis*, works as a weak partial agonist on CB₁ and CB₂, with preferential binding to CB₁, and is also an agonist on the PPAR- γ and TRPA1 receptors [30]. It is well-known for homeostatically regulating a myriad of physiological functions [27, 31]. On the contrary, CBD has much lower affinity for CB₁ and CB₂ receptors, with protean pharmacological effects on various other receptor systems including 5-HT_{1A}, TRPV1, adenosine A_{2A}. It acts as a non-competitive receptor antagonist that is responsible for its neutralizing actions on the side effects of THC [28]. **Table 1.2** shows the various cannabinoid classes, subtypes and their pharmacological properties.

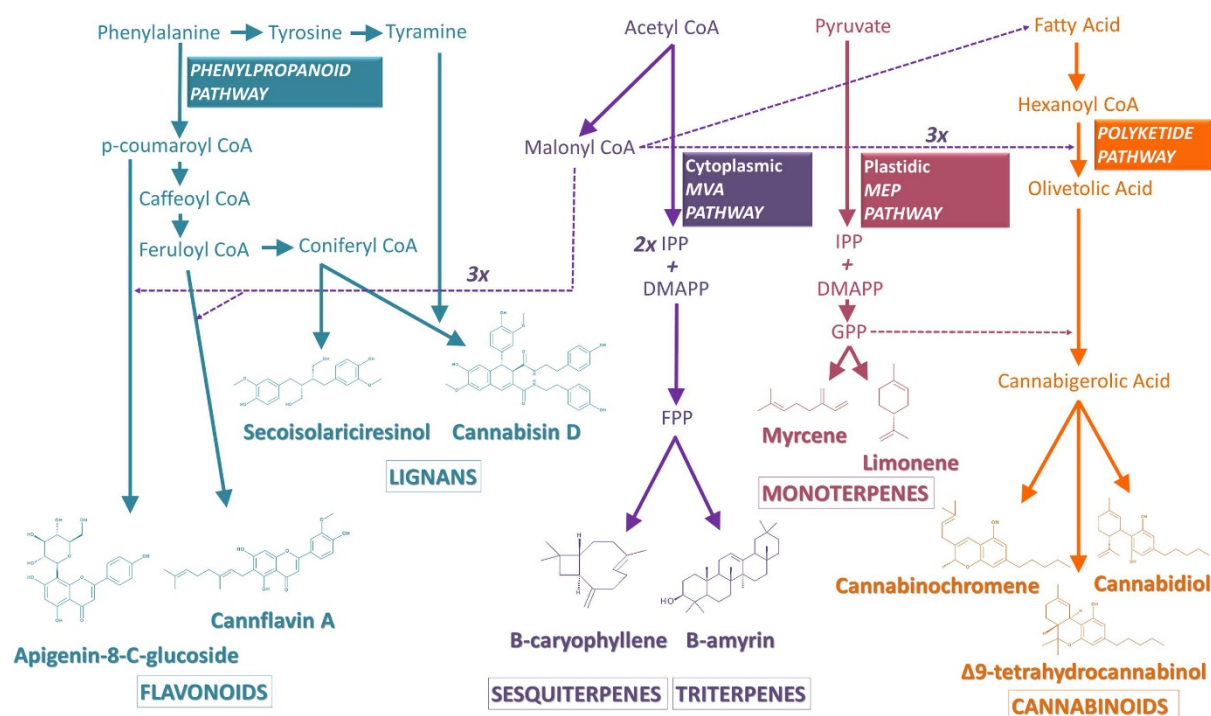


Figure 1.1 Biosynthetic pathways for bioactive compounds in *Cannabis* [29] – Published by the Frontiers publisher

Table 1.2 Classes of cannabinoids with their pharmacological attributes

Sr. No.	Cannabinoid class	Number of subtypes	Pharmacological attributes
1.	CBG	6	Antibiotic, antifungal, anti-inflammatory, analgesic
2.	CBC	5	Antibiotic, antifungal, anti-inflammatory, analgesic

3.	CBD	7	Anxiolytic, antipsychotic, analgesic, anti-inflammatory, antioxidant, antispasmodic
4.	Δ 9-THC	9	Euphoriant, analgesic, anti-inflammatory, antioxidant, antiemetic
5.	Δ 8-THC	2	Similar to THC (less potent)
6.	CBL	3	-
7.	CBE	5	-
8.	CBN and CBND	6+2	Sedative, antibiotic, anticonvulsant, anti-inflammatory, appetite-stimulant
9.	CBT	9	-
10.	Miscellaneous	11	-

1.3.2.2. *Chemotypes in Cannabis*

Apart from its utilization for medical purposes, *Cannabis* is the most extensively consumed drug of abuse in Europe. Based on the total THC content, it is categorized into three major chemotypes. Chemotype I or drug-type is predominant in THC with THC/CBD \gg 1.0, chemotype II or intermediate-type is mixed with THC/CBD \approx 1.0 and chemotype III or fibre-type is predominant in CBD with THC/CBD \ll 1.0. Due to the presence of psychoactive compound, law governs the plant cultivation in many countries. The fibre-type *Cannabis*, commonly known as hemp, is native to France, Hungary and Russia and has low THC content with presence of other non-psychoactive cannabinoids such as CBD or CBG. The maximum allowable limit for THC for hemp cultivation in Europe is 0.3% of the dry weight [32].

1.3.2.3. *Therapeutic potential of cannabinoids*

Cannabinoids have shown immense therapeutic potential (**Figure 1.2**). The most common ones include palliative effects such as treatment of nausea and emesis in patients undergoing chemotherapy, stimulation of appetite in HIV-positive patients and spasticity associated to multiple sclerosis in adults [29]. Cannabinoids have shown effects in treating ailments like epilepsy, schizophrenia, diseases related to the gut and ocular pathologies such as glaucoma. They exhibit analgesic effects through non-receptor mechanism and cannabinoid receptors, which has been used to treat muscle pain. The anti-inflammatory and anti-oxidant properties of cannabinoids have been exploited for neuro-degenerative disorders like Parkinson's disease, Huntington's disease, Alzheimer's disease, where they

were found to slow down the process of neurodegeneration [33]. Further, they have also shown promise as antitumor or anticancer agents [34, 35].

It is worth noting that the therapeutic potential and the observed biological effects of *Cannabis* vary among the different chemotypes (as discussed in section 1.3.2.2) as well as within the same chemotype depending on the chemical profile and the relative proportions of its constituents.

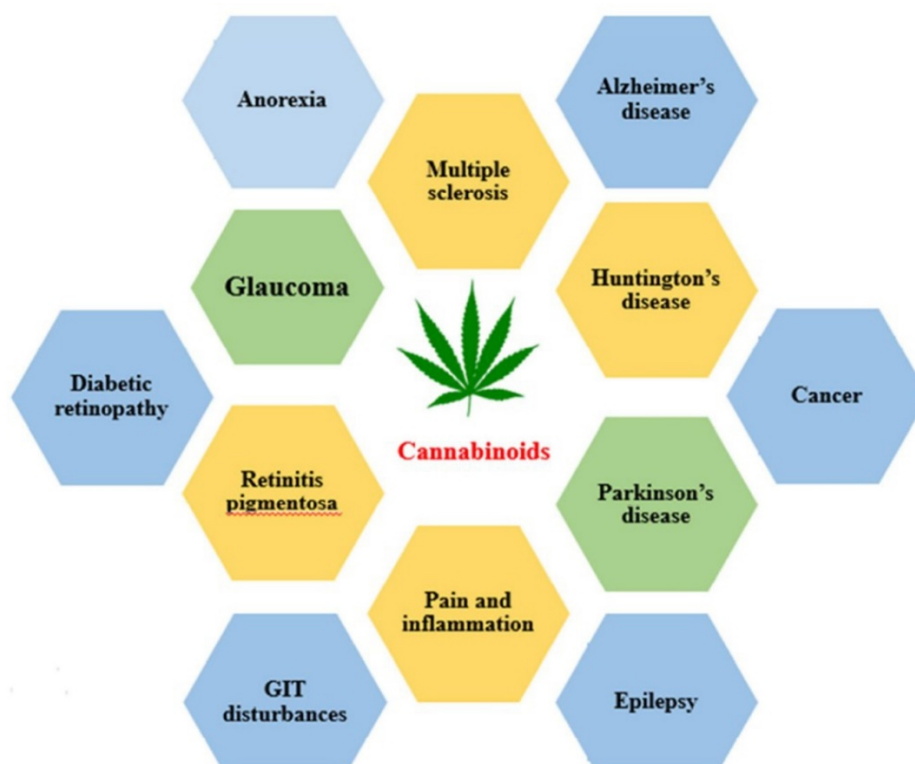


Figure 1.2 Therapeutic effects of cannabinoids for some diseases [Reproduced with permission from [36] ©2018 Elsevier publisher]

1.3.3. Extraction of phytoconstituents

Extraction is simply the separation of biologically active constituents of the plant by solvents using standard procedures with an aim to separate the soluble plant metabolites, leaving behind the insoluble cellular marc [15]. It can be achieved using conventional or modern techniques.

1.3.3.1. Using conventional methods

The isolation of these bioactive compounds and their separation from the plant matrix is made complicated due to their sensitivity to various process parameters such as temperature as well as the co-extraction of other undesirable components [23].

Conventional methods for extraction such as Soxhlet extraction, maceration and hydro-distillation have the major drawbacks of longer time needed for extraction and large amounts of solvent needed.

1.3.3.2. Using modern methods

In order to overcome these limitations, a number of modern techniques have been lately focussed on which include extractions assisted by ultrasound, microwave, enzymes, pulsed electric field, supercritical fluid extraction and pressurized liquid extraction (**Figure 1.3**) [14].

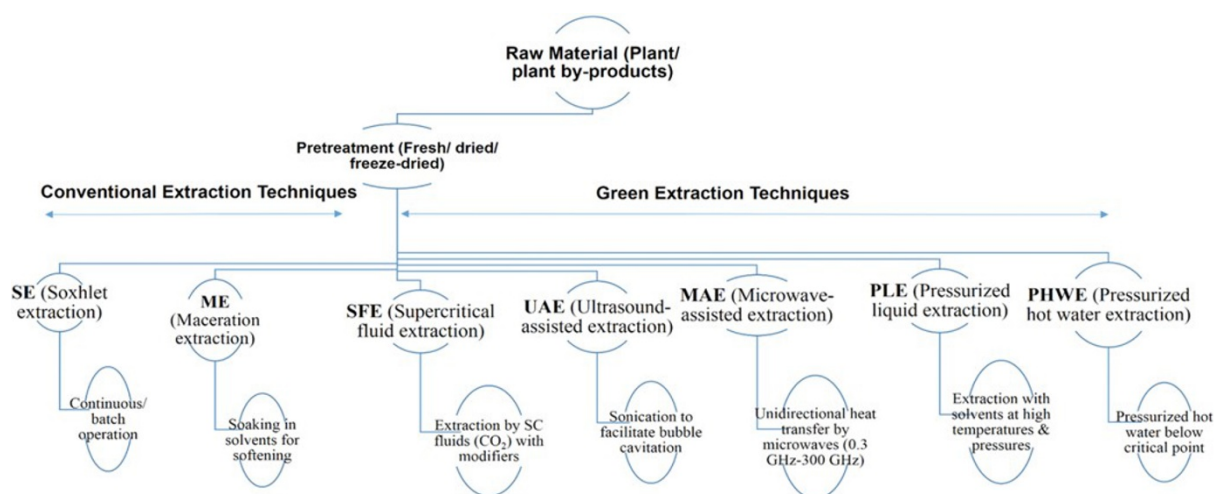


Figure 1.3 Conventional and modern methods of extraction for phytoconstituents [Reproduced with permission from [37] ©2017 JWS publisher]

Of these, ultrasonication has been widely employed for the extraction of bioactive compounds [21, 38, 39]. It is a simple technique with easy-to-operate equipment and relies on the phenomenon of bubble formation and their violent collapse called cavitation. As depicted in **Figure 1.4**, the phenomenon of cavitation occurs in the following steps:

- i. **Formation of bubble:** Similar to the sound waves, ultrasound is propagated through the liquid medium via a series of compression and rarefaction waves. At high power, the rarefaction cycle may exceed the attractive forces of the liquid molecules leading to the formation of cavitation bubbles [40].
- ii. **Growth of bubble:** The cavitation bubbles grow by a process known as rectified diffusion, where small amounts of vapour from the medium enter the bubble during its expansion phase and is not fully expelled during compression [40].

- iii. **Collapse of bubble:** Eventually, the bubbles collapse in succeeding compression cycles, which releases energy resulting in local hotspots with temperature of the order of 10^4 K and pressure as high as 10^3 bar [41, 42].

The energy released from implosion of cavitation bubbles brings about various physical effects such as turbulence due to circulation of solvent as well as chemical effects like free radical generation due to decomposition of water and pyrolysis of the trapped compounds. The shock waves generated because of cavitation are capable enough to break chemical bonds and cause cell lysis, thus assisting the process of extraction [18].

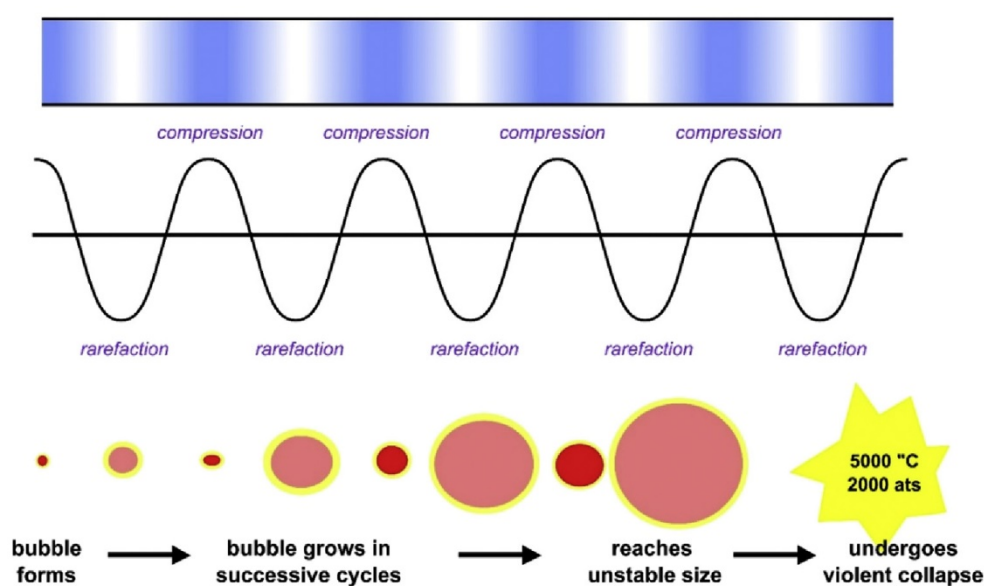


Figure 1.4 Formation and collapse of cavitation bubble [Reproduced with permission from [40] ©2017 Elsevier publisher]

Mechanism of ultrasonic extraction: The mechanism of ultrasonic extraction can be broadly described by the following two major phenomena occurring in the plant tissue/extraction solvent system [40, 43].

- i. **Swelling and hydration:** The solvent forms a layer around the plant tissue as soon as it is dispersed in the extraction solvent. Gradually, the solvent seeps into the tissue to replenish the water loss, leading to the swelling of the tissue [40]. During swelling, some phytoconstituents that are soluble in the solvent migrate into the solution due to concentration gradient inside and outside the tissue.
- ii. **Mass transfer:** Following the swelling of the plant tissue, mass transfer of soluble components into the solvent may take place by diffusion and osmotic processes in different ways (*Figure 1.5*) [40, 44]:

- a. Type I diffusion of phytoconstituents towards the outer stagnant layer
- b. Type II diffusion of phytoconstituents directly to the solvent
- c. Type III diffusion of phytoconstituents from the stagnant layer towards the bulk solvent
- d. Rinsing or washing out of the contents of broken cells

Advantages of ultrasonic extraction: Ultrasonication offers several advantages over the conventional techniques, which include improved mass transfer, cell disruption, milling and improved solvent penetration. Further, it also enhances the yield and provides better selectivity in the extraction of the phytoconstituents [16, 40]. Ultrasonication is environmental-friendly compared to the conventional techniques in terms of resources, time and energy. It avoids the use of large amounts of solvents and voluminous extraction vessels used for Soxhlet extraction and maceration. It has far less environmental impact in terms of carbon footprint- only 200 g CO₂/100 g of extracted material is released for ultrasonic extraction as against 6400 g CO₂/100 g of extracted material for Soxhlet extraction and 3600 g CO₂/100 g of extracted material for maceration [45].

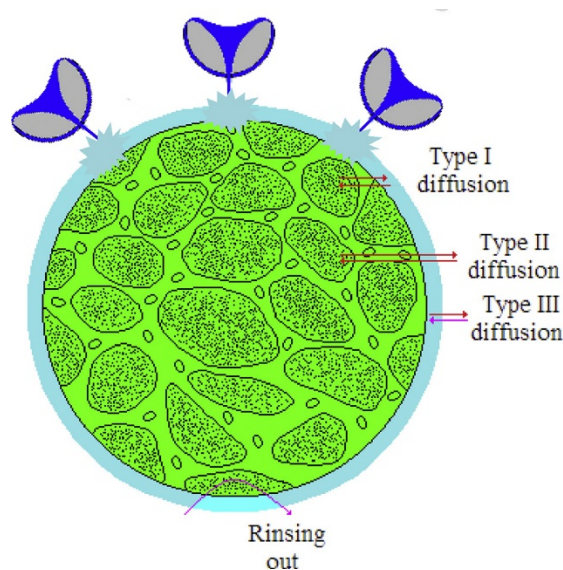


Figure 1.5 Diffusion in a plant tissue surrounded by a solvent layer during ultrasonic extraction [Reproduced with permission from [40] ©2017 Elsevier publisher]

1.3.4. Plant extract as a green reducing agent

A number of plant extracts have been explored as green reducing agents for the synthesis of nanomaterials (**Figure 1.6**). The plant extracts are free from corrosion, carcinogenicity, and toxicity, and hence are termed as “green reducing agents” [46]. A broad range of biomolecules in the extracts including alkaloids, terpenes, phenols,

flavonoids, tannins, quinines etc. are known to facilitate the reduction process [6]. The bio-reduction is influenced by the reaction conditions such as time and temperature. For instance, chrysanthemum extract has been employed as a green reductant for the chemical reduction of GO [47]. The dried flowers of chrysanthemum contain alkanes, flavonoids, unsaturated fatty acids, polysaccharides, which have a high tendency to get oxidized in presence of reactive oxygen. Likewise, Another study utilized the aqueous leaf extract of *Piper pedicellatum* C.DC to synthesize Ag, Au and Ag–Au bimetallic nanoparticles [13]. The reduction of nanoparticles was possibly facilitated by the adsorption of flavonoids and phenolic acids on the surface of metal nanoparticles through π -electrons interaction. Similarly, tea extract has been used to synthesize palladium nanoparticles at room temperature, where the polyphenols acted as a reducing agent as well as a capping agent for the ensuing nanoparticles in the range of 20–60 nm [11].

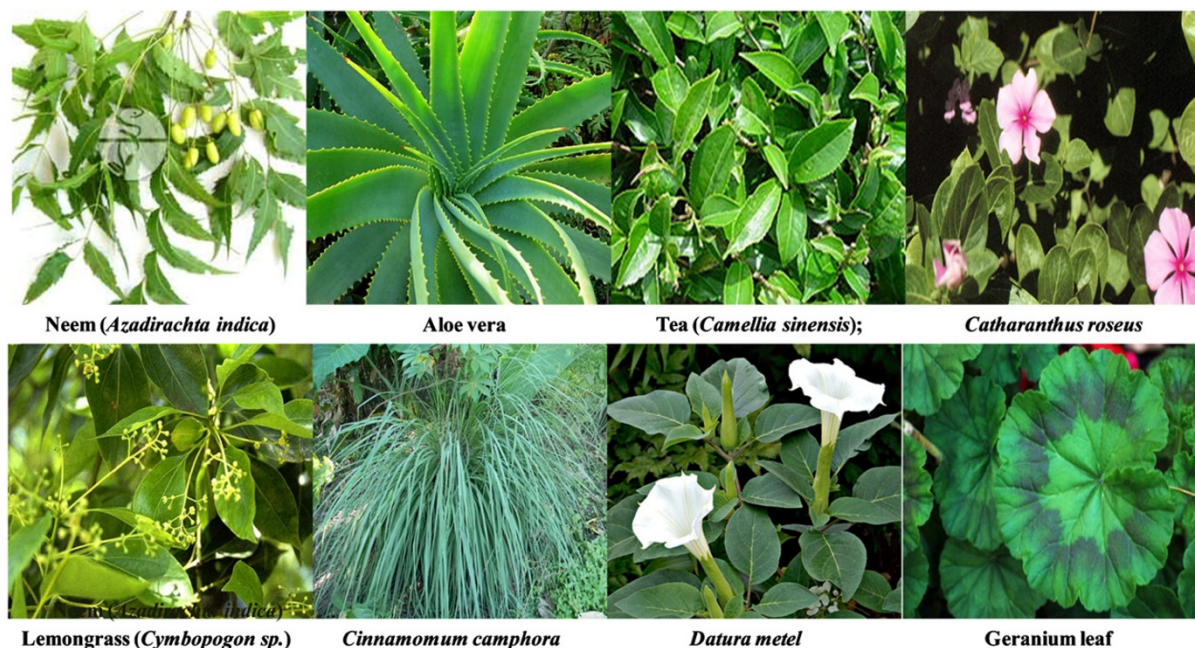


Figure 1.6 Plants used for the green reduction of materials such as nanoparticles [Reproduced with permission from [7] ©2013 Elsevier publisher]

1.4. Cellulose as a substrate for functionalization of materials

1.4.1. Cellulose background

1.4.1.1. Structure

In view of the growing concerns on sustainable and economic development, natural materials such as cellulose have drawn significant attention for various scientific purposes in the recent years. Cellulose, the most abundantly available biopolymer on earth, was first

isolated from plants by Anselme Payen in 1838 [48, 49]. Cellulose is a linear homopolysaccharide consisting of β -D-glucopyranose units with an empirical formula of $(C_6H_{10}O_5)_n$, 'n' ranging from a couple of hundreds to 15,000 depending on the source of cellulose [49, 50]. The smallest repeating unit is cellulose consists of two anhydroglucose units (cellobiose) linked together by a covalently bonded oxygen connecting C1 of one unit with C4 of the adjoining unit, hence also referred to as $\beta(1-4)$ glycosidic bonds as shown in **Figure 1.7a** [50, 51].

Natural cellulose from plants is synthesized in the form of chain bundles referred to as protofibrils, which are assembled to form microfibrils. The microfibrils contain regions, which are highly ordered (crystalline) and regions in-between that are not as ordered (amorphous) as depicted in **Figure 1.7b**. The ratio of the crystalline and amorphous regions depends on the origin and affects the density of cellulose [50, 51]. Wood is composed of 30 to 40 % cellulose, with almost an equal portion of the crystalline and amorphous phases [52]. The crystalline phase imparts mechanical strength, whereas the amorphous phase is associated with viscoelastic properties. The linearity in structure comes from the hydrogen bonding between hydroxyl groups and oxygen of the adjoining rings. The inter- and intra-chain hydrogen bonding imparts stability and stiffness to cellulose (**Figure 1.7c**). The morphology of cellulose is closely related to its reactivity, the hydroxyl groups in the crystalline region may not be accessible due to close packing and strong bonding, while those in amorphous region may react easily [52, 53].

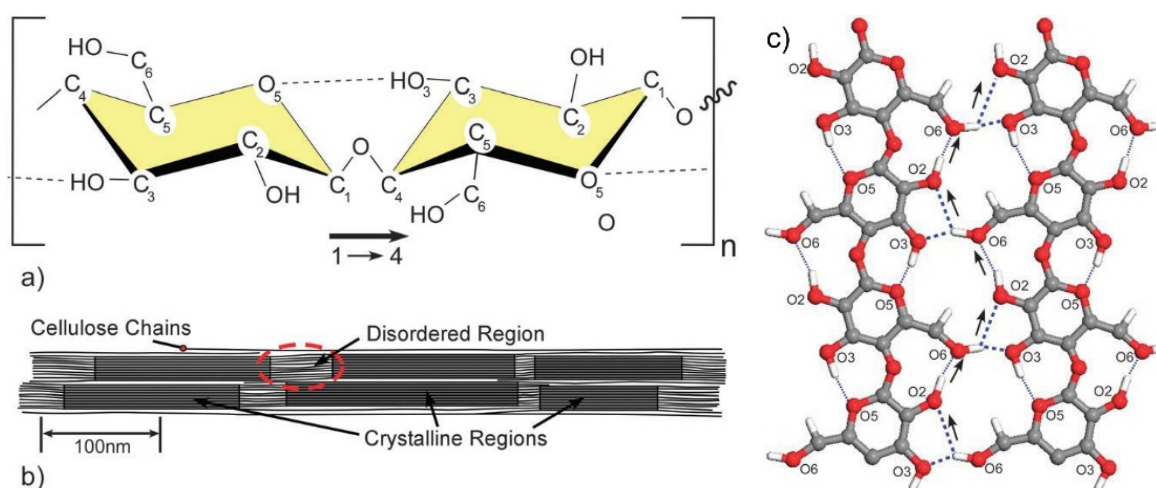


Figure 1.7 (a) Two glucose rings in cellulose chain connected by $\beta(1-4)$ glycosidic linkage; dotted line indicates the intra-chain hydrogen bonding, (b) amorphous and crystalline regions in a cellulose chain, (c) hydrogen bonding in cellulose, the thin dotted lines indicate

the intrachain bonding, while the thick dotted line represents the interchain bonding [Reproduced with permission from [50] ©2011 RSC publisher]

1.4.1.2. Polymorphs

Crystalline cellulose primarily has four polymorphs (I, II, III and IV). These polymorphs exhibit various conformations depending on the intra- and inter-molecular H-bonding. Of all, cellulose II is the most thermodynamically stable form with lowest energy [51]. Cellulose I is also called natural or native cellulose, by virtue of its predominate existence in most plants, trees and some sea animals. Cellulose II, reportedly found in bacteria cultivated in glycerol and in cold conditions, can be obtained from cellulose I by solubilisation, recrystallization (regeneration) and treating with sodium hydroxide (mercerization). Likewise, cellulose III can be obtained from either cellulose I (called cellulose III_I) or II (called cellulose III_{II}) by treating it with liquid ammonia while cellulose IV (IV_I or IV_{II}) can be formed on further thermal treatment (heating with glycerol at 250 °C) [54].

1.4.1.3. Sources

Cellulose can be obtained from both plant as well as animal sources. Being the fundamental strengthening component of plant cell wall, cellulose forms an inexhaustible source of raw material. Wood (softwood or hardwood) is the most important source of cellulose. Cellulose roughly constitutes 45 % of the dry weight of wood. Cellulose is commonly extracted from wood for production of pulp and paper by removal of lignin via the Kraft process [55]. Apart from wood, cellulose also occurs in many non-woody plants such as bamboo, sisal, flax, hemp, jute, cotton and agricultural residues obtained from bagasse, wheat, rice, corn, coconut, banana, pineapple and sugar beet pulp [50, 56]. Like wood, they also need to be processed for cellulose.

Tunicates, a class of sea animals, have a mantle of cellulose embedded in a matrix of proteins. Some of the widely investigated species include *Halocynthia roretzi* and *Metandrocarpa uedai*. Several algae such as green, red and grey algae produce cellulose. *Micrasterias denticulate* and *Caldophora* are some of the extensively studied species. Finally, some bacterial strains such as *Gluconacetobacter xylinus* and *Acetobacter xylinum* secrete cellulose under special culturing conditions to form biofilms. They do so in order to possibly protect themselves from UV rays or to hinder fungi and other organisms [50].

1.4.1.4. Properties

The cellulose fibres are naturally hydrophilic due to the presence of hydroxyl groups, which allow capillary wicking of fluids required in many LFAs [48]. The porosity of cellulose fibre network, as in paper, is also immensely useful for the incorporation of materials as well as their diffusion [57]. The biocompatibility, biodegradability and non-toxicity of cellulose make it ideal for a number of biomedical applications. All these attributes of cellulose have made possible for it to come a long way in making its place as an attractive biomaterial for a plethora of applications, ranging from simple wound-healing bandages to complex immunosensors.

1.4.2. Cellulose chemistry

The chemical functionality of native cellulose is because of its surface chemistry, which depends on the source of cellulose. Added functionality can be introduced on them by means of surface modification by physical adsorption of molecules or by chemical attachment of entities or by derivatisation by functional groups. The cellulose chain, with directional chemical asymmetry, consists of a hemiacetal hydroxyl group on the pyranose ring on the reducing end and a pendant hydroxyl group on the non-reducing end (**Figure 1.8a**).

Different sorts of interactions such as van der Waals, intra- and inter-chain hydrogen bonding between hydroxyl groups and oxygen atoms exist in cellulose. The abundance of hydroxyl groups on the surface of cellulose cause the surface to become very reactive which makes it possible to functionalize it with a number of moieties. **Figure 1.8b** depicts the major reactions for the chemical modification i.e. (1) esterification, (2) etherification, (3) replacement of the OH by amine or halogen groups, (4) replacement of hydrogen molecules by sodium, (5) oxidation or (6) addition compounds with acids, bases and salts [58]. These modifications only affect the terminal groups of cellulose without breaking down the chain. It is also to be noted that the reactivity of each of the three hydroxyl groups varies with its position in the glucose ring and is not the same due to steric effects arising by virtue of the structure [59].

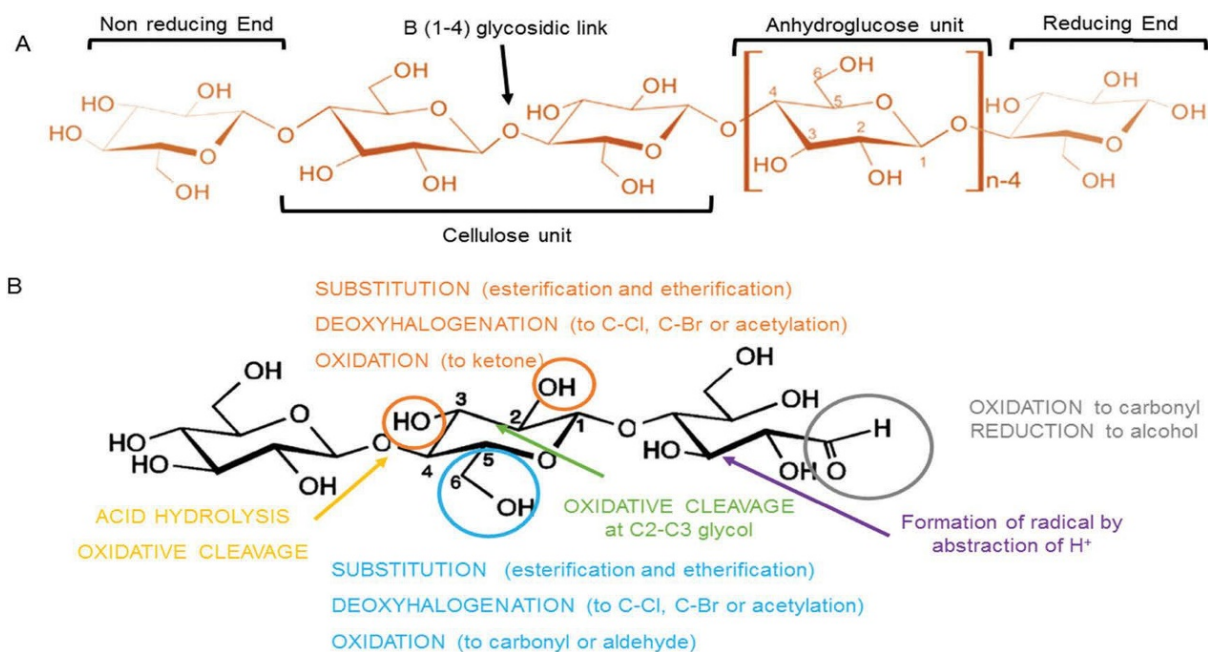


Figure 1.8 (a) Directional asymmetry of cellulose, (b) chemical reactions for modification of cellulose [Reproduced with permission from [58] ©2018 RSC publisher]

1.4.2.1. *Functionalization via physical adsorption*

Cellulose may be functionalized by adsorbing the molecules on its surface by electrostatic forces of attraction, as in case of polyelectrolytes used as dry and wet strength additives in paper industry. The layer-by-layer deposition is the most commonly used technique for employing physical adsorption [60]. Non-ionic dispersants such as xyloglucan that have a strong, specific adsorption towards cellulose have also been used [61].

1.4.2.2. *Functionalization via chemical bonding*

Alternatively, cellulose may be functionalized by direct chemical bonding or covalent attachment of molecules. Since cellulose has ample surface hydroxyl groups, species reacting with alcohols such as epoxides, isocyanates, acid halides and acid anhydrides are commonly used for chemical attachment. These reactions can further be used to form a number of alternate surface chemistries including ammonium, amine, alkyl, hydroxyalkyl, ester, acid, etc. [50].

Thus, the structure of cellulose allows its surface to be chemically modified by different processes such as oxidation, amination, esterification, which play an instrumental role in the immobilization of materials by imparting new properties to cellulose without destroying its appealing intrinsic properties [48], as depicted in **Figure 1.9**.

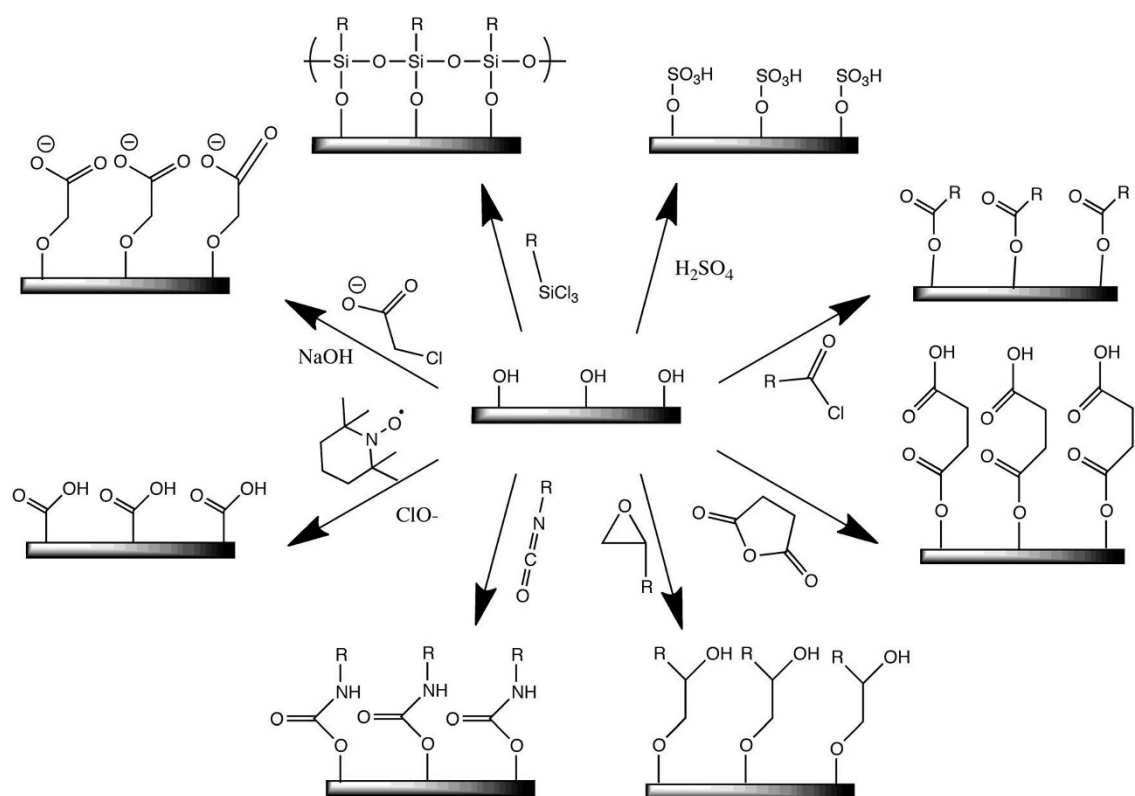


Figure 1.9 Common functionalization chemistries of cellulose surfaces: (clockwise from top-right) sulphuric acid treatment provides sulphate esters, carboxylic acid halides create ester linkages, acid anhydrides create ester linkages, epoxides create ether linkages, isocyanates create urethane linkages, TEMPO mediated hypochlorite oxidation creates carboxylic acids, halogenated acetic acids create carboxymethyl surfaces, and chlorosilanes create an oligomeric silylated layer [Reproduced with permission from [50] ©2011 RSC publisher]

1.4.3. Functionalization of cellulose

Cellulose has gained considerable attention of researchers as a versatile biomaterial, in the quest for sustainable and economical materials in a myriad of fields. The fact that cellulose fibres have reactive surface makes it easy to modify them with a range of functional groups to conjugate various species such as biomolecules, nanoparticles for targeted applications such as bio-sensing, catalysis, biomedical, packaging, etc. [1]. Cellulose is abundantly available, biodegradable, biocompatible, flexible, and readily modifiable, which make it an excellent choice for composites [56].

The functionalization of materials onto substrates has mitigated their recovery issues, leading to environmental remediation [2]. The immobilization of an entity simply refers to its attachment to a surface leading to reduction or loss of its mobility. It can occur

by different approaches- physical, chemical, biological or a combination of these processes [48, 62]. Cellulose fibre substrates, such as paper, provide an ideal platform for immobilization by favouring the growth of nanostructures due to their inherently oriented and organized network of fibres [63]. Within the fast growing field of nanotechnology, metal, metal oxide, quantum dots and carbon nanomaterials are gaining increasing interest of researchers due to their overwhelming characteristics [2, 3, 64]. Cellulosic substrates have been widely explored for embedding these nanomaterials for building simple, portable and disposable devices in theranostics, electronics, microfluidics, environmental and POC applications (**Figure 1.10**) [48, 57]. Paper, being a sheet of randomly interwoven cellulose fibres, possesses all the aforementioned intriguing features of cellulose, which make an excellent platform for anchoring of materials. It also easily complies with the requirements of WHO for diagnostic devices, which should be ASSURED- Affordable, Sensitive, Specific, User-friendly, Rapid and robust, Equipment free and Deliverable to end-users [48].

Cellulose has been functionalized with several materials mainly including metals, metal oxides, quantum dots, carbon and biomolecules. Considering the vast potential and demand of natural and renewable resources in virtually every sector, functionalized cellulosic materials show promise to overcome many hurdles and challenges posed during material synthesis and application.

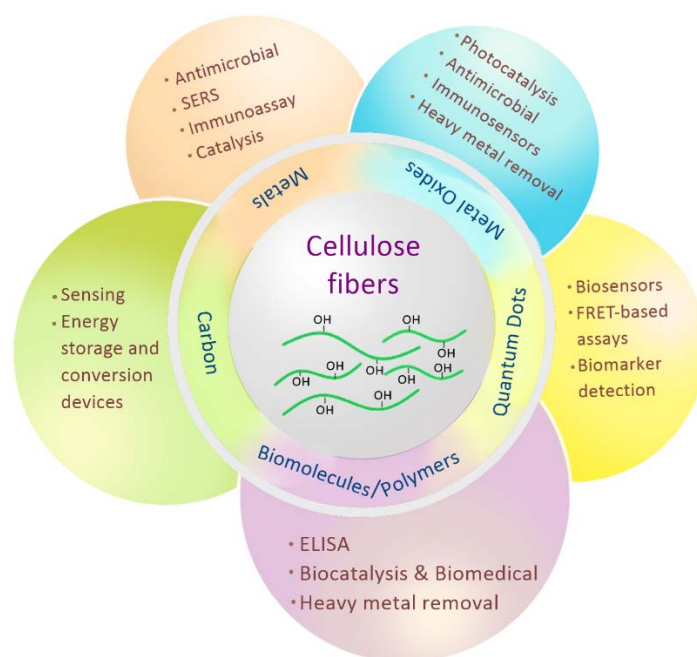


Figure 1.10 Applications of cellulose fibres modified with nanomaterials

1.4.4. Functionalization of cellulose with carbonaceous materials

Various nanomaterials based on carbon such as fullerenes, graphene and CNTs have attracted significant attention in the past three decades. In view of their extraordinary mechanical, optical, electrical, thermal and chemical properties, they have been extensively explored for electronics, optoelectronics, photovoltaics and sensing applications [3]. Since the discovery of CNTs by Iijima in 1991, considerable efforts have been devoted to uncover their underlying potential. CNTs are seamless cylinders of single or few layered graphene with an aspect ratio ranging from 10^2 to 10^7 . Apart from having a high surface area, CNTs have shown remarkable mechanical properties, good electrical conductivity, high thermal conductivity and stability as well as unique mesoporosity. These attributes have made them very attractive for various piezoelectric and thermoelectric energy-harvesting devices, cells, batteries and sensors [65]. Graphene is a two-dimensional, single atom thick building block for other carbon materials, comprising of planar sheets of sp^2 -bonded carbon atoms that are closely packed in a honeycomb crystal lattice. It has many similarities to CNTs in structure and property, which make it a promising candidate for use in similar areas as CNTs, including supercapacitors, solar cells, lithium-ion batteries, fuel cells, actuators and transistors [65, 66].

1.4.4.1. Carbon nanotubes

Carbon nanomaterials have been widely used to sense a variety of analytes including gases, solvents and biomolecules. Cellulose-based sensors using CNTs have been developed for the detection of glucose [67], ammonia [68, 69], tumour markers [70-73], chemical vapours [74], environmental toxins [75], water [76-78] and ions [79]. Different approaches used to anchor CNTs to cellulosic substrates include simple paper-making technique [78, 80], coating [81], mechanical drawing [69] and ink-jet printing [74]. A humidity sensor was fabricated by conformally coating single-walled CNTs functionalized with carboxylic acid on paper surface [81]. The roughness and porosity of paper were advantageous as they increased the contact area with the ambient air and promoted the adhesion to CNTs. The SEM images confirmed firm entanglement of the CNTs with the cellulose fibres. A shift in conductance of CNT network entangled on the fibres was used for humidity sensing. Since cellulose is an insulator, no current flowed in the bare paper up to 80% RH. Current, however, began to flow at higher RH due to ionic conduction from the dissociation of water. On the other hand, the CNT-coated paper showed linear decrease

in conductance with increasing RH up to 75% RH, after which there was marginal rise in conductance. On comparing to a control sensor on glass substrate, cellulose facilitated the charge transport on the paper substrate thus enhancing its sensitivity. Further, the wettability of paper allowed it to soak the CNT suspension leading to better adhesion [81].

In a different study, ink-jet printed films of CNTs on 100% acid-free paper demonstrated the use of cellulose as substrates for sensing chemically aggressive vapours [74]. It was shown that the instability of cellulose towards highly oxidizing vapours is not intrinsic to it but instead, it is an outcome of the surface finishes used during paper manufacture. The detection of NO₂ and Cl₂ vapours up to 250 and 500 ppb, respectively, was made possible by acid-free paper in ambient conditions by recording the resistance changes. Unlike as in case of PET-based substrate, the paper sensor exhibited spontaneous signal recovery and repeated use over multiple cycle without loss of functionality. It suggested that cellulosic substrates can meaningfully mitigate the aggressive behaviour of vapours such as Cl₂ toward thin organic films by reducing the residence time of vapours [74].

Paper-based supercapacitors were prepared by depositing single-walled CNTs on a paper substrate *via* Meyer rod coating and ink-jet printing. The paper was treated with polyvinylidene fluoride prior to printing of CNTs in order to prevent short circuit and yet allow it to function as an electrolyte membrane and separator [82]. Earlier, they had deposited a combination of single-walled CNTs and AgNWs on paper using printable solution processing technique. The values of specific capacitance, energy, power and life were found to be better than those devices using plastic substrates due to the intrinsic properties of paper such as high solvent absorption and strong binding with nanomaterials. Superior mechanical properties resulted from the porous nature of paper, which relaxed the bending strain. Additionally, the conductive paper also showed potential as a current collector in Li-ion batteries to replace the metallic counterparts [83]. Similar other works on CNT-coated paper supercapacitors have been reported [84-86].

1.4.4.2. Graphene/reduced-GO

Like CNTs, graphene [87-90], reduced-GO [91, 92], graphene quantum dots [93, 94] and carbon nanodots [95, 96] anchored to cellulosic substrates have also shown extraordinary sensing potential. The exceptional physical, mechanical, thermal, chemical and electrical properties of graphene have made it a versatile choice of research for material

scientists the world over. It has been widely used to develop a wide range of functional materials for a plethora of applications from electronics to antibacterial materials [97]. The top-down approach, with GO as the precursor, is the most-promising and a widely used technique for the preparation of graphene-based materials. GO is typically highly reactive due to the presence of a number of functional groups such as $-OH$, $-COOH$, epoxy and alkoxy. Hence, reducing the functionalities on the surface of GO is desirable for many biological applications as well as in the electronics sector, in order to regain the electrical activity by recovery of conjugated network of graphitic lattice [98, 99].

Graphene stands out as a material for sensing owing to its single atom thickness, which makes it extremely sensitive to changes in its environment. Graphene layers were directly transferred on paper for resistive sensing of NO_2 with remarkably low limit of detection at 300 ppt [100]. As shown in **Figure 1.11**, graphene on copper foil was spin coated with a layer of PMMA and etched to foil. The PMMA-graphene film was then dredged on to paper and PMMA was dissolved with acetone. The normal paper yielded a patchy coverage while complete transfer occurred on smooth glossy paper [100].

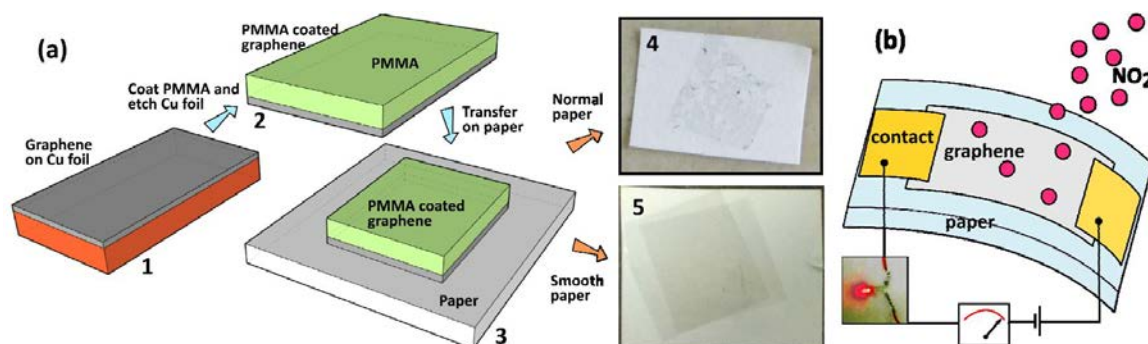


Figure 1.11 (a) Schematic depicting transfer of graphene on to paper, (b) Graphene paper strip in action as a gas sensor may glow an LED bulb [Reproduced with permission from ref. [100] ©2015 ACS publisher]

A pressure sensor was developed by soaking tissue paper in GO solution and subsequently reducing thermally into reduced-GO (rGO paper) [89]. Optimization between sensor sensitivity and working range was achieved in the range of 0-20 kPa and sensitivity up to 17.2 kPa^{-1} . Significant differences in the sensor performance was observed with number of tissue layers (**Figure 1.12a**). With increasing number of layers, the sensitivity rose 17.2 kPa^{-1} in the range of 0-2 kPa while it fell to 0.1 kPa^{-1} in the range of 2-20 kPa. This was attributed to the presence of air gaps between the layers of tissue paper resulting

in their poor contact, which led to a large origin resistance when no pressure was applied on the sensor. The sensor showed good response for detection of pulse, respiration and other human movements (**Figure 1.12 b&c**) [89].

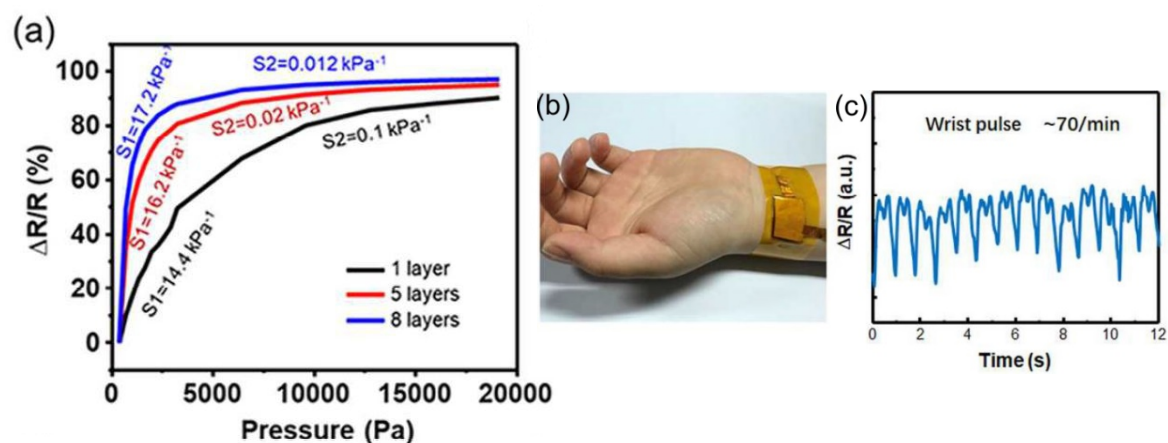


Figure 1.12 (a) Increase in resistance change with pressure for graphene-based pressure sensor for different number of layers of tissue paper, (b) Sensor application for detection of wrist pulse, (c) Pulse waveform of the sensor [Reproduced with permission from ref. [89] ©2017 ACS publisher]

Likewise, rGO on paper with AuPd alloy nanoparticles has been used for real time and *in situ* analysis of hydrogen sulphide released from cancer cells [101]. rGO-paper electrode modified with ZnO nanorods was used as an electrochemical sensor platform for various antigens [102]. Flower-like rGO-modified paper biosensor showed a good linear response for the detection of Pb^{2+} from 0.005 to 2000 nM [103]. Long graphene nanoribbons (150 nm wide) synthesized *via* nanoscale cutting of graphite were cleaved to produce graphene quantum dots (100-200 nm) for humidity and pressure sensors [104]. Electrochemical immunoassays with graphene-based sensing have been used to detect biomolecules such as DNA and biomarker [105-107].

Apart from sensing, graphene-based materials have found a plethora of applications in energy storage and energy conversion devices. Supercapacitors fabricated from graphene/cellulose composites as flexible electrodes have demonstrated good capacitance, low resistance and high strength [66, 108]. The graphene-cellulose paper (GCP) was prepared by simply filtering a suspension of graphene nanosheets (GNSs) through a filter paper under vacuum. Electrostatic attraction between the functional groups on cellulose fibres and the negatively charged graphene caused the GNSs to strongly bind to fibres and

penetrate the voids to form a conductive interwoven network, as shown in **Figure 1.13**. The low strength and porosity of graphene was overcome by combining it with the cellulose matrix. Further, the GCP also inherited mechanical flexibility from paper and could endure over 1000 repeated bend tests with little increase in resistivity for good supercapacitor performance [108].

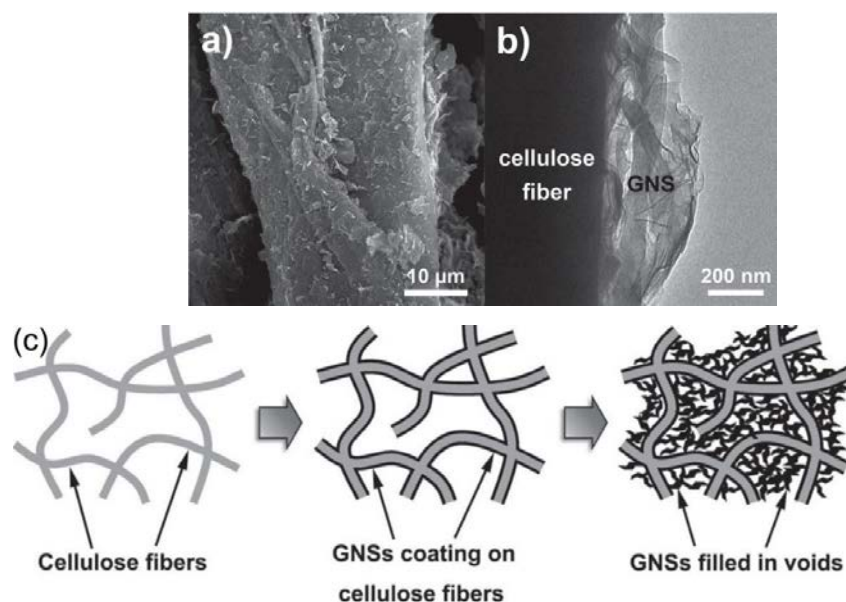


Figure 1.13 a) SEM and b) TEM images of a cellulose fibre in a GCP membrane showing GNSs anchored on the fibre surface, c) cellulose-GNSs binding in GCP [Reproduced with permission from ref. [108] ©2011 JWS publisher]

Similarly, GNS/paper composite was synthesized by dispersing chemically synthesized GNSs in a cellulose pulp and followed by infiltration. The tough paper composite could be bent and restored fully, forming a good contact with the copper foil while remaining flexible without separation (**Figure 1.14**). It also showed higher modulus of elasticity than pure cellulose paper due to the mechanical locking of the cellulose fibres by the GNS coating making it less vulnerable to inter-fibre sliding. It exhibited a high electrochemical activity as an electrode in a supercapacitor and lithium battery with a promising electrochemical performance [109]. Likewise, flexible electrodes from graphene/polyaniline composite paper have been reported [110].

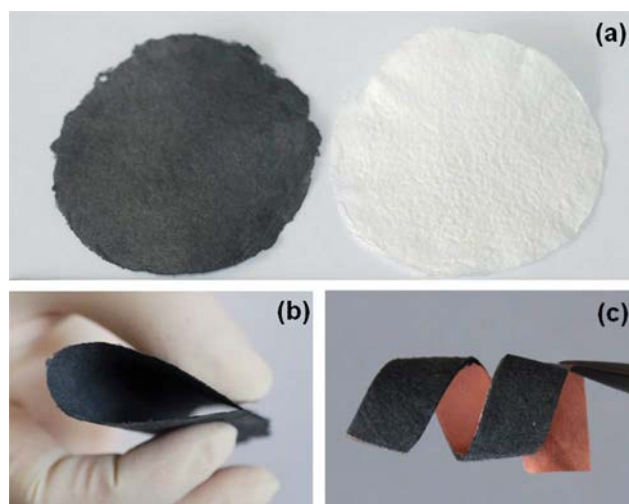


Figure 1.14 (a) GNS/cellulose composite paper (black) against pure cellulose paper (white), (b) the bent composite paper, showing flexibility of the paper and (c) composite paper adhered to conducting copper foil to make a flexible supercapacitor [Reproduced with permission from ref. [109] ©2012 RSC publisher]

1.5. Green reduction of GO

Conventionally, the reduction of GO has been achieved by means of chemical reducing agents such as dimethylhydrazine, sodium borohydride and hydroquinone [8, 46]. However, the highly toxic nature and high costs of the chemical reducing agents, along with their inability to prevent the irreversible aggregation of GO have led the scientific community to look for natural and eco-friendly reducing agents [9]. The thirst for finding suitable alternatives paved the way for green nanotechnology, especially in the last decade, which has employed various biomolecules such as vitamins, saccharides, amino acids and hormones, plant extracts as well as microorganisms as green reducing agents [8-10]. For instance, ascorbic acid (vitamin C) is a common green reducing agent and performs well in the reduction of GO; however, in most cases, the reduced product has exhibited a highly agglomerated morphology without an external stabilizer [111-113]. This limitation can be overcome by using phytoextracts, which are being widely exploited as eco-friendly reducing agents due to their availability, non-toxicity and low cost.

The extracts from plants abound in phytoconstituents such as polyphenols and flavonoids, which are the fundamental secondary metabolites with an excellent reducing ability and antioxidant potential. The reducing ability is a function of the number of free hydroxyl groups present in the molecular structure of the compound and is strengthened by

stearic hindrance [114]. Another advantage of bio-reductants is their ability to act as both reducing and capping or stabilizing agents, thus eliminating the need for additional chemical stabilizers. Nevertheless, there may be instances where stabilizers or supporting agents are required for effective reduction [115]. Recently, various plants including *Ocimum sanctum* (holy basil) [99], *Aloe vera* [116], green tea [117] and *Salvadora persica* L. (miswak) [118] were used for the green reduction of GO. Studies have shown that the naturally reduced-GO has excellent dispersibility, stability and biocompatibility compared to the chemically reduced one [115, 119].

The mechanism for the reduction of GO by plant extracts is illustrated in **Figure 1.15** [10]. GO has different oxygen groups such as epoxide, hydroxyl and carbonyl. The polyphenols react with the epoxide group through S_N2 mechanism resulting in the opening of the oxirane ring. The carbonyl and hydroxyl groups experience nucleophilic attack by polyphenols with the elimination of a water molecule, thus leading to the conversion of GO to RGO [10].

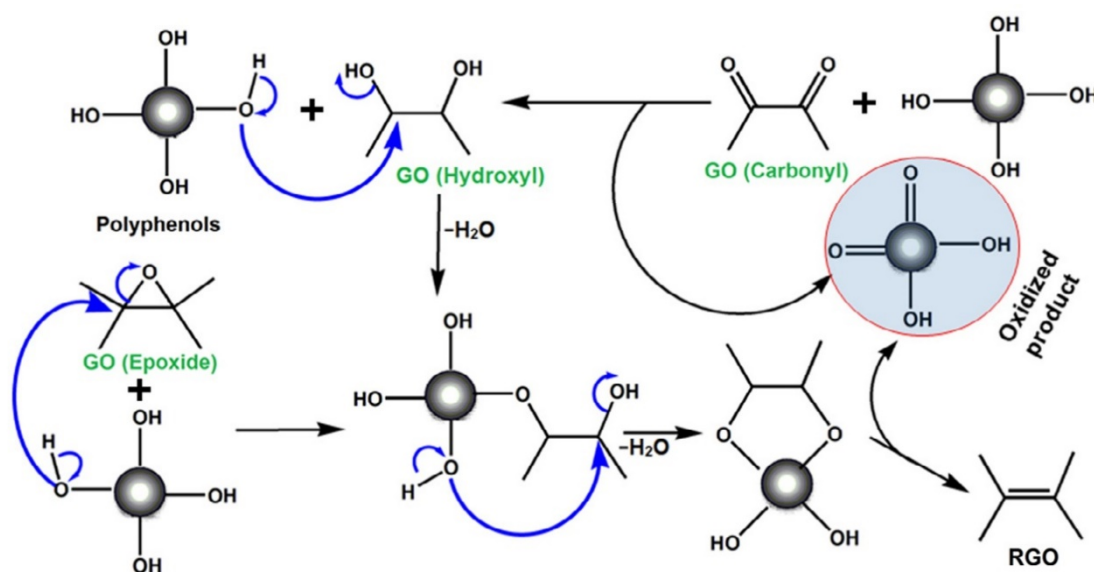


Figure 1.15 Mechanism for the reduction of GO with plant extracts [Reproduced with permission from ref. [10] ©2015 Elsevier publisher]

1.6. Research rationale & objectives

The advent of nanotechnology has opened new avenues for a plethora of applications in biomedical healthcare, food and pharmaceutical, electronics, to name a few. The chemical reducing agents commonly used for the synthesis of nanomaterials are generally toxic in nature and have hazardous reaction products. In order to overcome the limitations

associated with the chemical reducing agents, phytoconstituents have been employed for the eco-friendly synthesis of nanomaterials.

The present research endeavours to extract phytoconstituents using one of the modern extraction techniques and employ them as eco-friendly agents for the in situ reduction and simultaneous functionalization on cellulose fibres. It will encourage the exploration of the potentially useful compounds present in *Cannabis* by their facile extraction achieved by ultrasonication.

In light of this, the following research objectives were proposed:

- ✓ Extraction of bioactive compounds (cannabinoids, terpenes, flavonoids, etc.) from the inflorescence of *Cannabis* using ultrasonication at varying experimental conditions
- ✓ Evaluation of the extracts to obtain the response values (total phenolics, total flavonoids, ferric reducing ability of plasma and extraction yield)
- ✓ Optimization of the extraction parameters (time, ultrasonic power and extraction solvent) by response surface methodology
- ✓ Qualitative analysis of the extract using chromatographic techniques (HPLC-DAD-MS/MS and GC-MS)
- ✓ Utilization of the extract for in situ reduction of GO on cellulose fibres
- ✓ Characterization of the reduced-GO/cellulose composites using advanced analytical techniques (FTIR, SEM, XRD and XPS) and study of their electrical performance

1.7. Dissertation outline

This dissertation has been structured into six chapters as follows:

i. Chapter I

This chapter outlines the problem statement and the research objectives. It reviews the phytoconstituents in *Cannabis* and their extraction using the conventional and modern. It also discusses the potential of the phytoextracts as greens reducing agents for the synthesis of materials. Further, a brief discussion on cellulose chemistry and the functionalization of cellulose with special focus on carbon materials such as carbon nanotubes and graphene along with the functionalization strategies has been put in. Finally, the chapter throws light on the reduction of GO using various phytoextracts.

ii. Chapter II

This chapter deals with the detailed experimental procedures employed for the extraction of bioactive compounds from the inflorescences of *Cannabis* using the principle of ultrasound, their evaluation and experimental design for the optimization of extraction conditions. The reduction of GO in situ on the cellulose fibres using *Cannabis* extract and the characterization of the synthesized composites by advanced analytical tools has been discussed.

iii. Chapter III

This chapter presents the ultrasonic extraction of bioactive compounds from *Cannabis* and analysis of the influence of ultrasonic parameters on the extract properties using response surface methodology. It shows a comparative evaluation of cannabinoids using HPLC-DAD-MS/MS technique for the ultrasonic and control extractions.

iv. Chapter IV

This chapter deals with the identification and qualitative assessment of the ultrasonically extracted cannabinoid and other bioactive compounds using advanced chromatographic techniques. It describes the biosynthesis and pharmacology of the cannabinoids. It discusses the various advantages of using *Cannabis* extracts exhibiting entourage effects over the pure cannabinoids as well as their safety concerns.

v. Chapter V

This chapter deals with the green reduction and simultaneous functionalization of GO on cellulose fibres using the aqueous extract of *Cannabis*. The GO was reduced in situ on the cellulose matrix in presence of the extract in order to functionalize the fibres with reduced-GO. It thoroughly discusses the characterization of RGO/cellulose composites using advanced analytical techniques and their electrical performance.

vi. Chapter VI

This chapter presents the conclusions of the research work and recommendations for future research. The facile ultrasonic technique employed for the extraction of phytoconstituents in this work can be extended for the extraction of other biological components.

1.8. Summary

The bioactive compounds in *Cannabis* including terpenes, flavonoids and cannabinoids have described followed by the extraction of these phytoconstituents using both the conventional and modern techniques for extraction with focus on ultrasonication.

The use of phytoextracts as eco-friendly reducing agents for the synthesis of materials has been elaborated, considering the limitations of the chemical reducing agents. Cellulose is an attractive material owing to its huge abundance, easy availability, low-cost, biocompatibility, non-toxicity, while cellulose-based devices are promising due to their flexibility, portability, disposability and eco-friendliness. The chemical structure of cellulose with end hydroxyl groups has facilitated its surface modification with functional species. The hydrophilic nature and porosity of native cellulose play a key role to anchor the nanomaterials such as graphene by way of either physical sorption or covalent linkage. Finally, the potential of phytoextracts for the reduction of GO has been evaluated. The research objectives have been formulated bearing in mind the needs of the current times as well as the challenges associated with the extraction of phytoconstituents and employing them as green reducing agents for the in situ reduction of GO on cellulose fibre matrix.

References

- [1] Agarwal, C., and Csóka, L., "Functionalization of Wood/Plant-Based Natural Cellulose Fibers with Nanomaterials: A Review," *Tappi J.* Vol. 17, no. 2, 2018, 92-111.
- [2] Chauhan, I., Aggrawal, S., Chandravati, C., and Mohanty, P., "Metal Oxide Nanostructures Incorporated/Immobilized Paper Matrices and Their Applications: A Review," *RSC Adv.* Vol. 5, no. 101, 2015, 83036-83055.
- [3] Jariwala, D., Sangwan, V. K., Lauhon, L. J., Marks, T. J., and Hersam, M. C., "Carbon Nanomaterials for Electronics, Optoelectronics, Photovoltaics, and Sensing," *Chem. Soc. Rev.* Vol. 42, no. 7, 2013, 2824-2860.
- [4] Ahmed, S., Ahmad, M., Swami, B. L., and Ikram, S., "A Review on Plants Extract Mediated Synthesis of Silver Nanoparticles for Antimicrobial Applications: A Green Expertise," *J. Adv. Res.* Vol. 7, no. 1, 2016, 17-28.
- [5] Elia, P., Zach, R., Hazan, S., Kolusheva, S., Porat, Z. E., and Zeiri, Y., "Green Synthesis of Gold Nanoparticles Using Plant Extracts as Reducing Agents. ," *Int. J. Nanomedicine* Vol. 9, 2014, 4007-4021.
- [6] Kavitha, K. S., Baker, S., Rakshith, D., Kavitha, H. U., Yashwantha Rao, H. C., Harini, B. P., and Satish, S., "Plants as Green Source Towards Synthesis of Nanoparticles," *Int. Res. J. Biol. Sci.* Vol. 2, no. 6, 2013, 66-76.

- [7] Mittal, A. K., Chisti, Y., and Banerjee, U. C., "Synthesis of Metallic Nanoparticles Using Plant Extracts," *Biotechnol. Adv.* Vol. 31, no. 2, 2013, 346-356.
- [8] Agharkar, M., Kochrekar, S., Hidouri, S., and Azeez, M. A., "Trends in Green Reduction of Graphene Oxides, Issues and Challenges: A Review," *Mater. Res. Bull.* Vol. 59, 2014, 323-328.
- [9] Thakur, S., and Karak, N., "Green Reduction of Graphene Oxide by Aqueous Phytoextracts," *Carbon* Vol. 50, no. 14, 2012, 5331-5339.
- [10] Thakur, S., and Karak, N., "Alternative Methods and Nature-Based Reagents for the Reduction of Graphene Oxide: A Review," *Carbon* Vol. 94, 2015, 224-242.
- [11] Nadagouda, M. N., and Varma, R. S., "Green Synthesis of Silver and Palladium Nanoparticles at Room Temperature Using Coffee and Tea Extract," *Green Chem.* Vol. 10, no. 8, 2008, 859-862.
- [12] Sharma, D., Kanchi, S., and Bisetty, K., "Biogenic Synthesis of Nanoparticles: A Review," *Arab. J. Chem.* 2015, doi:10.1016/j.arabjc.2015.11.002
- [13] Tamuly, C., Hazarika, M., Borah, S. C., Das, M. R., and Boruah, M. P., "In Situ Biosynthesis of Ag, Au and Bimetallic Nanoparticles Using *Piper Pedicellatum* C.DC: Green Chemistry Approach," *Colloids Surf. B Biointerfaces* Vol. 102, 2013, 627-634.
- [14] Azmir, J., Zaidul, I. S. M., Rahman, M. M., Sharif, K. M., Mohamed, A., Sahena, F., Jahurul, M. H. A., Ghafoor, K., Norulaini, N. A. N., and Omar, A. K. M., "Techniques for Extraction of Bioactive Compounds from Plant Materials: A Review," *J. Food Eng.* Vol. 117, no. 4, 2013, 426-436.
- [15] Azwanida, N. N., "A Review on the Extraction Methods Use in Medicinal Plants, Principle, Strength and Limitation," *Med. Aromat. Plants* Vol. 4, no. 3, 2015, 3-8.
- [16] Gupta, A., Naraniwal, M., and Kothari, V., "Modern Extraction Methods for Preparation of Bioactive Plant Extracts," *Int. J. Appl. Nat. Sci.* Vol. 1, no. 1, 2012, 8-26.
- [17] Shirsath, S. R., Sable, S. S., Gaikwad, S. G., Sonawane, S. H., Saini, D. R., and Gogate, P. R., "Intensification of Extraction of Curcumin from *Curcuma Amada* Using Ultrasound Assisted Approach: Effect of Different Operating Parameters," *Ultrason. Sonochem.* Vol. 38, 2017, 437-445.

- [18] Shirsath, S. R., Sonawane, S. H., and Gogate, P. R., "Intensification of Extraction of Natural Products Using Ultrasonic Irradiations—a Review of Current Status," *Chem. Eng. Proc. Proc. Intens.* Vol. 53, 2012, 10-23.
- [19] Agarwal, C., Aggrawal, S., Dutt, D., and Mohanty, P., "Cerium Oxide Immobilized Paper Matrices for Bactericidal Application," *Mater. Sci. Eng. B* Vol. 232, 2018, 1-7.
- [20] Herrera, M. C., and de Castro, M. D., "Ultrasound-Assisted Extraction of Phenolic Compounds from Strawberries Prior to Liquid Chromatographic Separation and Photodiode Array Ultraviolet Detection," *J. Chromatogr. A* Vol. 1100, 2005, 1-7.
- [21] Spigno, G., Tramelli, L., and De Faveri, D. M., "Effects of Extraction Time, Temperature and Solvent on Concentration and Antioxidant Activity of Grape Marc Phenolics," *J. Food Eng.* Vol. 81, no. 1, 2007, 200-208.
- [22] Thaipong, K., Boonprakob, U., Crosby, K., Cisneros-Zevallos, L., and Hawkins Byrne, D., "Comparison of ABTS, DPPH, FRAP, and ORAC Assays for Estimating Antioxidant Activity from Guava Fruit Extracts," *J. Food Compos. Anal.* Vol. 19, no. 6-7, 2006, 669-675.
- [23] Bimakr, M., Rahman, R. A., Taip, F. S., Ganjloo, A., Salleh, L. M., Selamat, J., Hamid, A., and Zaidul, I. S. M., "Comparison of Different Extraction Methods for the Extraction of Major Bioactive Flavonoid Compounds from Spearmint (*Mentha Spicata* L.) Leaves," *Food Bioprod. Process.* Vol. 89, no. 1, 2011, 67-72.
- [24] Happyana, N., Agnolet, S., Muntendam, R., Van Dam, A., Schneider, B., and Kayser, O., "Analysis of Cannabinoids in Laser-Microdissected Trichomes of Medicinal *Cannabis Sativa* Using LCMS and Cryogenic NMR," *Phytochemistry* Vol. 87, 2013, 51-59.
- [25] Mechoulam, R., and Hanuš, L. r., "A Historical Overview of Chemical Research on Cannabinoids," *Chem. Phys. Lipids* Vol. 108, no. 1-2, 2000, 1-13.
- [26] Andre, C. M., Larondelle, Y., and Evers, D., "Dietary Antioxidants and Oxidative Stress from a Human and Plant Perspective: A Review," *Curr. Nutr. Food Sci.* Vol. 6, no. 1, 2010, 2-12.
- [27] ElSohly, M. A., *Marijuana and the Cannabinoids*, Humana Press Inc., New Jersey, 2007.

- [28] Baron, E. P., "Medicinal Properties of Cannabinoids, Terpenes, and Flavonoids in *Cannabis*, and Benefits in Migraine, Headache, and Pain: An Update on Current Evidence and *Cannabis* Science," *Headache* Vol. 58, no. 7, 2018, 1139-1186.
- [29] Andre, C. M., Hausman, J. F., and Guerriero, G., "*Cannabis Sativa*: The Plant of the Thousand and One Molecules," *Front. Plant Sci.* Vol. 7, 2016, 1-17.
- [30] Pertwee, R. G., "The Diverse CB₁ and CB₂ Receptor Pharmacology of Three Plant Cannabinoids: Δ^9 -Tetrahydrocannabinol, Cannabidiol and Δ^9 -Tetrahydrocannabivarin," *Br. J. Pharmacol.* Vol. 153, no. 2, 2008, 199-215.
- [31] MacCallum, C. A., and Russo, E. B., "Practical Considerations in Medical *Cannabis* Administration and Dosing," *Eur. J. Intern. Med.* Vol. 49, 2018, 12-19.
- [32] De Backer, B., Debrus, B., Lebrun, P., Theunis, L., Dubois, N., Decock, L., Verstraete, A., Hubert, P., and Charlier, C., "Innovative Development and Validation of an HPLC/DAD Method for the Qualitative and Quantitative Determination of Major Cannabinoids in *Cannabis* Plant Material," *J. Chromatogr. B* Vol. 877, no. 32, 2009, 4115-4124.
- [33] Baker, D., and Pryce, G., "The Endocannabinoid System and Multiple Sclerosis," *Curr. Pharm. Des.* Vol. 14, no. 23, 2008, 2326-2336.
- [34] Alexander, S. P., "Therapeutic Potential of *Cannabis*-Related Drugs," *Prog. Neuropsychopharmacol. Biol. Psychiatry* Vol. 64, 2016, 157-166.
- [35] Guzman, M., "Cannabinoids: Potential Anticancer Agents," *Nat. Rev. Cancer* Vol. 3, no. 10, 2003, 745-755.
- [36] Maurya, N., and Velmurugan, B. K., "Therapeutic Applications of Cannabinoids," *Chem. Biol. Interact.* Vol. 293, 2018, 77-88.
- [37] Ameer, K., Shahbaz, H. M., and Kwon, J. H., "Green Extraction Methods for Polyphenols from Plant Matrices and Their Byproducts: A Review," *Compr. Rev. Food Sci. Food Saf.* Vol. 16, no. 2, 2017, 295-315.
- [38] Muniz-Marquez, D. B., Martinez-Avila, G. C., Wong-Paz, J. E., Belmares-Cerda, R., Rodriguez-Herrera, R., and Aguilar, C. N., "Ultrasound-Assisted Extraction of Phenolic Compounds from *Laurus Nobilis* L. And Their Antioxidant Activity," *Ultrason. Sonochem.* Vol. 20, no. 5, 2013, 1149-1154.

- [39] Khan, M. K., Abert-Vian, M., Fabiano-Tixier, A.-S., Dangles, O., and Chemat, F., "Ultrasound-Assisted Extraction of Polyphenols (Flavanone Glycosides) from Orange (*Citrus Sinensis* L.) Peel," *Food Chem.* Vol. 119, no. 2, 2010, 851-858.
- [40] Vinatoru, M., Mason, T. J., and Calinescu, I., "Ultrasonically Assisted Extraction (UAE) and Microwave Assisted Extraction (MAE) of Functional Compounds from Plant Materials," *Trends Anal. Chem.* Vol. 97, 2017, 159-178.
- [41] Iskalieva, A., Yimmou, B. M., Gogate, P. R., Horvath, M., Horvath, P. G., and Csóka, L., "Cavitation Assisted Delignification of Wheat Straw: A Review," *Ultrason. Sonochem.* Vol. 19, no. 5, 2012, 984-993.
- [42] Mohammad Azmin, S. N. H., Abdul Manan, Z., Wan Alwi, S. R., Chua, L. S., Mustaffa, A. A., and Yunus, N. A., "Herbal Processing and Extraction Technologies," *Sep. Purif. Rev.* Vol. 45, no. 4, 2016, 305-320.
- [43] Mason, T. J., Chemat, F., and Vinatoru, M., "The Extraction of Natural Products Using Ultrasound or Microwaves," *Curr. Org. Chem.* Vol. 15, no. 2, 2011, 237-247.
- [44] Vinatoru, M., "An Overview of the Ultrasonically Assisted Extraction of Bioactive Principles from Herbs," *Ultrason. Sonochem.* Vol. 8, no. 3, 2001, 303-313.
- [45] Chemat, F., Rombaut, N., Sicaire, A. G., Meullemiestre, A., Fabiano-Tixier, A. S., and Abert-Vian, M., "Ultrasound Assisted Extraction of Food and Natural Products. Mechanisms, Techniques, Combinations, Protocols and Applications. A Review," *Ultrason. Sonochem.* Vol. 34, 2017, 540-560.
- [46] Aunkor, M. T. H., Mahbulul, I. M., Saidur, R., and Metselaar, H. S. C., "The Green Reduction of Graphene Oxide," *RSC Adv.* Vol. 6, no. 33, 2016, 27807-27828.
- [47] Hou, D., Liu, Q., Cheng, H., Li, K., Wang, D., and Zhang, H., "Chrysanthemum Extract Assisted Green Reduction of Graphene Oxide," *Mater. Chem. Phys.* Vol. 183, 2016, 76-82.
- [48] Credou, J., and Berthelot, T., "Cellulose: From Biocompatible to Bioactive Material," *J. Mater. Chem. B* Vol. 2, no. 30, 2014, 4767-4788.
- [49] Hokkanen, S., Bhatnagar, A., and Sillanpaa, M., "A Review on Modification Methods to Cellulose-Based Adsorbents to Improve Adsorption Capacity," *Water Res.* Vol. 91, 2016, 156-173.

- [50] Moon, R. J., Martini, A., Nairn, J., Simonsen, J., and Youngblood, J., "Cellulose Nanomaterials Review: Structure, Properties and Nanocomposites," *Chem. Soc. Rev.* Vol. 40, no. 7, 2011, 3941-3994.
- [51] Eyley, S., and Thielemans, W., "Surface Modification of Cellulose Nanocrystals," *Nanoscale* Vol. 6, no. 14, 2014, 7764-7779.
- [52] Postek, M. T., Vladár, A., Dagata, J., Farkas, N., Ming, B., Wagner, R., Raman, A., Moon, R. J., Sabo, R., and Wegner, T. H., "Development of the Metrology and Imaging of Cellulose Nanocrystals," *Meas. Sci. Technol.* Vol. 22, no. 2, 2010, 024005.
- [53] Pérez, J., Munoz-Dorado, J., De la Rubia, T., and Martinez, J., "Biodegradation and Biological Treatments of Cellulose, Hemicellulose and Lignin: An Overview," *Int. Microbiol.* Vol. 5, no. 2, 2002, 53-63.
- [54] Kamel, S., Ali, N., Jahangir, K., Shah, S., and El-Gendy, A., "Pharmaceutical Significance of Cellulose: A Review," *Express Polym. Lett.* Vol. 2, no. 11, 2008, 758-778.
- [55] Casey, J. P., *Pulp and Paper: Chemistry and Chemical Technology*, Wiley Interscience Publishers, New York, 1952.
- [56] Siqueira, G., Bras, J., and Dufresne, A., "Cellulosic Bionanocomposites: A Review of Preparation, Properties and Applications," *Polymers* Vol. 2, no. 4, 2010, 728-765.
- [57] Ge, S., Zhang, L., Zhang, Y., Lan, F., Yan, M., and Yu, J., "Nanomaterials-Modified Cellulose Paper as a Platform for Biosensing Applications," *Nanoscale* Vol. 9, no. 13, 2017, 4366-4382.
- [58] Pinho, E., and Soares, G., "Functionalization of Cotton Cellulose for Improved Wound Healing," *J. Mater. Chem. B* Vol. 6, no. 13, 2018, 1887-1898.
- [59] Hebeish, A., and Guthrie, T. J., *The Chemistry and Technology of Cellulosic Copolymers*, Springer Science & Business Media, 2012.
- [60] Cranston, E. D., and Gray, D. G., "Morphological and Optical Characterization of Polyelectrolyte Multilayers Incorporating Nanocrystalline Cellulose," *Biomacromolecules* Vol. 7, no. 9, 2006, 2522-2530.
- [61] Zhou, Q., Brumer, H., and Teeri, T. T., "Self-Organization of Cellulose Nanocrystals Adsorbed with Xyloglucan Oligosaccharide– Poly (Ethylene Glycol)– Polystyrene Triblock Copolymer," *Macromolecules* Vol. 42, no. 15, 2009, 5430-5432.

- [62] Liu, Y., and Chen, J. Y., "Enzyme Immobilization on Cellulose Matrixes," *J. Bioact. Compat. Polym.* Vol. 31, no. 6, 2016, 553-567.
- [63] Tiwari, S., Vinchurkar, M., Rao, V. R., and Garnier, G., "Zinc Oxide Nanorods Functionalized Paper for Protein Preconcentration in Biodiagnostics," *Sci. Rep.* Vol. 7, 2017, 43905-43914.
- [64] Ngo, Y. H., Li, D., Simon, G. P., and Garnier, G., "Paper Surfaces Functionalized by Nanoparticles," *Adv. Colloid Interface Sci.* Vol. 163, no. 1, 2011, 23-38.
- [65] Dai, L., Chang, D. W., Baek, J. B., and Lu, W., "Carbon Nanomaterials for Advanced Energy Conversion and Storage," *Small* Vol. 8, no. 8, 2012, 1130-1166.
- [66] Liu, W.-w., Yan, X.-b., Lang, J.-w., Peng, C., and Xue, Q.-j., "Flexible and Conductive Nanocomposite Electrode Based on Graphene Sheets and Cotton Cloth for Supercapacitor," *J. Mater. Chem.* Vol. 22, no. 33, 2012, 17245-17253.
- [67] Figueredo, F., Garcia, P. T., Corton, E., and Coltro, W. K., "Enhanced Analytical Performance of Paper Microfluidic Devices by Using Fe₃O₄ Nanoparticles, MWCNT, and Graphene Oxide," *ACS Appl. Mater. Interfaces* Vol. 8, no. 1, 2016, 11-15.
- [68] Han, J.-W., Kim, B., Li, J., and Meyyappan, M., "A Carbon Nanotube Based Ammonia Sensor on Cellulose Paper," *RSC Adv.* Vol. 4, no. 2, 2014, 549-553.
- [69] Mirica, K. A., Weis, J. G., Schnorr, J. M., Esser, B., and Swager, T. M., "Mechanical Drawing of Gas Sensors on Paper," *Angew. Chem. Int. Ed. Engl.* Vol. 51, no. 43, 2012, 10740-10745.
- [70] Liu, W., Yang, H., Ding, Y., Ge, S., Yu, J., Yan, M., and Song, X., "Paper-Based Colorimetric Immunosensor for Visual Detection of Carcinoembryonic Antigen Based on the High Peroxidase-Like Catalytic Performance of ZnFe₂O₄-Multiwalled Carbon Nanotubes," *Analyst* Vol. 139, no. 1, 2014, 251-258.
- [71] Wang, P., Ge, L., Yan, M., Song, X., Ge, S., and Yu, J., "Paper-Based Three-Dimensional Electrochemical Immunodevice Based on Multi-Walled Carbon Nanotubes Functionalized Paper for Sensitive Point-of-Care Testing," *Biosens. Bioelectron.* Vol. 32, no. 1, 2012, 238-243.
- [72] Ge, S., Ge, L., Yan, M., Song, X., Yu, J., and Huang, J., "A Disposable Paper-Based Electrochemical Sensor with an Addressable Electrode Array for Cancer Screening," *Chem. Commun.* Vol. 48, no. 75, 2012, 9397-9399.

- [73] Feng, Q. M., Pan, J. B., Zhang, H. R., Xu, J. J., and Chen, H. Y., "Disposable Paper-Based Bipolar Electrode for Sensitive Electrochemiluminescence Detection of a Cancer Biomarker," *Chem. Commun. (Camb.)* Vol. 50, no. 75, 2014, 10949-10951.
- [74] Ammu, S., Dua, V., Agnihotra, S. R., Surwade, S. P., Phulgirkar, A., Patel, S., and Manohar, S. K., "Flexible, All-Organic Chemiresistor for Detecting Chemically Aggressive Vapors," *J. Am. Chem. Soc.* Vol. 134, no. 10, 2012, 4553-4556.
- [75] Wang, L., Chen, W., Xu, D., Shim, B. S., Zhu, Y., Sun, F., Liu, L., Peng, C., Jin, Z., Xu, C., and Kotov, N. A., "Simple, Rapid, Sensitive, and Versatile SWNT–Paper Sensor for Environmental Toxin Detection Competitive with ELISA," *Nano Lett.* Vol. 9, no. 12, 2009, 4147-4152.
- [76] Qi, H., Liu, J., Deng, Y., Gao, S., and Mäder, E., "Cellulose Fibres with Carbon Nanotube Networks for Water Sensing," *J. Mater. Chem. A* Vol. 2, no. 15, 2014, 5541-5547.
- [77] Qi, H., Mäder, E., and Liu, J., "Unique Water Sensors Based on Carbon Nanotube–Cellulose Composites," *Sens. Actuators B Chem.* Vol. 185, 2013, 225-230.
- [78] Dichiara, A. B., Song, A., Goodman, S. M., He, D., and Bai, J., "Smart Papers Comprising Carbon Nanotubes and Cellulose Microfibers for Multifunctional Sensing Applications," *J. Mater. Chem. A* Vol. 5, no. 38, 2017, 20161-20169.
- [79] Guinovart, T., Parrilla, M., Crespo, G. A., Rius, F. X., and Andrade, F. J., "Potentiometric Sensors Using Cotton Yarns, Carbon Nanotubes and Polymeric Membranes," *Analyst* Vol. 138, no. 18, 2013, 5208-5215.
- [80] Anderson, R. E., Guan, J., Ricard, M., Dubey, G., Su, J., Lopinski, G., Dorris, G., Bourne, O., and Simard, B., "Multifunctional Single-Walled Carbon Nanotube–Cellulose Composite Paper," *J. Mater. Chem.* Vol. 20, no. 12, 2010, 2400-2407.
- [81] Han, J.-W., Kim, B., Li, J., and Meyyappan, M., "Carbon Nanotube Based Humidity Sensor on Cellulose Paper," *J. Phys. Chem. C* Vol. 116, no. 41, 2012, 22094-22097.
- [82] Hu, L., Wu, H., and Cui, Y., "Printed Energy Storage Devices by Integration of Electrodes and Separators into Single Sheets of Paper," *Appl. Phys. Lett.* Vol. 96, no. 18, 2010, 183502(1-3).

- [83] Hu, L., Choi, J. W., Yang, Y., Jeong, S., La Mantia, F., Cui, L. F., and Cui, Y., "Highly Conductive Paper for Energy-Storage Devices," *Proc. Natl. Acad. Sci. USA* Vol. 106, no. 51, 2009, 21490-21494.
- [84] Kang, Y. J., Chung, H., Han, C.-H., and Kim, W., "All-Solid-State Flexible Supercapacitors Based on Papers Coated with Carbon Nanotubes and Ionic-Liquid-Based Gel Electrolytes," *Nanotechnology* Vol. 23, no. 6, 2012, 289501.
- [85] Kang, Y. J., Kim, B., Chung, H., and Kim, W., "Fabrication and Characterization of Flexible and High Capacitance Supercapacitors Based on MnO₂/CNT/Papers," *Synth. Met.* Vol. 160, no. 23-24, 2010, 2510-2514.
- [86] Ge, L., Wang, P., Ge, S., Li, N., Yu, J., Yan, M., and Huang, J., "Photoelectrochemical Lab-on-Paper Device Based on an Integrated Paper Supercapacitor and Internal Light Source," *Anal. Chem.* Vol. 85, no. 8, 2013, 3961-3970.
- [87] Ruecha, N., Rangkupan, R., Rodthongkum, N., and Chailapakul, O., "Novel Paper-Based Cholesterol Biosensor Using Graphene/Polyvinylpyrrolidone/Polyaniline Nanocomposite," *Biosens. Bioelectron.* Vol. 52, 2014, 13-19.
- [88] Li, L., Li, W., Yang, H., Ma, C., Yu, J., Yan, M., and Song, X., "Sensitive Origami Dual-Analyte Electrochemical Immunodevice Based on Polyaniline/Au-Paper Electrode and Multi-Labeled 3D Graphene Sheets," *Electrochim. Acta* Vol. 120, 2014, 102-109.
- [89] Tao, L. Q., Zhang, K. N., Tian, H., Liu, Y., Wang, D. Y., Chen, Y. Q., Yang, Y., and Ren, T. L., "Graphene-Paper Pressure Sensor for Detecting Human Motions," *ACS Nano* Vol. 11, no. 9, 2017, 8790-8795.
- [90] Yang, G., Lee, C., Kim, J., Ren, F., and Pearton, S. J., "Flexible Graphene-Based Chemical Sensors on Paper Substrates," *Phys. Chem. Chem. Phys.* Vol. 15, no. 6, 2013, 1798-1801.
- [91] Kumar, S., Kumar, S., Srivastava, S., Yadav, B. K., Lee, S. H., Sharma, J. G., Doval, D. C., and Malhotra, B. D., "Reduced Graphene Oxide Modified Smart Conducting Paper for Cancer Biosensor," *Biosens. Bioelectron.* Vol. 73, 2015, 114-122.
- [92] Ling, Y., Li, X., Zhou, S., Wang, X., and Sun, R., "Multifunctional Cellulosic Paper Based on Quaternized Chitosan and Gold Nanoparticle-Reduced Graphene Oxide Via Electrostatic Self-Assembly," *J. Mater. Chem. A* Vol. 3, no. 14, 2015, 7422-7428.

- [93] Zhang, L., Li, L., Ma, C., Ge, S., Yan, M., and Bian, C., "Detection of α -Fetoprotein with an Ultrasensitive Electrochemiluminescence Paper Device Based on Green-Luminescent Nitrogen-Doped Graphene Quantum Dots," *Sens. Actuators B Chem.* Vol. 221, 2015, 799-806.
- [94] Carrasco, P. M., García, I., Yate, L., Tena Zaera, R., Cabañero, G., Grande, H. J., and Ruiz, V., "Graphene Quantum Dot Membranes as Fluorescent Sensing Platforms for Cr (VI) Detection," *Carbon* Vol. 109, 2016, 658-665.
- [95] Kim, Y., Jang, G., and Lee, T. S., "New Fluorescent Metal-Ion Detection Using a Paper-Based Sensor Strip Containing Tethered Rhodamine Carbon Nanodots," *ACS Appl. Mater. Interfaces* Vol. 7, no. 28, 2015, 15649-15657.
- [96] Wang, Y., Wang, S., Ge, S., Wang, S., Yan, M., Zang, D., and Yu, J., "Facile and Sensitive Paper-Based Chemiluminescence DNA Biosensor Using Carbon Dots Dotted Nanoporous Gold Signal Amplification Label," *Anal. Methods* Vol. 5, no. 5, 2013, 1328-1336.
- [97] Luong, N. D., Pahimanolis, N., Hippi, U., Korhonen, J. T., Ruokolainen, J., Johansson, L.-S., Nam, J.-D., and Seppälä, J., "Graphene/Cellulose Nanocomposite Paper with High Electrical and Mechanical Performances," *J. Mater. Chem.* Vol. 21, no. 36, 2011, 13991-13998.
- [98] Yang, W., Zhao, Z., Wu, K., Huang, R., Liu, T., Jiang, H., Chen, F., and Fu, Q., "Ultrathin Flexible Reduced Graphene Oxide/Cellulose Nanofiber Composite Films with Strongly Anisotropic Thermal Conductivity and Efficient Electromagnetic Interference Shielding," *J. Mater. Chem. C* Vol. 5, no. 15, 2017, 3748-3756.
- [99] Shubha, P., Namratha, K., Aparna, H. S., Ashok, N. R., Mustak, M. S., Chatterjee, J., and Byrappa, K., "Facile Green Reduction of Graphene Oxide Using *Ocimum Sanctum* Hydroalcoholic Extract and Evaluation of Its Cellular Toxicity," *Mater. Chem. Phys.* Vol. 198, 2017, 66-72.
- [100] Kumar, S., Kaushik, S., Pratap, R., and Raghavan, S., "Graphene on Paper: A Simple, Low-Cost Chemical Sensing Platform," *ACS Appl. Mater. Interfaces* Vol. 7, no. 4, 2015, 2189-2194.

- [101] Yang, H., Zhang, Y., Li, L., Sun, G., Zhang, L., Ge, S., and Yu, J., "Real-Time and In Situ Enzyme Inhibition Assay for the Flux of Hydrogen Sulfide Based on 3D Interwoven AuPd-Reduced Graphene Oxide Network," *Biosens. Bioelectron.* Vol. 87, 2017, 53-58.
- [102] Sun, G., Zhang, L., Zhang, Y., Yang, H., Ma, C., Ge, S., Yan, M., Yu, J., and Song, X., "Multiplexed Enzyme-Free Electrochemical Immunosensor Based on ZnO Nanorods Modified Reduced Graphene Oxide-Paper Electrode and Silver Deposition-Induced Signal Amplification Strategy," *Biosens. Bioelectron.* Vol. 71, 2015, 30-36.
- [103] Ge, S., Wu, K., Zhang, Y., Yan, M., and Yu, J., "Paper-Based Biosensor Relying on Flower-Like Reduced Graphene Guided Enzymatically Deposition of Polyaniline for Pb(2⁺) Detection," *Biosens. Bioelectron.* Vol. 80, 2016, 215-221.
- [104] Sreeprasad, T. S., Rodriguez, A. A., Colston, J., Graham, A., Shishkin, E., Pallem, V., and Berry, V., "Electron-Tunneling Modulation in Percolating Network of Graphene Quantum Dots: Fabrication, Phenomenological Understanding, and Humidity/Pressure Sensing Applications," *Nano Lett.* Vol. 13, no. 4, 2013, 1757-1763.
- [105] Li, M., Wang, Y., Zhang, Y., Yu, J., Ge, S., and Yan, M., "Graphene Functionalized Porous Au-Paper Based Electrochemiluminescence Device for Detection of DNA Using Luminescent Silver Nanoparticles Coated Calcium Carbonate/Carboxymethyl Chitosan Hybrid Microspheres as Labels," *Biosens. Bioelectron.* Vol. 59, 2014, 307-313.
- [106] Zhang, Y., Li, L., Yang, H., Ding, Y.-n., Su, M., Zhu, J., Yan, M., Yu, J., and Song, X., "Gold-Silver Nanocomposite-Functionalized Graphene Sensing Platform for an Electrochemiluminescent Immunoassay of a Tumor Marker," *RSC Adv.* Vol. 3, no. 34, 2013, 14701-14709.
- [107] Li, L., Zhang, L., Yu, J., Ge, S., and Song, X., "All-Graphene Composite Materials for Signal Amplification toward Ultrasensitive Electrochemical Immunosensing of Tumor Marker," *Biosens. Bioelectron.* Vol. 71, 2015, 108-114.
- [108] Weng, Z., Su, Y., Wang, D.-W., Li, F., Du, J., and Cheng, H.-M., "Graphene-Cellulose Paper Flexible Supercapacitors," *Adv. Energy Mater.* Vol. 1, no. 5, 2011, 917-922.
- [109] Kang, Y. R., Li, Y. L., Hou, F., Wen, Y. Y., and Su, D., "Fabrication of Electric Papers of Graphene Nanosheet Shelled Cellulose Fibres by Dispersion and Infiltration as Flexible Electrodes for Energy Storage," *Nanoscale* Vol. 4, no. 10, 2012, 3248-3253.

- [110] Wang, D. W., Li, F., Zhao, J., Ren, W., Chen, Z. G., Tan, J., Wu, Z. S., Gentle, I., Lu, G. Q., and Cheng, H. M., "Fabrication of Graphene/Polyaniline Composite Paper Via In Situ Anodic Electropolymerization for High-Performance Flexible Electrode," *ACS Nano* Vol. 3, no. 7, 2009, 1745-1752.
- [111] Dua, V., Surwade, S. P., Ammu, S., Agnihotra, S. R., Jain, S., Roberts, K. E., Park, S., Ruoff, R. S., and Manohar, S. K., "All-Organic Vapor Sensor Using Inkjet-Printed Reduced Graphene Oxide," *Angew. Chem. Int. Ed.* Vol. 49, no. 12, 2010, 2154-2157.
- [112] Fang, M., Long, J., Zhao, W., Wang, L., and Chen, G., "pH-Responsive Chitosan-Mediated Graphene Dispersions," *Langmuir* Vol. 26, no. 22, 2010, 16771-16774.
- [113] Gao, J., Liu, F., Liu, Y., Ma, N., Wang, Z., and Zhang, X., "Environment-Friendly Method to Produce Graphene That Employs Vitamin C and Amino Acid," *Chem. Mater.* Vol. 22, no. 7, 2010, 2213-2218.
- [114] Rice-Evans, C. A., Miller, N. J., and Paganga, G., "Structure-Antioxidant Activity Relationships of Flavonoids and Phenolic Acids," *Free Radic. Biol. Med.* Vol. 20, no. 7, 1996, 933-956.
- [115] De Silva, K. K. H., Huang, H. H., Joshi, R. K., and Yoshimura, M., "Chemical Reduction of Graphene Oxide Using Green Reductants," *Carbon* Vol. 119, 2017, 190-199.
- [116] Bhattacharya, G., Sas, S., Wadhwa, S., Mathur, A., McLaughlin, J., and Roy, S. S., "Aloe Vera Assisted Facile Green Synthesis of Reduced Graphene Oxide for Electrochemical and Dye Removal Applications," *RSC Adv.* Vol. 7, no. 43, 2017, 26680-26688.
- [117] Wang, Y., Shi, Z., and Yin, J., "Facile Synthesis of Soluble Graphene Via a Green Reduction of Graphene Oxide in Tea Solution and Its Biocomposites," *ACS Appl. Mater. Interfaces* Vol. 3, no. 4, 2011, 1127-1133.
- [118] Khan, M., Al-Marri, A. H., Khan, M., Shaik, M. R., Mohri, N., Adil, S. F., Kuniyil, M., Alkathlan, H. Z., Al-Warthan, A., Tremel, W., Tahir, M. N., and Siddiqui, M. R., "Green Approach for the Effective Reduction of Graphene Oxide Using *Salvadora Persica* L. Root (Miswak) Extract," *Nanoscale Res. Lett.* Vol. 10, no. 1, 2015, 281-289.
- [119] Khan, M., Al-Marri, A. H., Khan, M., Mohri, N., Adil, S. F., Al-Warthan, A., Siddiqui, M. R. H., Alkathlan, H. Z., Berger, R., Tremel, W., and Tahir, M. N., "*Pulicaria*

Glutinosa Plant Extract: A Green and Eco-Friendly Reducing Agent for the Preparation of Highly Reduced Graphene Oxide," *RSC Adv.* Vol. 4, no. 46, 2014, 24119-24125.

CHAPTER II-
MATERIALS & METHODS

2.1. Chapter synopsis

This chapter presents the experimental details on the extraction of bioactive compounds such as polyphenols, flavonoids and cannabinoids using the principle of ultrasound from the inflorescences of fibre-type *Cannabis*. The evaluation of the extracts for total phenolics, flavonoids, ferric reducing ability of plasma assay and the overall yield has been described. The experimental design and statistical modelling of the evaluated data (responses) has been detailed based on the response surface methodology. The regression and analysis of variance was performed in order to determine the significance of the model and the ultrasonic extraction parameters of time, power and solvent (factors). Finally, the extraction parameters were optimized and the predicted values of the responses were compared to the experimentally obtained values to validate the model.

The identification of the cannabinoids and other bioactive compounds in the *Cannabis* extract using HPLC-DAD-MS/MS and GC-MS techniques, respectively has also been discussed. Further, procedures for the synthesis of GO using modified Hummer's method and its subsequent reduction with simultaneous functionalization on the surface of cellulose fibres by aqueous *Cannabis* extract have been elucidated. Different analytical techniques such as SEM, FTIR, XRD and XPS were used to characterize the reduced-GO (RGO)/cellulose composites and to relate the morphology-structure relationship to the electrical properties of the composites have been described.

2.2. Materials

2.2.1. Chemicals

Methanol (Scharlab Magyarorszag Kft.), Folin & Ciocalteu's phenol reagent (2N, Sigma Aldrich), gallic acid (Sigma Aldrich), sodium acetate buffer solution (3M, Sigma Aldrich), ferric chloride hexahydrate (Reanal, Hungary), sodium carbonate (Reanal, Hungary), L-ascorbic acid (Reanal, Hungary), 2-aminoethyl diphenyl borinate (Alfa Aesar), 2,4,6-tri(2-pyridyl)-1,3,5-triazine (TCI), quercetin dihydrate (Fluka AG, Chem. Fabrik.), concentrated sulphuric acid (95-98%, Merck), potassium permanganate (99.5%, Merck), hydrogen peroxide (30%, Merck) and fuming hydrochloric acid (37%, Merck), expanded graphite sheets (Torok & Tarsai Ltd., Hajduszoboszlo, Hungary), linter sheets (Buckeye Technologies Inc.).

All the reagents were of analytical grade and used as such without further purification. All the aqueous solutions were prepared using deionized water.

2.2.2. *Plant material*

The inflorescences of fibre-type hemp (*Cannabis sativa* L., Hungary), comprising mainly of the top portions of the plant including the flowers, leaves, stems and seed husks, were harvested in the previous summer (**Figure 2.1**). They were dried well and stored in a dark room at ambient temperature until further analysis.



Figure 2.1 Inflorescence of fibre-type *Cannabis*

2.2.3. *Instrumentation*

2.2.3.1. *Probe sonicator*

A Tesla 150 WS ultrasonicator fitted with 18 mm diameter titanium probe (horn) was used to extract bioactive components from the plant material (**Figure 2.2a**). The frequency of operation was 20 kHz with a maximum power output of 150 W.

2.2.3.2. *Spectrophotometer*

For all the absorbance measurements, WPA lightwave S2000 UV/vis spectrophotometer consisting of a diode array detector with tungsten and deuterium lamps was used, having range of wavelength between 200 and 800 nm (**Figure 2.2b**).

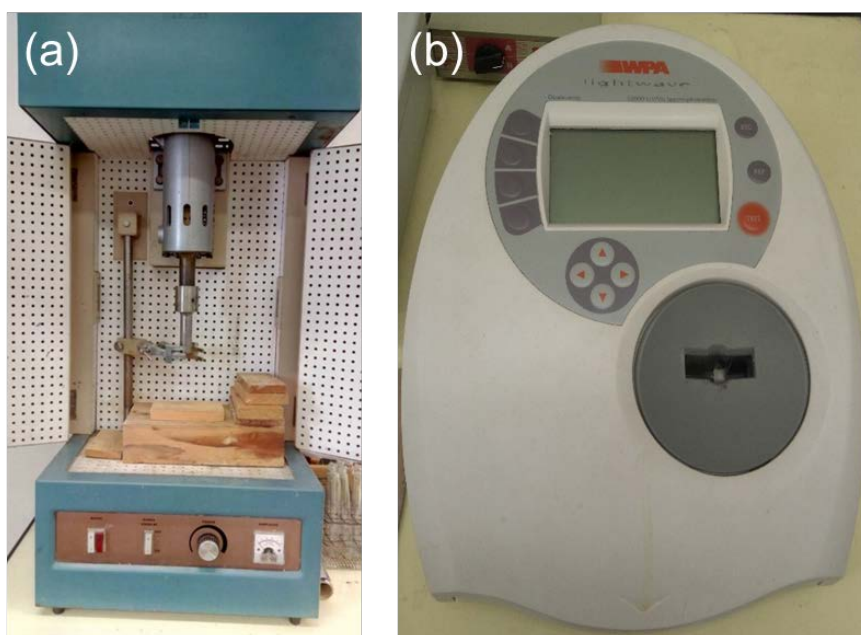


Figure 2.2 Photographs of (a) Probe-type ultrasonicator used for the extraction of phytoconstituents from *Cannabis*, (b) UV/vis spectrophotometer for the measurement of absorbance

2.3. Methods

2.3.1. Ultrasonic extraction

Plant samples weighed to 2.5 g were mixed with 50 ml of methanol/water solvent in ratios of 20, 50 and 80% (V/V) in slender glass beakers, covered with a parafilm in order to avoid solvent evaporation. The probe was inserted in the beaker such that the distance from the tip to the base of the beaker was approximately half the calculated ultrasonic wavelength to achieve maximum cavitation and efficiency of sonication. Extractions were carried out at low, medium and full power inputs of 90, 120 and 150 W, respectively. The time for sonication was varied at 5, 10 and 15 min. The sonicated samples were allowed to cool down naturally and thereafter, filtered through filter paper in glass bottles. The extracts were stored away from light at ambient temperature (around 5 °C) until further analysis.

The energy efficiency of the ultrasonic horn was calculated by calorimetrically determining the actual energy dissipated according to an already documented method [1]. The input power levels adjusted to amplitudes of 60, 80 and 100% consumed 90, 120 and 150 W, respectively. The actual power dissipated from the probe tip into the bulk of the medium was calculated by measuring the rise in temperature of a given quantity of water in a given time. The actual power dissipation values corresponding to power inputs of 90,

120 and 150 W were calculated as 31.4, 41.8 and 52.3 W, respectively. The average energy efficiency of the horn was found to be around 34.9% from the calorimetric studies.

2.3.2. *Control extraction without ultrasound treatment*

A control experiment was run without ultrasound treatment in order to make a comparative study. The plant sample (2.5 g) was mixed with 50% methanol (50 ml) in a beaker and stirred continuously on a magnetic stirrer at 300 rpm at 60 °C for 30 min. After cooling it, the filtered extract was also stored away from light in ambient conditions until further analysis.

2.3.3. *Determination of total phenolic content (TPC)*

The TPC of extracts was determined by the Folin & Ciocalteu (FC) assay. The addition of FC reagent to phenolic compounds leads to the formation of blue-coloured phosphomolybdic/phosphotungstic complex due to electron transfer in alkaline medium [2]. In a typical procedure, 0.5 ml each of extract followed by FC reagent were mixed vigorously in a 10 ml volumetric flask. After 2 min, 2.5 ml of 7.5% Na₂CO₃ solution was added and the remaining volume was made up with distilled water. A blank solution was prepared with the same procedure without the extract. All the samples were kept in dark and ambient temperature for 2 h. Thereafter, the absorbance was measured using the UV/vis spectrophotometer at 765 nm against the blank sample as the reference. Standard solutions of gallic acid in the concentration range of 0.1 to 0.5 mg/ml were used for plotting the calibration curve. All the measurements were made in triplicate and mean values were expressed in mg gallic acid equivalent per g dry weight of plant (mg GAE/g DW).

2.3.4. *Determination of total flavonoids (TF)*

The flavonoids were determined by slightly modifying a method previously reported [3]. In a 10 ml volumetric flask, 1 ml of extract was mixed with 0.1 ml of 1% (V/V) methanolic solution of 2-aminoethyl diphenyl borinate and the remaining volume was made up with distilled water. The absorbance was measured spectrophotometrically at 404 nm after 'zeroing' the blank solution. Quercetin solutions in the range of 0.05 to 0.3 mg/ml were used as standards for the calibration curve. The mean results were reported in mg quercetin equivalent per g dry weight of plant (mg QE/g DW).

2.3.5. *Determination of ferric reducing ability of plasma (FRAP) antioxidant capacity*

The FRAP assay measures the antioxidant power by reduction of the ferric ions through electron transfer reactions. The FRAP reagents were freshly prepared each time

before analysis. As given in a similar procedure by Benzie and Strain [4], 100 ml of sodium acetate buffer (0.3 M, 3.6 pH) was mixed with 10 ml of TPTZ solution (10 mM) by dissolving it in 40 mM HCl in a hot water bath. This was followed by the addition of 10 ml of ferric chloride solution (20 mM) and 12 ml of distilled water to give a straw-coloured reagent. This ferric-TPTZ complex changes to its ferrous form in the presence of antioxidants that act as electron donors, which can be confirmed by the appearance of a dark violet colour. 0.1 ml of extract was mixed with 5 ml of FRAP reagent and incubated at 37 °C in a water bath in a dark room for 30 min. The blank was also prepared in a similar fashion without the extract. The absorbance was determined at 593 nm by the spectrophotometer against the blank as the reference. Ascorbic acid standards in the range of 0.1 to 1.6 mM were used for the calibration curve. The mean values were expressed in mmol ascorbic acid equivalent per g dry weight of plant (mM AAE/g DW).

2.3.6. Determination of extraction yield

The yield of the extracts was determined by drying a known weight of extract in a glass Petri dish, in an oven at 50 °C for 4 h. After ensuring complete evaporation of the solvent, the extracts were re-weighed and the yield was calculated as a percentage of the dry weight of plant.

2.3.7. Experimental design of & statistical analysis

A response surface methodology (RSM) approach was used to investigate the effect of different input variables on the studied output parameters and to optimize the extraction process. The experiment was conducted based on face-centred central composite design (CCD), which is one of the most commonly used designs for process optimization. The CCD is known for obtaining a good amount of information from least number of experiments. Three independent variables or factors- time, input power and solvent, were the predictors (denoted by A, B and C) for the design, which uses coded levels for modelling the experimental data instead of the actual values. As shown in **Table 2.1**, each predictor had three levels of -1, 0 and 1 corresponding to the lower, central and upper values, respectively. In the present study, the time (A) was varied at 5, 10 and 15 min; the input power (B) varied at 90, 120 and 150 W; while the solvent (methanol) composition (C) varied at 20, 50 and 80%. In a face-centred design, the distance from the centre to a star point, represented by ' α ' is ± 1 since the star points lie at the centre of each of the faces in the design space. For a 3-factor CCD, 20 experimental runs with various combinations of the predictors and comprising of 8 factorial points (coded as ± 1), 6 star or axial points

(coded as $\pm\alpha$) along with 6 replicates of the centre point (coded as 0) were performed randomly. The dependent parameters or responses (denoted by R) studied were total phenolic content (TPC, mg GAE/g DW) (R1), total flavonoids (TF, mg QE/g DW) (R2), ferric reducing ability of plasma (FRAP, mM AAE/g DW) (R3) and yield (%) (R4).

Design Expert Software (Version 10.0.5.0, Stat-Ease Incorporation, Minneapolis, USA, 2017) was used for carrying out the statistical and regression analysis of the design and fit an appropriate mathematical model to the experimental data. The ANOVA for each of the responses was performed with a 95% confidence interval to determine significant differences within means based on the probability or ‘p-value’ ($p < 0.05$) and Fisher or ‘F-value’. Finally, design optimization of the predictors was done for optimal values of the responses based on desirability function after testing the model for its significance and reliability.

Table 2.1 Design space factors and levels

Factor	Unit	Factor levels		
		-1	0	1
Time, A	min	5	10	15
Power, B	W	90	120	150
Solvent, C	%	20	50	80

2.3.8. Synthesis of GO

GO was synthesized by modified Hummer’s method reported earlier [5, 6]. In a typical procedure, expanded graphite powder (5 g) was dispersed in concentrated sulfuric acid (100 ml) in a 600 ml beaker and cooled on an ice-bath to 5 °C over a magnetic stirrer. Small portions of KMnO_4 (15 g) were intermittently added with constant stirring over a period of 2 h in order to ensure the consumption of the oxidizing agent indicated by the fading of the green color. The beaker was then transferred from the ice-bath into a water bath at 30 °C resulting in an instantaneous volumetric expansion and the stirring was continued for another 30 min for further oxidation. After adding deionized water (250 ml) very slowly, the yellowish-brown reaction mixture was heated to 80°C and held for 30 min to achieve complete hydrolysis and exfoliation of graphite oxide. In the end, the residual oxidants were reduced by gradually pouring in 30% H_2O_2 (25 ml) with vigorous stirring. Finally, the suspension was filtered and subsequently washed with deionized water and 1

M HCl (500 ml) several times. The synthesized GO was oven-dried and stored for further use.

2.3.9. Green reduction of GO and preparation of composites

GO was reduced to RGO using the aqueous extract from *Cannabis*. The extract was prepared by dispersing the dried plant (3 g) in deionized water (60 ml) and sonicating it for 15 min at full power using a horn-type sonicator (Tesla 150 WS, 150 W output and 20 kHz frequency) followed by filtration. Before mixing the extract, the GO powder was reconstituted in deionized water and the suspension was sonicated for 15 min at full power in order to fully exfoliate it. To synthesize RGO powder, a known quantity of the extract was added to the sonicated GO suspension and the reaction was carried out at 80 °C for 3 h. The black powder thus obtained was filtered, washed with deionized water and dried in the oven. The dried powder was stored for further characterization.

RGO/cellulose composites were fabricated by in situ reduction of GO on the cellulose fibres in presence of the extract (**Figure 2.3**). The cellulose pulp was prepared by disintegrating the linter sheets in a Lorentzen and Wettre pulp disintegrator at 1% consistency for 10 min and then taking a volume corresponding to 5 g of air-dried fibres. GO suspensions were made by dispersing the GO powder (0.05 g) in deionized water (70 ml) followed by sonication for 15 min. The sonicated suspensions were treated with the extract (10 ml) in the optimized ratio of about 0.2 ml extract/mg GO, followed by heating to 80 °C for 1 h with occasional stirring. Next, the partially reduced GO suspensions were again sonicated for another 15 min and subsequently poured into the cellulose pulps (500 ml) already preheated to 75-80 °C in different volumes corresponding to weight fractions of GO from 0.1 to 10 m/m %, as shown in **Table 2.2**. After 2 h, the pulp mixtures were removed and allowed to cool naturally.

Table 2.2 Different weight fractions of RGO functionalized on cellulose fibres

Sr. No.	Specimen name	GO m/m %	Linter weight, g
1.	Blank	0	5
2.	RGO-0.1	0.1	5
3.	RGO-1	1	5
4.	RGO-2	2	5
5.	RGO-5	5	5
6.	RGO-10	10	5

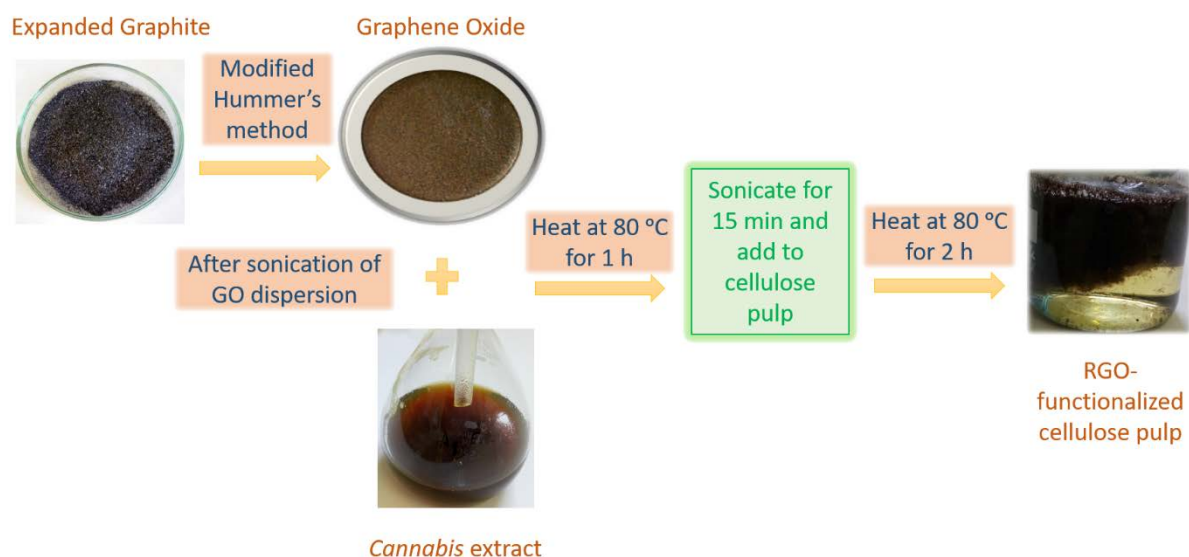


Figure 2.3 Schematic illustration for the fabrication of RGO/cellulose composites

2.3.10. Handsheet-making

Handsheets were made from the treated pulps in a semi-automated sheet machine (HAAGE D-4330 System Laboratory sheet former) with vacuum press-drying (9.0×10^4 Pa, 90 °C) using the DIN EN ISO 5269-2 standard test method (**Figure 2.4**) [7]. The handsheets were named according to their RGO contents- specimens with 0.1, 1, 2, 5 and 10 m/m % of RGO were labeled as RGO-0.1, RGO-1, RGO-2, RGO-5 and RGO-10, respectively (**Figure 2.5**). A “blank” handsheet consisting of only cellulose fibres without any RGO was also made.



Figure 2.4 Photograph of laboratory sheet former with vacuum press-drying

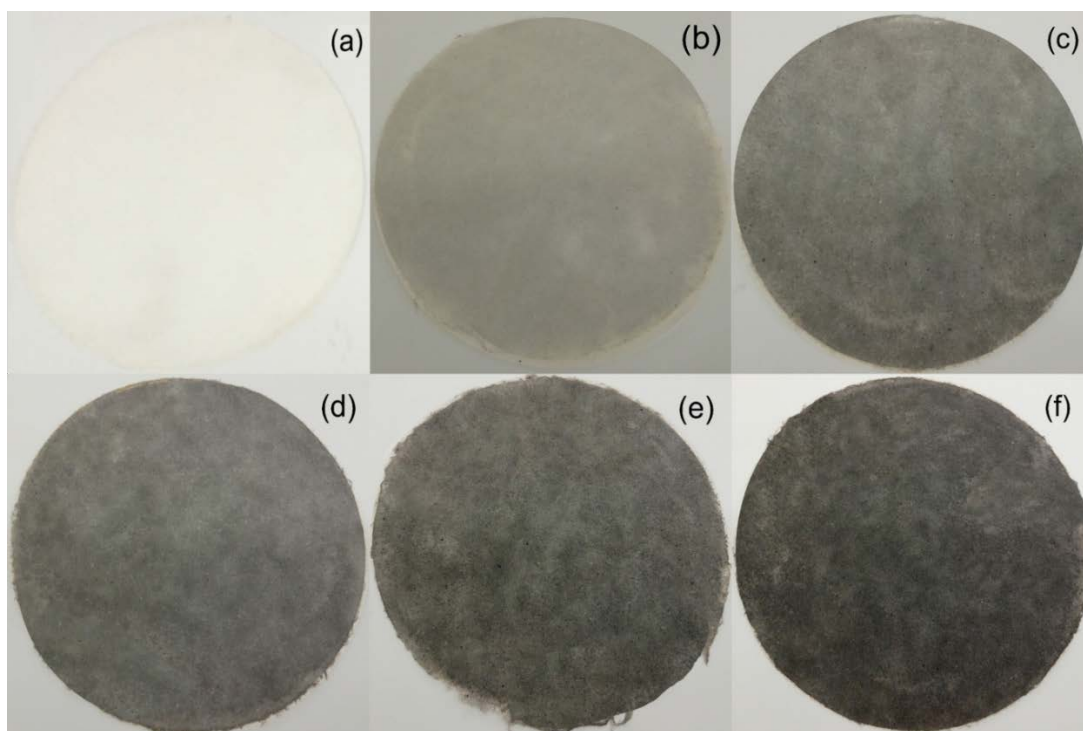


Figure 2.5 RGO/cellulose composites with various loadings of RGO- (a) 0 m/m %, (b) 0.1 m/m %, (c) 1 m/m %, (d) 2 m/m %, (e) 5 m/m % and (f) 10 m/m %

2.4. Characterization

2.4.1. High pressure liquid chromatography/mass spectrometry (HPLC-DAD-MS/MS)

HPLC coupled with MS is a very powerful analytical tool for the identification, characterization and quantification of compounds [8, 9]. In this work, this technique was used for the identification of cannabinoids in the *Cannabis* extract as well as to analyse the efficacy of ultrasonication against the conventional extraction method.

Selected extracts were analysed using a Shimadzu LC-20 type liquid chromatograph coupled with a Shimadzu SPD-M20A type diode array detector (DAD) (Shimadzu Corporation, Kyoto, Japan) in the 210 to 250 nm range and an AB Sciex 3200 QTrap triple quadrupole/linear ion trap LC/MS/MS detector (AB Sciex, Framingham, USA) (**Figure 2.6**). A Phenomenex Kinetex C18, 150 mm × 4.6 mm, 2.6 μm core-shell column was used for the separation with a Phenomenex Security Guard ULTRA LC type guard column (Phenomenex Inc., Torrance, USA) at 40 °C. The injection volume was 15 μL. The mobile phase consisted of A (H₂O + 0.1% HCOOH) and B (CH₃CN + 0.1% HCOOH). A gradient elution was run with 1.2 mL/min flow-rate using the following time gradient: 20% B (0–1 min), 30% B (9 min), 44% B (13.5 min), 100% B (16.5–18 min), 20% B (18.5–20 min).

The mass spectrometric identification of cannabinoid compounds was carried out by recording on-line MS/MS spectra of the separated compounds in negative electrospray ionization mode using the IDA scanning function of the mass spectrometer which utilizes time programming and the linear ion trap function of the MS detector to perform automatic on-line MS/MS experiments during the chromatographic separation: survey (Q1) scans were performed between 150 and 1300 m/z. After selection of a particular m/z ion and Q2 fragmentation, the dependent (Q3) product ion scans were performed between 80 and 1300 m/z. Because of the relatively high flow rate of the mobile phase, flow-splitting was applied using a split valve, which allowed 0.6 mL/min flow to enter the ion source. In the ion source ion spray voltage was set at -4500 V, the curtain gas (N_2) pressure was set at 2.7×10^5 Pa, spray gas (N_2) pressure at 2.0×10^5 Pa, drying gas (N_2) pressure at 2.0×10^5 Pa, and ion source temperature at 500 °C. Identification of the major cannabinoids was done by their MS/MS spectra and characteristic fragments using literature data [10-12]. After identification, the relative quantitative assessment of cannabinoid compounds was carried out by comparing their respective peak heights in the DAD chromatogram. Chromatographic data were acquired and evaluated using the Analyst 1.6.1 software.



Figure 2.6 Photograph of HPLC-DAD-MS/MS

2.4.2. Gas chromatography/mass spectrometry (GC-MS)

GC-MS is a widely used tool for metabolite profiling, it can facilitate the identification and robust quantification of a few hundred metabolites in a single plant extract. It has a relatively broad coverage of compound classes from gases, volatile and semi-volatile compounds to non-volatile low-molecular compounds such as amino acids, sugars, alcohols, phosphorylated intermediates and lipophilic compounds [13-15]. In this work, this technique was used for the identification of non-cannabinoid bioactive compounds in the *Cannabis* extract.

Methanolic extract of *Cannabis* was analysed using a Shimadzu TQ8040 GC-MS equipped with a Shimadzu AOC 6000 autosampler and a Thermo Scientific TG-5MS, 30 m \times 0.25 mm \times 0.25 μ m column (**Figure 2.7**). The mobile phase comprised of He 6.0 (Linde). The scanning was performed in Q3 scan mode with an injection volume of 1 μ l at 280 $^{\circ}$ C. The ion source temperature was 250 $^{\circ}$ C while the interface temperature was 300 $^{\circ}$ C with a split ratio of 10. The temperature program was as follows: initial temperature 35 $^{\circ}$ C, hold time 5 min, final temperature 300 $^{\circ}$ C, hold time 20 min, rate 15 $^{\circ}$ C/min.

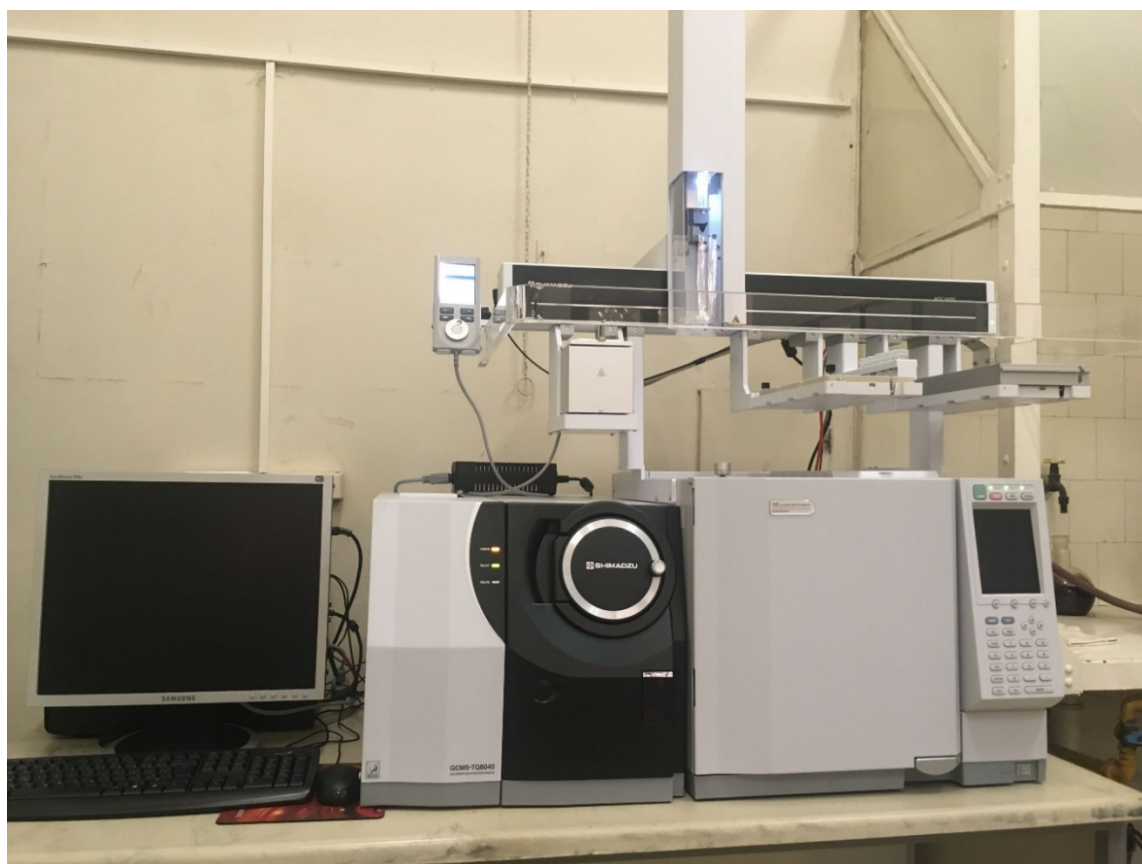


Figure 2.7 Photograph of GC-MS

2.4.3. Fourier transform infrared spectroscopy (FTIR)

FTIR is a spectroscopic technique based on the absorption of infrared radiations by molecules to detect the functional groups and bonding patterns in the specimen. A change in the dipole moment of IR active molecules leads to stretching or bending molecular vibrations [16-18].

In this work, FTIR was used for investigating the structural composition of the RGO/cellulose composites as well as the potential of the *Cannabis* extract to cause reduction. The FTIR spectra were collected using a Jasco FT/IR6300 equipped with an ATR PRO 470-H spectrometer (**Figure 2.8**). Full scan spectra were recorded in the mid-IR region of 4000-400 cm^{-1} in the transmission mode with a resolution of 4 cm^{-1} and 16 scans per sample at ambient conditions. The spectra were analyzed using OriginPro 2016 software (OriginLab Corporation).



Figure 2.8 Photographs of (a) FTIR and (b) ATR probe

2.4.4. Scanning electron microscopy (SEM)

SEM is a microscopic technique, which uses a beam of electrons to create an image of the specimen and extensively used for the physical characterization of materials. It provides finer details on the surface morphology, composition, crystallography and topography of the samples [19].

In this work, SEM was used for morphological analysis of the synthesized composites and determine the surface interactions occurring. The morphology of the composites was investigated by SEM (Hitachi S-3400N) at an operating voltage of 20 kV (**Figure 2.9**).



Figure 2.9 Photograph of SEM

2.4.5. Synchrotron X-ray diffraction (XRD)

XRD is a non-destructive technique based on the Bragg's law of constructive interference between the X-rays, and primarily used for phase identification, crystal structure determination and quantitative phase analysis [20, 21]. The synchrotron XRD has the advantage of combining high brightness and fine vertical collimation of synchrotron radiation with a broad range of wavelength tunability as compared to conventional laboratory X-ray sources.

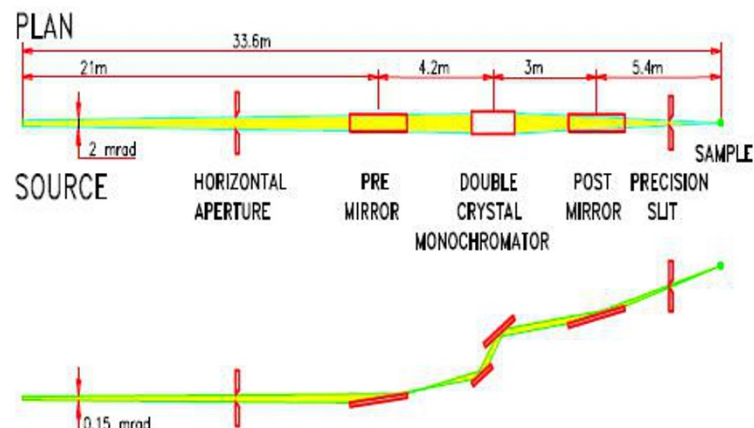


Figure 2.10 Schematic layout of XRD beamline (BL-12) at Indus 2 synchrotron, RRCAT (India) [22, 23]

In this work, XRD was used to study the structural composition of the composites and the efficacy of reduction by the *Cannabis* extract. The XRD data were collected at ADXRD beamline BL-12 of Indus-2 synchrotron source, RRCAT, India (**Figure 2.10**). The XRD data, obtained using MAR345 image plate detector at a wavelength of 1.1 Å, were integrated using Fit2D software in the 2θ range of 3-60°. The wavelength was calibrated using NIST LaB₆ standard.

2.4.6. Synchrotron X-ray photoelectron spectroscopy (XPS)

XPS is a surface technique, widely used to probe the surface composition and properties such as the elemental composition, chemical and electronic states of the elements including their bond energy. The sample is irradiated with a beam of monoenergetic X-ray, exciting the core electrons and ejecting them [24, 25]. The elements are identified by comparing the peak energies in the spectra to the standard binding or kinetic energies in the database, which are characteristic for each element. Unlike lab-based XPS that provides information up to a depth of about 1 nm due to the small mean free path of the emitted electrons, the synchrotron XPS provides information at larger depths, as the mean free path increases with electron energy.

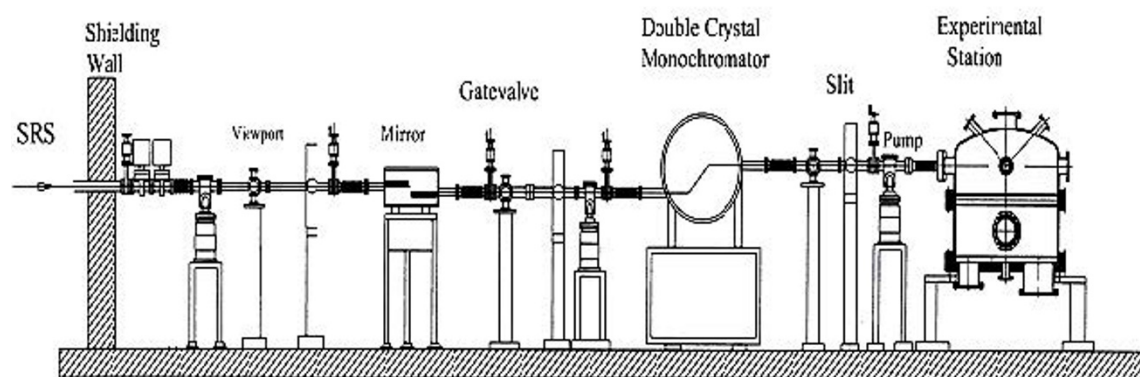


Figure 2.11 Schematic layout of XPS beamline (BL-14) at Indus 2 synchrotron, RRCAT (India) [26]

In this work, XPS was used to study the chemical composition of the synthesized GO and reduced-GO obtained after reduction with the *Cannabis* extract. The XPS data were collected at XPS beamline BL-14 of Indus-2 synchrotron source, RRCAT, India (**Figure 2.11**). The chemical composition was studied using data from XPS beamline equipped with a double-crystal monochromator [Si (111)], a platinum-coated X-ray mirror, a high-energy hemispherical analyzer with a microchannel plate and CCD detector. High-resolution spectra were obtained with an excitation energy of 4404 eV and an analyzer pass

energy of 150 eV focused on a spot size of 400 x 400 μm . The deconvolution of the peaks was done using PeakFit software (Systat Software, Inc.)

2.5. Electrical measurements

Surface resistivity, a fundamental property of insulators, may be defined as the electrical resistance of a known surface of the insulator composites. The resistivity measurement was used to determine the dielectric properties of the RGO/cellulose composites. The resistivity of 7 x 7 cm composites was measured using Keithley 6517B electrometer and Keithley 8009 resistivity test fixture by sourcing a known voltage for 60 s (**Figure 2.12**). Measurements were done at varying voltages of 0.5, 1, 2.5, 5, 10, 20, 40, 60, 80 and 100 V. Because the surface resistivity is measured from a known length of ring electrode to a guarded electrode along the surface of the composites, the measurement is independent of the physical dimensions (thickness, length and width) of the samples. The distance between the ring and guarded electrode was 4 mm and the effective D_0 diameter was 54 mm. The specimens were conditioned at 23 °C and 50% relative humidity for 2 hours prior to the measurement.

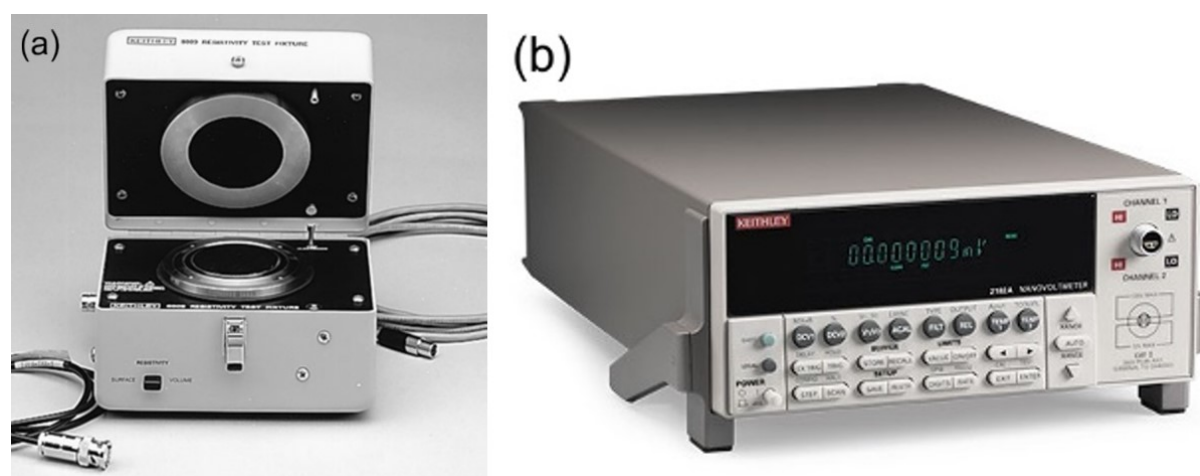


Figure 2.12 Photographs of (a) Keithley resistivity test fixture and (b) Keithley electrometer

2.6. Summary

Bioactive compounds were extracted using the technique of ultrasonication from the inflorescences of fibre-type *Cannabis*. The extracts were evaluated for TPC, TF, FRAP and yield at varying ultrasonic parameters of time, power and extraction solvent. Statistical modelling using a 3-factor central composite design approach of the response surface methodology was used to carry out the optimization of the extraction parameters. The

extract was analysed for cannabinoids and other bioactive compounds using HPLC-DAD-MS/MS and GC-MS, respectively. A green and facile method for the simultaneous reduction and functionalization of GO in situ on cellulose fibres using the aqueous *Cannabis* extract was developed. Composites were fabricated with different contents of RGO from 0.1 to 10 m/m %, characterized using advanced analytical techniques and evaluated for their electrical properties.

References

- [1] Gogate, P. R., Shirgaonkar, I. Z., Sivakumar, M., Senthilkumar, P., Vichare, N. P., and Pandit, A. B., "Cavitation Reactors: Efficiency Analysis Using a Model Reaction," *AIChE J.* Vol. 47, no. 11, 2001, 2526-2538.
- [2] Ainsworth, E. A., and Gillespie, K. M., "Estimation of Total Phenolic Content and Other Oxidation Substrates in Plant Tissues Using Folin-Ciocalteu Reagent," *Nat. Protoc.* Vol. 2, no. 4, 2007, 875-877.
- [3] Teh, S. S., and Birch, E. J., "Effect of Ultrasonic Treatment on the Polyphenol Content and Antioxidant Capacity of Extract from Defatted Hemp, Flax and Canola Seed Cakes," *Ultrason. Sonochem.* Vol. 21, no. 1, 2014, 346-353.
- [4] Benzie, I. F. F., and Strain, J. J., "The Ferric Reducing Ability of Plasma (FRAP) as a Measure of "Antioxidant Power": The FRAP Assay," *Anal. Biochem.* Vol. 239, no. 1, 1996, 70-76.
- [5] Yu, H., Zhang, B., Bulin, C., Li, R., and Xing, R., "High-Efficient Synthesis of Graphene Oxide Based on Improved Hummers Method," *Sci. Rep.* Vol. 6, 2016, 36143-36149.
- [6] Pendolino, F., Armata, N., Masullo, T., and Cuttitta, A., "Temperature Influence on the Synthesis of Pristine Graphene Oxide and Graphite Oxide," *Mater. Chem. Phys.* Vol. 164, 2015, 71-77.
- [7] Pulps - Preparation of Laboratory Sheets for Physical Testing Part 2: Rapid-Kothen Method, DIN EN ISO 5269-2, 2005.
- [8] Klencsár, B., Li, S., Balcaen, L., and Vanhaecke, F., "High-Performance Liquid Chromatography Coupled to Inductively Coupled Plasma–Mass Spectrometry (HPLC-ICP-MS) for Quantitative Metabolite Profiling of Non-Metal Drugs," *Trends Anal. Chem.* Vol. 104, 2018, 118-134.
- [9] Zoccali, M., Tranchida, P. Q., and Mondello, L., "On-Line Combination of High Performance Liquid Chromatography with Comprehensive Two-Dimensional Gas

Chromatography-Triple Quadrupole Mass Spectrometry: A Proof of Principle Study," *Anal. Chem.* Vol. 87, no. 3, 2015, 1911-1918.

[10] De Backer, B., Debrus, B., Lebrun, P., Theunis, L., Dubois, N., Decock, L., Verstraete, A., Hubert, P., and Charlier, C., "Innovative Development and Validation of an HPLC/DAD Method for the Qualitative and Quantitative Determination of Major Cannabinoids in Cannabis Plant Material," *J. Chromatogr. B* Vol. 877, no. 32, 2009, 4115-4124.

[11] Aizpurua-Olaizola, O., Omar, J., Navarro, P., Olivares, M., Etxebarria, N., and Usobiaga, A., "Identification and Quantification of Cannabinoids in *Cannabis Sativa* L. Plants by High Performance Liquid Chromatography-Mass Spectrometry," *Anal. Bioanal. Chem.* Vol. 406, no. 29, 2014, 7549-7560.

[12] Hazekamp, A., Peltenburg, A., Verpoorte, R., and Giroud, C., "Chromatographic and Spectroscopic Data of Cannabinoids from *Cannabis Sativa* L.," *J. Liq. Chromatogr. Relat. Technol.* Vol. 28, no. 15, 2005, 2361-2382.

[13] Lisec, J., Schauer, N., Kopka, J., Willmitzer, L., and Fernie, A. R., "Gas Chromatography Mass Spectrometry-Based Metabolite Profiling in Plants," *Nat. Protoc.* Vol. 1, no. 1, 2006, 387-396.

[14] Milman, B. L., "General Principles of Identification by Mass Spectrometry," *Trends Anal. Chem.* Vol. 69, 2015, 24-33.

[15] Mondello, L., Tranchida, P. Q., Dugo, P., and Dugo, G., "Comprehensive Two-Dimensional Gas Chromatography-Mass Spectrometry: A Review," *Mass Spectrom. Rev.* Vol. 27, no. 2, 2008, 101-124.

[16] Fayer, M. D., *Ultrafast Infrared and Raman Spectroscopy*, CRC Press, 2001.

[17] Smith, B. C., *Fundamentals of Fourier Transform Infrared Spectroscopy*, CRC Press, 2011.

[18] Stuart, B., "Infrared Spectroscopy," *Kirk-Othmer Encyclopedia of Chemical Technology*, 2000, 1-18.

[19] Goldstein, J. I., Newbury, D. E., Michael, J. R., Ritchie, N. W., Scott, J. H. J., and Joy, D. C., *Scanning Electron Microscopy and X-Ray Microanalysis*, Springer, 2017.

[20] Cullity, B. D., and Stock, S. R., *Elements of X-Ray Diffraction*, Pearson Education 2014.

[21] He, B. B., Preckwinkel, U., and Smith, K. L., "Fundamentals of Two-Dimensional X-Ray Diffraction (XRD2)," *Adv. X-ray Anal.* Vol. 43, 2000, 273-280.

- [22] Sinha, A. K., Sagdeo, A., Gupta, P., Upadhyay, A., Kumar, A., Singh, M. N., Gupta, R. K., Kane, S. R., Verma, A., and Deb, S. K., Angle Dispersive X-Ray Diffraction Beamline on Indus-2 Synchrotron Radiation Source: Commissioning and First Results, 11th International Conference on Synchrotron Radiation Instrumentation, 2013, pp. 072017.
- [23] Sinha, A., Sagdeo, A., Gupta, P., Kumar, A., Singh, M., Gupta, R., Kane, S., and Deb, S., Commissioning of Angle Dispersive X-Ray Diffraction Beamline on Indus-2, AIP Conference Proceedings, AIP, 2011, pp. 503-504.
- [24] Castle, J. E., Practical Surface Analysis by Auger and X-Ray Photoelectron Spectroscopy, in: D.B.a.M. Seah (Ed.) Surface and Interface Analysis, John Wiley and Sons Ltd., Chichester, 1984.
- [25] Weightman, P., X-Ray-Excited Auger and Photoelectron Spectroscopy, Electronic Properties of Surfaces, Routledge, 2018, pp. 135-195.
- [26] Sharma, R. K., Goutam, U. K., Mithal, N., Sule, U. S., Gadkari, S. C., Yakhmi, J. V., and Sahni, V. C., A High Energy Hemispherical Analyzer for Experimental Station of PES Beamline at Indus-2 (No. Barc--2009/E/006). , in: T.P.P.E. Division (Ed.) Bhabha Atomic Research Centre, Mumbai, 2009.

CHAPTER III-
ULTRASONIC EXTRACTION OF BIOACTIVE
COMPOUNDS FROM *CANNABIS SATIVA* L.
OPTIMIZED BY RESPONSE SURFACE
METHODOLOGY

3.1. Chapter synopsis

This chapter deals with the discussion on the ultrasonic extraction of bioactive compounds from fibre-type *Cannabis*. Detailed analysis of the influence of ultrasonic parameters (design factors) on the extract properties using response surface methodology has been presented. A comparative evaluation of cannabinoids using HPLC-DAD-MS/MS technique has been elucidated. Finally, the optimization of the extraction parameters and experimental model validation have been discussed.

3.2. Extraction process and factor selection

For proper resource utilization and process optimization, the selection of the right technique and the governing factors plays a crucial role. The extraction of bioactive compounds was assisted by ultrasonic waves (20 kHz), which create compression and expansion in the medium causing the formation, growth and collapse of bubbles known as cavitation. It causes the swelling and rupture of cell walls, followed by leaching of cellular components by mass transfer into the solvent due to the diffusion across the plant cell wall and subsequent washing-out of the contents [1]. The low frequency of sonication used here leads to stronger physical effects which aid the extraction process [2]. Compared to the conventional extraction techniques, ultrasonication facilitates faster mass and energy transfer, uniform mixing and reduced thermal gradients, thus leading to shorter extraction times at lower temperatures. Temperature, time, solvent, power and frequency are the main parameters affecting the efficiency of ultrasonication [1]. The time and temperature can have either positive or negative impact on extraction and hence, should be considered cautiously. Longer sonication time may result in the degradation of some thermolabile compounds due to higher temperature. Additionally, it also increases the energy and operational costs [3]. In this study, time was chosen as one of the influencing factors for the design, as it is easier to monitor and control time over temperature. Further, they are also directly linked as the temperature increases with time due to the large amount of heat generated continuously in the process. Another factor considered for process study was the power of sonication. It affects the intensity of ultrasonic waves passing through the solvent medium and thereby, can have a profound impact on the extraction process. The third factor, solvent plays a key role during sonication by dissolving the compounds of interest and chosen based on the selectivity of the targeted compounds. Methanol has been widely employed as a preferred solvent for extraction of plant components such as the phenolic

antioxidants [1]. The selection of solvent also depends on its safety or toxicity, cost and availability.

Table 3.1 Central composite design factors in coded and actual forms along with the investigated responses of TPC, TF, FRAP and yield for various experimental runs

Run No.	Coded factors			Decoded factors			Responses [#]			
	A	B	C	Time (min)	Power (W)	Solvent (%)	TPC (R1)	TF (R2)	FRAP (R3)	Yield (R4)
1	-1	1	-1	5	150	20	205.89	45.02	15.97	12.1
2	0	0	1	10	120	80	262.626	25.395	11.41	8.73
3	0	0	0	10	120	50	244.709	39.224	10.72	9.57
4	-1	1	1	5	150	80	267.403	23.064	16.3	8.36
5	-1	0	0	5	120	50	229.779	32.577	10.16	8.71
6	-1	-1	1	5	90	80	200.515	16.89	9.18	7.02
7	1	1	1	15	150	80	313.389	39.255	19.51	11.37
8	0	0	-1	10	120	20	210.071	42.752	13.68	10.91
9	0	1	0	10	150	50	240.529	39.192	10.07	9.68
10	1	1	-1	15	150	20	197.828	46.5	12.01	12.21
11	0	0	0	10	120	50	245.306	50.973	7.58	10.31
12	1	-1	1	15	90	80	313.986	37.239	18.11	9.99
13	0	-1	0	10	90	50	228.584	31.443	8.13	8.75
14	1	0	0	15	120	50	254.563	39.728	12.39	10.62
15	0	0	0	10	120	50	265.313	40.389	18.15	11.29
16	-1	-1	-1	5	90	20	189.467	34.908	9.72	10.02
17	0	0	0	10	120	50	249.487	47.193	6.2	10.2
18	0	0	0	10	120	50	271.285	49.389	19	11.58
19	1	-1	-1	15	90	20	218.432	47.036	14.06	12.77
20	0	0	0	10	120	50	239.035	33.522	8.65	8.85

[#] Values of TPC in mg GAE/g DW, TF in mg QE/g DW, FRAP in mM AAE/g DW and yield in %.

3.3. Modelling and regression analysis

The influence of the selected design factors viz. time (A), input power (B) and solvent concentration (C) was evaluated on four responses- TPC (R1), TF (R2), FRAP (R3) and the extraction yield (R4), according to a face-centred central composite design to

optimize the extraction conditions for *Cannabis*. **Table 3.1** presents the experimentally obtained values for the responses (R1, R2, R3 and R4) under different factor (A, B, C) conditions, which have been given in both coded and actual forms. The conversion of factors from their actual into the coded forms is as per eq. (1), where C is the coded level (-1, 0 or 1), A_c and A_v are the actual and average factor values, respectively; while R is the range or difference between the highest and lowest factor values.

$$C = 2 (A_c - A_v) / R \quad (1)$$

The experimental data for each response was fitted to a second order polynomial equation as represented by eq. (2), where Y is the response variable, X_i and X_j are independent factors, β_0 is the intercept, β_i , β_{ii} and β_{ij} are coefficients for linear, quadratic and factor interaction terms while k is the number of design variables.

$$Y = \beta_0 + \sum_{i=1}^k \beta_i X_i + \sum_{i=1}^k \beta_{ii} X_i^2 + \sum_{i=1}^{k-1} \sum_{j=i+1}^k \beta_{ij} X_i X_j \quad (2)$$

The data modelling revealed that the quadratic terms did not show any appreciable effect on any of the four responses under investigation as indicated by their higher than 0.05 p-values and hence were redundant. The model reduction showed that two-factor interaction model well fitted TPC while linear models fitted the other responses of TF, FRAP and yield. The predictive equations in terms of coded factors (A, B and C) for TPC (mg GAE/g DW), TF (mg QE/g DW), FRAP (mM AAE/g DW) and yield (%) are given by eq. (3), (4), (5) and (6), respectively.

$$\text{TPC} = 242.41 + 20.51 A + 7.41 B + 33.62 C - 13.06 AB + 17.32 AC + 8.81 BC \quad (3)$$

$$\text{TF} = 38.08 + 5.73 A + 2.55 B - 7.44 C \quad (4)$$

$$\text{FRAP} = 12.55 + 1.48 A + 1.47 B + 0.91 C \quad (5)$$

$$\text{Yield} = 10.15 + 1.07 A + 0.52 B - 1.25 C \quad (6)$$

They can be used to make predictions about the responses at the coded levels for each factor. Moreover, their coefficients also show the relative impact or contribution of each factor term on the response as a whole. Similar predictive equations in terms of actual factors of time, input power and solvent (denoted by T, P and S, respectively) are given by eq. (7), (8), (9) and (10) for each response. Since their coefficients are scaled (according to eq. 1) in order to accommodate the units of each factor, they do not determine the relative impact of each term in the equation.

$$\text{TPC} = 127.66605 + 8.78100 T + 0.62839 P - 1.20838 S - 0.087093 TP + 0.11546 TS + 9.78778E-003 PS \quad (7)$$

$$\text{TF} = 28.81415 + 1.14598 T + 0.085050 P - 0.24791 S \quad (8)$$

$$\text{FRAP} = 2.22433 + 0.29500 T + 0.048867 P + 0.030233 S \quad (9)$$

$$\text{Yield} = 8.02400 + 0.21500 T + 0.017233 P - 0.041800 S \quad (10)$$

The regression coefficients of the intercept, linear and interaction terms for each response and ANOVA are shown in **Table 3.2**. The relative significance in terms of p and F-values are presented for each term as well as for the model and lack of fit. It was found that the interaction terms were significant only for TPC while other responses obeyed the linear model. The values of the coefficient of regression (R^2) ranged from 0.90 for TPC to 0.16 for FRAP. The exceptionally low R^2 for FRAP and low p and F-values implied that the model was not significant relative to the noise with no significant terms. However, despite low p_M and F_M , it showed an insignificant lack of fit relative to the pure error as is evident from p_{LoF} and F_{LoF} for FRAP. All other responses (TPC, TF and yield) showed a very good statistical significance for the model, as can be clearly observed from the low p-values ($p_M < 0.01$) with no significant lack of fit ($p_{LoF} > 0.5$). This was also confirmed from the F-values for the model (high F_M) and lack of fit (low F_{LoF}) which also indicated that the fitted models were capable of drawing a relationship between the experimental factors and the investigated responses. Further, all the responses had an adequate precision (AP) or signal to noise ratio ($AP > 4$) strong enough to be used for optimization and navigation through the design space.

Table 3.2 Regression coefficient estimates for second order polynomial model for TPC, TF, FRAP and yield along with their ANOVA parameters

Term	Coefficient estimates			
	TPC	TF	FRAP	Yield
Intercept	242.41	38.08	12.55	10.15
Linear				
A (time)	20.51*	5.73**	1.48	1.07*
B (power)	7.41***	2.55	1.47	0.52***
C (solvent)	33.62*	-7.44*	0.91	-1.25*
Interaction				

AB	-13.06 ^{**}	-1.85	-1.75	-0.33
AC	17.32 [*]	2.87	1.47	0.39
BC	8.81 ^{***}	-0.17	0.54	0.15
σ^a	12.96	6.27	4.13	0.86
R ^{2b}	0.9036	0.6101	0.1621	0.7147
AP ^c	16.06	8.47	4.05	11.13
CV ^d	5.34	16.15	32.5	8.52
p _M ^e	0.0001	0.0014	0.4051	0.0001
p _{LoF} ^e	0.5072	0.6911	0.9372	0.7918
F _M ^f	20.30	4.40	0.93	7.18
F _{LoF} ^f	1.04	0.76	0.29	0.53

^{*} $p \leq 0.01$

^{**} $0.01 < p \leq 0.05$

^{***} $0.05 < p \leq 0.1$

^a σ Standard deviation

^bR² Coefficient of regression

^cAP adequate precision

^dCV Coefficient of variation (%)

^ep_M & p_{LoF} p-values for the model and lack of fit, respectively

^fF_M & F_{LoF} F-values for the model and lack of fit, respectively

3.4. Influence of ultrasonic parameters (design factors) on the responses

3.4.1. Influence of design factors on TPC

The obtained values of TPC have been given in **Table 3.1** while its regression analysis is done in **Table 3.2**. As evident from eq. (3), the linear terms of time and solvent have a very significant and positive influence on the extraction of TPC from *Cannabis*. Their interactive term also has the same effect ($p < 0.01$). Likewise, the interaction between time and power has a significant but negative impact on TPC. The third interactive term of power/ solvent and the linear term of power alone does not significantly affect TPC extraction.

The 3D response surface plots further supported the findings by the regression analysis graphically. These plots, being three dimensional, provide a clear view of the potential relationship established by varying two factors or predictor variables (on the X-

and Y- axes) against a response (on the Z- axis) by holding the third factor constant (at the central value).

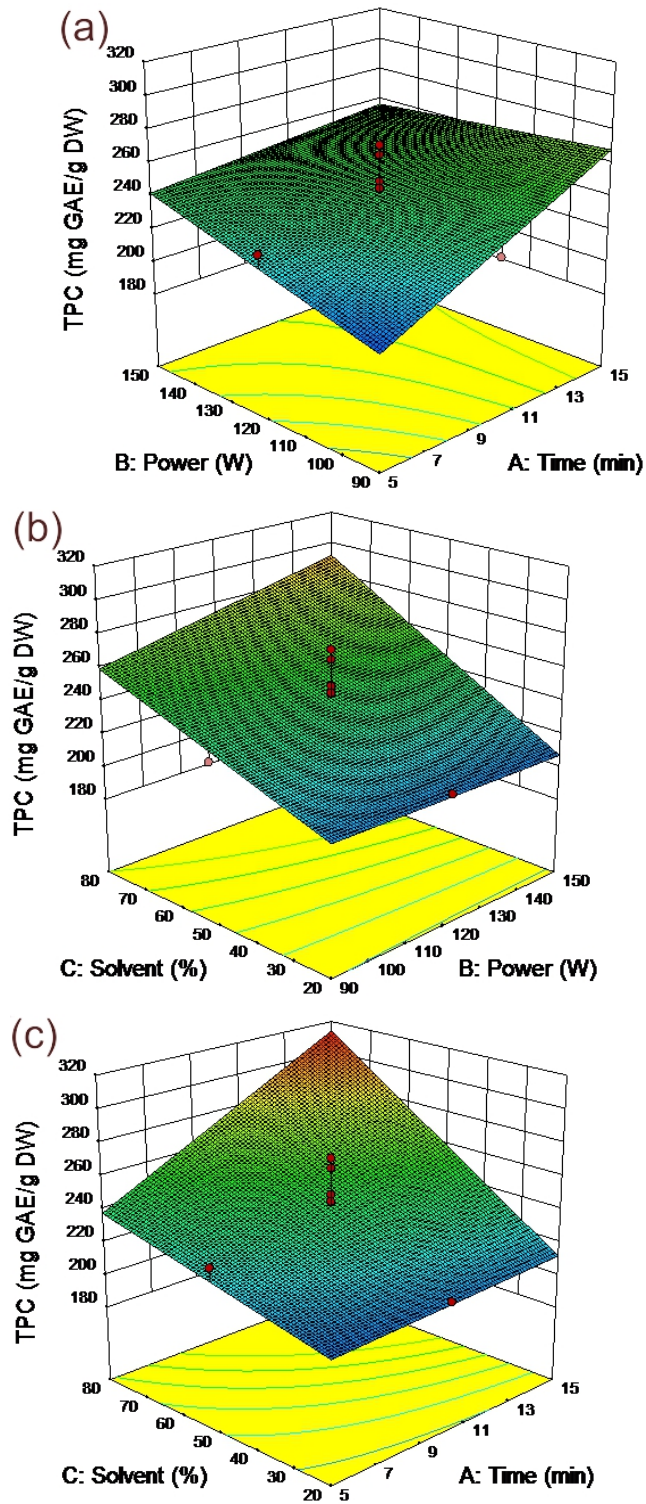


Figure 3.1 Response surface plots depicting the influence of design factors on TPC

Figure 3.1 shows the surface plots exhibiting the interaction and effect of varying the design factors on TPC. Maximum TPC obtained was for longest extraction time of 15

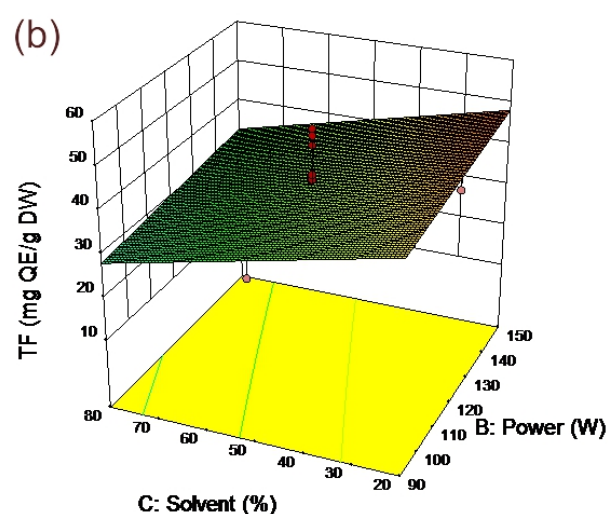
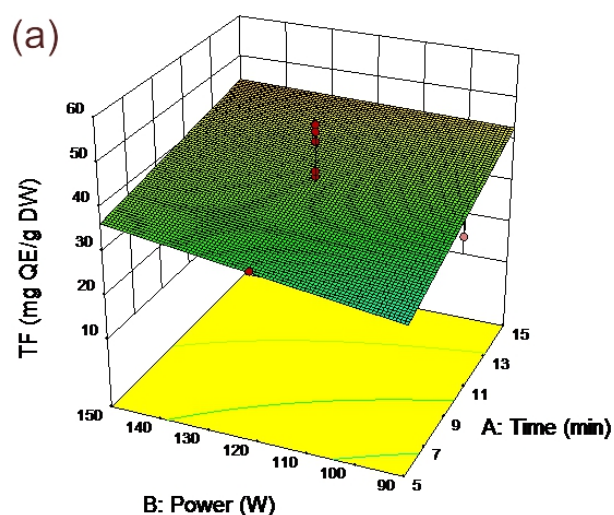
min and highest methanol concentration of 80% but with lowest power input of 90 W. As expected, the minimum TPC obtained was for shortest time, lowest methanol concentration with same power. This also suggests strong positive influence of both time and solvent can be observed in plots (**Figure 3.1 a,b,c**) indicating that TPC extraction would appreciably increase by increasing either of time or solvent or both. Longer sonication time aids in enhanced penetration of the solvent into the plant matrix leading to improved extraction of its contents [4]. More methanol content in the extraction solvent favouring TPC extraction could be attributed to the altered polarity of the alcohol-water mixture, which has also been reported previously [5]. Polar solvents increase the permeability of the cell wall thereby enhancing the extraction [6]. It is worth noting that power itself does not significantly affect TPC, which has also been observed earlier [3]. On the contrary, the interactive effect of time and power as seen in **Figure 3.1a** influences the extraction negatively. However, the interaction between power and solvent has a positive impact on TPC, though not significant as shown in **Figure 3.1b**.

3.4.2. Influence of design factors on TF

The values for TF are presented in **Table 3.1** with their statistical parameters in **Table 3.2**. TF shows a similar response to the extraction conditions as TPC except that the two-factor interaction terms are insignificant for the TF model, reducing it to a linear one. As given in eq. 4, the solvent is the most dominant factor affecting the flavonoid extraction ($p < 0.01$), although negatively. Time has a positive and moderately significant influence on TF extraction. Again, power does not significantly affect TF as in case of TPC. Maximum flavonoid content was obtained for extraction conditions of 10 min, 120 W power and 50% methanol whereas, the minimum extraction was at 5 min, 90 W power and 80% methanol. This also clearly indicated the positive impact of both time and power on TF but reverse for solvent.

The response surface plots shown in **Figure 3.2** provide a better visualization of the influence of design factors on flavonoid extraction. Like TPC, the positive influence of interactive effect of time and solvent can be observed for the extraction of TF as well (**Figure 3.2c**). However, contrary to TPC, the solvent negatively affected TF, meaning that the extraction of flavonoids decreased with increasing concentration of methanol. Similar highly significant effect of solvent on flavonoid extraction has already been reported earlier [3]. This shows that the presence of water in the solvent mixture assisted the ultrasonic removal of flavonoids from the plant. This has been attributed to the swelling action of the

plant matrix caused by water, thereby enhancing the effective contact surface area available for the solvent [7]. Moreover, water also generates hydroxyl radicals during cavitation, which may assist in the extraction process [8]. It can thus be conclusively established that there is an optimum ratio of alcohol to water for maximum extraction and ultrasound reduces methanol requirement for similar levels of extraction, which has also been observed before [9]. The polarity of the solvent mixture plays a crucial role in ultrasonic extraction and determines not only the quantity of flavonoids extracted but also their composition in the extract [3]. Further, the interactive effect of power with time had a negative impact on TF extraction, although insignificant (*Figure 3.2a*). This suggests the probability of possible degradation of flavonoids when sonicated for longer duration at higher power input. Such decomposition by the ultrasonic waves at prolonged sonication time has been observed in the past for polyphenols [10]. Likewise, the negative interactive effect of power and solvent has been shown in *Figure 3.2b*. Thus, mild conditions of time, power and solvent can be used TF extraction leading to cost and energy savings.



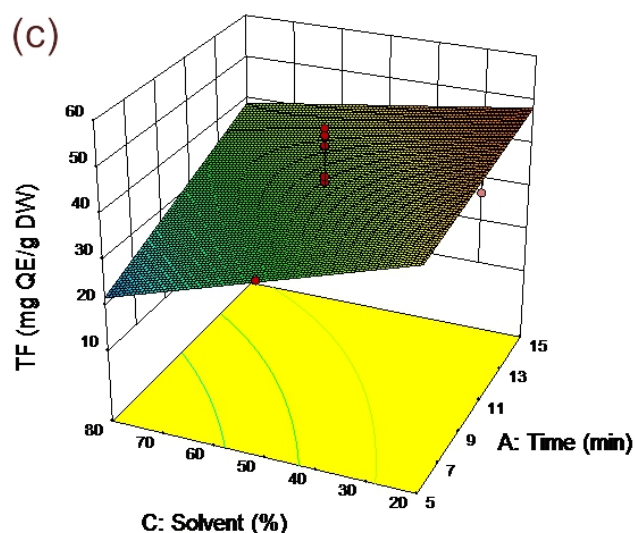


Figure 3.2 Response surface plots depicting the influence of design factors on TF

3.4.3. Influence of design factors on FRAP

The antioxidant activity of the extracts determined by the FRAP assay are presented in **Table 3.1**. It is clear from the regression analysis in **Table 3.2** that the model fitted was statistically insignificant ($p > 0.05$) with none of the experimental factors affecting FRAP in a significant way. The relative impact of the factors can be seen from eq. 5. The values for the antioxidant assay varied from 6.2 to 19.5 mM AAE/g DW. Interestingly, previous reports have also found such insignificance of studied factors in the determination of FRAP, where the effect of time was not significant [11].

Although the factors do not significantly influence the antioxidant assay, the response surface plots in **Figure 3.3** may lead to some valuable insights into the response. It can be said that the impact of all the factors, in general, is affirmative to the assay. The interactive effect of solvent with time or power may positively affect the FRAP as seen in **Figure 3.3 b,c**. Further, prolonging the sonication at higher power input may result in reduced antioxidant activity (**Figure 3.3a**). Similar behaviour was also observed for TPC. Many reports confirm a good correlation between the total phenolic content of the extract and its antioxidant activity [12]. However, no adequate correlation was found between TPC and FRAP in the present study with correlation coefficient of 0.54 indicating no linear relation between the two responses. There is also evidence of their non-linear relation, even though both colorimetric assays rely on the same concept of electron transfer [13]. This is possible as the FC reagent for TPC interacts with many reducing substances and not just the phenolic compounds. Contrary to TPC, the FRAP assay needs an acidic pH

environment, which alters the reaction behaviour of antioxidants [14]. Also, since the exact nature of the FC reagent is still unknown, there may be compounds in TPC which do not react with the FRAP assay and vice versa [15].

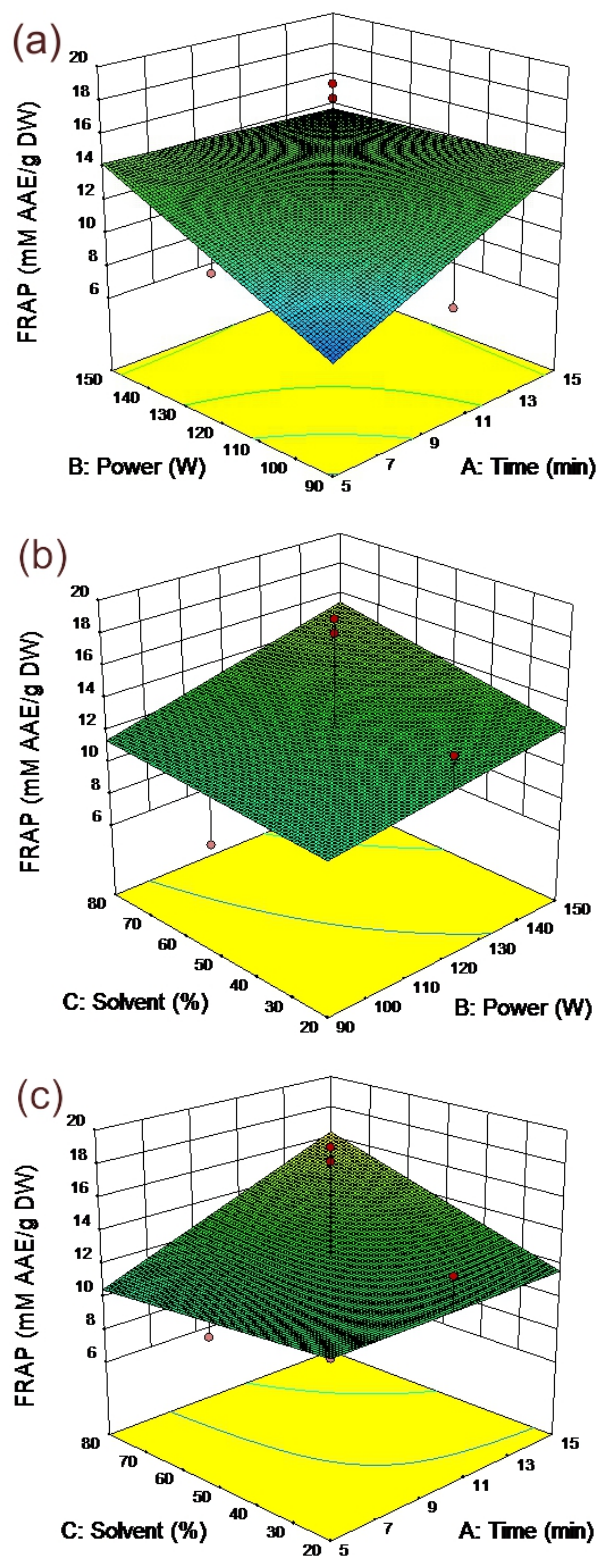


Figure 3.3 Response surface plots depicting the influence of design factors on FRAP

3.4.4. Influence of design factors on yield

The experimentally obtained values for the yield of *Cannabis* are shown in **Table 3.1**. As indicated in eq. 6 and from ANOVA in **Table 3.2**, the linear terms of time and solvent are highly significant ($p < 0.01$) and predominant factors, which determine the yield. The time shows a positive impact while solvent has a negative effect on yield, similar as in case of TF. On the other hand, the linear term of power does not so significantly influence the extraction yield. The model being linear, the interaction terms were insignificant. The maximum yield obtained was at extraction conditions of 15 min, 90 W power and 20% methanol. The corresponding values for minimum yield were 5 min, 90 W power and 80% methanol. This clearly indicated that yield increased as a function of time while it decreased with increasing concentration of methanol, power remaining the same.

The response surface plots shown in **Figure 3.4** depict the interaction and influence of factors on the extraction yield. The strong positive influence of time (**Figure 3.4 a,c**) can well be explained by the fact that more mass is extracted as the time passes. Contrary to time factor, the solvent intensely reduces the yield (**Figure 3.4 b,c**) implying that higher methanol content is detrimental to yield. Previous study has also reported the same observation [13]. The higher solubility of plant components in water occurs owing to the fact that the diffusivity of water is more than that of methanol. According to another study, more water in the solvent mixture favours the extraction of other concomitant compounds, which results in lower phenolic content in the extract [16]. Thus, although extraction solvents with higher water content improve the overall yield, they have lower phenolic antioxidants. As shown in **Figure 3.4c**, the slight positive impact of the interactive effect of time with solvent may suggest the use of more methanol in solvent at prolonged ultrasonication, which could enhance the phenolic yield. However, care should be taken that no decomposition of extracted components occurs during longer exposure period. As for the effect of power, the yield of some phenolic compounds has been shown to increase as a function of power while the opposite occurs for the rest [17]. Improved extraction yield obtained at higher ultrasonic power is due to the enhanced physical effects such as cracked cell walls, interfacial turbulence, solute diffusion and energy dissipation, which are caused by larger amplitude of ultrasound waves travelling through the solvent medium giving rise to intense collapse of the cavitation bubbles [6]. On the contrary, high acoustic power increases the dissipation of heat in the medium, which may reduce the yield due to the degradation of heat sensitive compounds [18]. Thus, the combined effect of power with

time or solvent may lead to an improved or reduced yield (*Figure 3.4 a,b*) depending on the nature of compounds present in the extract.

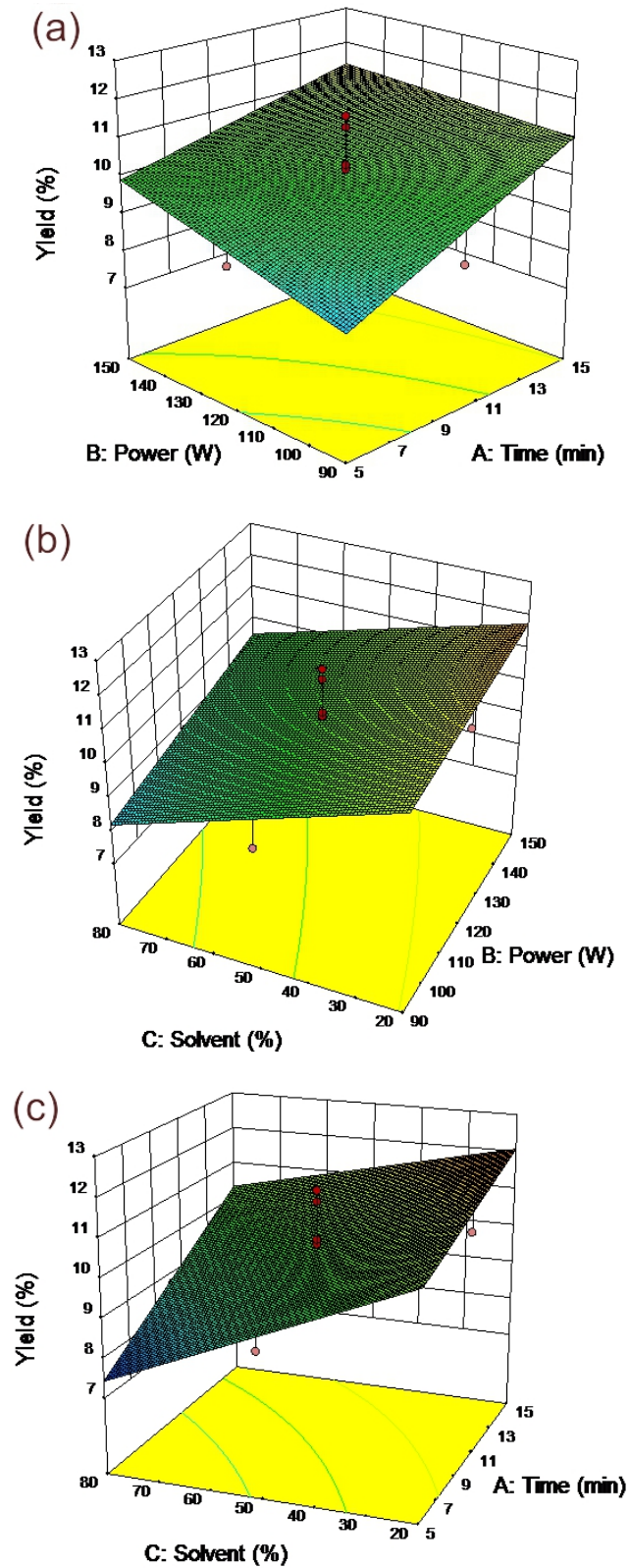


Figure 3.4 Response surface plots depicting the influence of design factors on extraction yield

3.5. Optimization of extraction conditions

The numerical optimization of ultrasonic extraction of *Cannabis* bioactive compounds would enable to carry out the process in the most efficient way leading to maximum output with minimum input conditions. In the present study, the optimal factors were obtained by maximising the desirability function, $D = 0.730$. For the investigated range of factors, the optimal conditions for extractions were 15 min time, 130 W power and 80% methanol for all the responses. At these conditions, the predicted values of the responses were: TPC- 314.822 mg GAE/g DW, TF- 28.173 mg QE/g DW, FRAP- 18.79 mM AAE/g DW and yield- 10.86%. These were experimentally confirmed to validate the predicted modelling on the responses and the obtained values were: TPC- 312.452 mg GAE/g DW, TF- 32.254 mg QE/g DW, FRAP- 17.84 mM AAE/g DW and yield- 10.68%. A close resemblance between the predicted and experimental values validated the model for the investigated responses at the optimal conditions of design factors.

3.6. Ultrasonic vs control extraction

In order to prove the merits of ultrasonication, a control extraction was performed and the responses were quantitatively compared. **Figure 3.5** shows the experimental values for each of the four responses in both types of extractions. It is obvious that ultrasonically extracted *Cannabis* demonstrated markedly higher values for all of the responses. Ultrasonic extraction done for just 15 min resulted in over twice the TPC, TF and yield than that obtained after a control extraction for 30 min. It undoubtedly confirms that ultrasonication saves time, energy and cost.

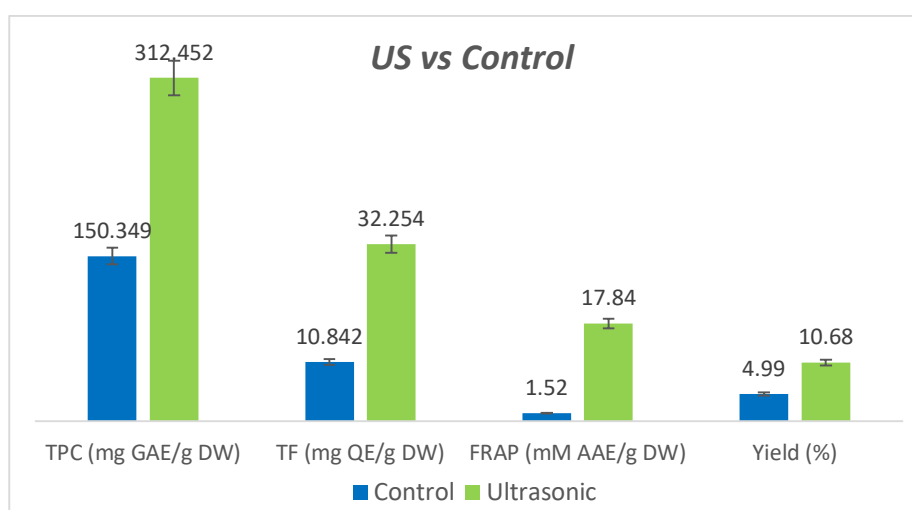


Figure 3.5 Comparison between ultrasonic (green) and control (blue) extractions for the responses (The error bars indicate percentage error)

The energy released from the collapse of the cavitation bubbles brings about various physical and chemical effects such as turbulence as well as free radical generation due to decomposition of water and pyrolysis of the trapped compounds. The shock waves generated because of cavitation are capable enough to break chemical bonds and cause cell lysis, thus assisting the process of extraction [2, 19]. Higher extraction in lesser time occurs due to the mechanical impact on plant cell walls caused by ultrasonic waves [20]. Moreover, the combination of localized stirring effect occurring due to cavitation along with the repeated washing of cellular components with solvent further intensified the extraction of compounds in case of ultrasonication [9]. Also, the degradation of phenols is less likely to happen than that of the more volatile compounds, which readily diffuse into the cavitation bubble [20]. Likewise, there was also a sharp rise in the antioxidant activity (FRAP) for the sonicated extract. This was due to the higher phenolic content of the sonicated extract, which reduced the reactive oxygen species or free radicals and protected the biomolecules against oxidation [21].

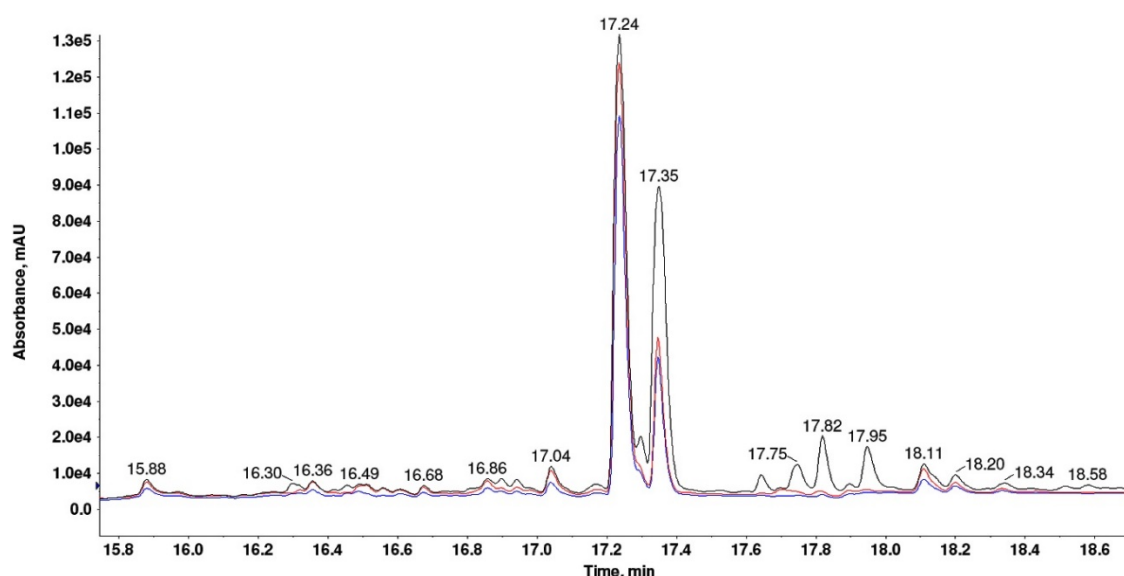


Figure 3.6 Qualitative HPLC chromatograms for ultrasonic (black represents optimal conditions & red represents central values) and control (blue) extracts of *Cannabis*

Furthermore, ultrasonication also proved extremely efficient for the extraction of cannabinoids, predominantly present in *Cannabis*. The HPLC separation as well as the relative quantitative assessment by DAD peak heights of the cannabinoids is shown in **Figure 3.6** (detailed qualitative analysis of the cannabinoids in the extract is presented in *Chapter IV*). The major cannabinoids identified by MS/MS spectra were CBG and THC at

retention times of 17.24 and 17.35 min, respectively. Clearly, the amounts of the cannabinoids were higher in the sonicated extracts compared to the control one, as depicted by the peak heights. It is worth noting that maximum extraction was of these cannabinoids was obtained at optimal conditions of ultrasonication. Thus, ultrasound considerably enhanced the extraction of compounds in far lesser time than the control extraction.

3.7. Summary and inferences

The extraction of bioactive compounds using the technique of ultrasonication from *Cannabis* has been elucidated. Statistical modelling using a 3-factor central composite design approach for the optimization of the extraction parameters has been demonstrated. Each of the responses was analysed by fitting a second order polynomial; the TPC was well described by the factor interaction model while linear models described the TF, FRAP and yield. The regression and graphical analysis revealed the solvent composition and time to be the most predominant factors influencing the extraction process, except in case of the FRAP assay. The time had a positive effect on the responses. More methanol content in the solvent favoured the TPC while it negatively affected TF and the extraction yield. The ultrasonic power, on the other hand, did not have any significant impact on any of the responses investigated. The response predictions obtained at optimum extraction conditions of 15 min time, 130 W power and 80% methanol were found to be 314.822 mg GAE/g DW of TPC, 28.173 mg QE/g DW of TF, 18.79 mM AAE/g DW of FRAP and 10.86% of yield. Appreciably higher values of all the responses were obtained for the ultrasonic extraction than the control process. Further, ultrasonication also considerably enhanced the extraction of cannabinoids, which was confirmed by HPLC chromatograms. On the whole, ultrasonication proved its merits as an efficient and green extraction technique, over the conventional method leading to substantial savings in resources, time, energy and cost.

References

- [1] Azmir, J., Zaidul, I. S. M., Rahman, M. M., Sharif, K. M., Mohamed, A., Sahena, F., Jahurul, M. H. A., Ghafoor, K., Norulaini, N. A. N., and Omar, A. K. M., "Techniques for Extraction of Bioactive Compounds from Plant Materials: A Review," *J. Food Eng.* Vol. 117, no. 4, 2013, 426-436.
- [2] Iskalieva, A., Yimmou, B. M., Gogate, P. R., Horvath, M., Horvath, P. G., and Csóka, L., "Cavitation Assisted Delignification of Wheat Straw: A Review," *Ultrason. Sonochem.* Vol. 19, no. 5, 2012, 984-993.

- [3] Tomsik, A., Pavlic, B., Vladic, J., Ramic, M., Brindza, J., and Vidovic, S., "Optimization of Ultrasound-Assisted Extraction of Bioactive Compounds from Wild Garlic (*Allium Ursinum* L.)," *Ultrason. Sonochem.* Vol. 29, 2016, 502-511.
- [4] Sališová, M., Toma, Š., and Mason, T. J., "Comparison of Conventional and Ultrasonically Assisted Extractions of Pharmaceutically Active Compounds from *Salvia Officinalis*," *Ultrason. Sonochem.* Vol. 4, no. 2, 1997, 131-134.
- [5] Muniz-Marquez, D. B., Martinez-Avila, G. C., Wong-Paz, J. E., Belmares-Cerda, R., Rodriguez-Herrera, R., and Aguilar, C. N., "Ultrasound-Assisted Extraction of Phenolic Compounds from *Laurus Nobilis* L. And Their Antioxidant Activity," *Ultrason. Sonochem.* Vol. 20, no. 5, 2013, 1149-1154.
- [6] Shirsath, S. R., Sable, S. S., Gaikwad, S. G., Sonawane, S. H., Saini, D. R., and Gogate, P. R., "Intensification of Extraction of Curcumin from *Curcuma Amada* Using Ultrasound Assisted Approach: Effect of Different Operating Parameters," *Ultrason. Sonochem.* Vol. 38, 2017, 437-445.
- [7] Liu, Q., Yang, X., Zhang, L., and Majetich, G., "Optimization of Ultrasonic-Assisted Extraction of Chlorogenic Acid from *Folium Eucommiae* and Evaluation of Its Antioxidant Activity," *J. Med. Plants Res.* Vol. 4, no. 23, 2010, 2503-2511.
- [8] Tsalagkas, D., Lagana, R., Poljansek, I., Oven, P., and Csóka, L., "Fabrication of Bacterial Cellulose Thin Films Self-Assembled from Sonochemically Prepared Nanofibrils and Its Characterization," *Ultrason. Sonochem.* Vol. 28, 2016, 136-143.
- [9] Jadhav, D., B.N, R., Gogate, P. R., and Rathod, V. K., "Extraction of Vanillin from Vanilla Pods: A Comparison Study of Conventional Soxhlet and Ultrasound Assisted Extraction," *J. Food Eng.* Vol. 93, no. 4, 2009, 421-426.
- [10] Jahouach-Rabai, W., Trabelsi, M., Van Hoed, V., Adams, A., Verhé, R., De Kimpe, N., and Frikha, M. H., "Influence of Bleaching by Ultrasound on Fatty Acids and Minor Compounds of Olive Oil. Qualitative and Quantitative Analysis of Volatile Compounds (by SPME Coupled to GC/MS)," *Ultrason. Sonochem.* Vol. 15, no. 4, 2008, 590-597.
- [11] Tabaraki, R., and Nateghi, A., "Optimization of Ultrasonic-Assisted Extraction of Natural Antioxidants from Rice Bran Using Response Surface Methodology," *Ultrason. Sonochem.* Vol. 18, no. 6, 2011, 1279-1286.

- [12] Thaipong, K., Boonprakob, U., Crosby, K., Cisneros-Zevallos, L., and Hawkins Byrne, D., "Comparison of ABTS, DPPH, FRAP, and ORAC Assays for Estimating Antioxidant Activity from Guava Fruit Extracts," *J. Food Compos. Anal.* Vol. 19, no. 6-7, 2006, 669-675.
- [13] Izadiyan, P., and Hemmateenejad, B., "Multi-Response Optimization of Factors Affecting Ultrasonic Assisted Extraction from Iranian Basil Using Central Composite Design," *Food Chem.* Vol. 190, 2016, 864-870.
- [14] Hofmann, T., Nebehaj, E., Stefanovits-Bányai, É., and Albert, L., "Antioxidant Capacity and Total Phenol Content of Beech (*Fagus Sylvatica* L.) Bark Extracts," *Ind. Crops Prod.* Vol. 77, 2015, 375-381.
- [15] Ainsworth, E. A., and Gillespie, K. M., "Estimation of Total Phenolic Content and Other Oxidation Substrates in Plant Tissues Using Folin-Ciocalteu Reagent," *Nat. Protoc.* Vol. 2, no. 4, 2007, 875-877.
- [16] Spigno, G., Tramelli, L., and De Faveri, D. M., "Effects of Extraction Time, Temperature and Solvent on Concentration and Antioxidant Activity of Grape Marc Phenolics," *J. Food Eng.* Vol. 81, no. 1, 2007, 200-208.
- [17] Ma, Y. Q., Chen, J. C., Liu, D. H., and Ye, X. Q., "Simultaneous Extraction of Phenolic Compounds of Citrus Peel Extracts: Effect of Ultrasound," *Ultrason. Sonochem.* Vol. 16, no. 1, 2009, 57-62.
- [18] Purohit, A. J., and Gogate, P. R., "Ultrasound-Assisted Extraction of β -Carotene from Waste Carrot Residue: Effect of Operating Parameters and Type of Ultrasonic Irradiation," *Sep. Sci. Technol.* Vol. 50, no. 10, 2015, 1507-1517.
- [19] Badve, M. P., Alpar, T., Pandit, A. B., Gogate, P. R., and Csóka, L., "Modeling the Shear Rate and Pressure Drop in a Hydrodynamic Cavitation Reactor with Experimental Validation Based on KI Decomposition Studies," *Ultrason. Sonochem.* Vol. 22, 2015, 272-277.
- [20] Khan, M. K., Abert-Vian, M., Fabiano-Tixier, A.-S., Dangles, O., and Chemat, F., "Ultrasound-Assisted Extraction of Polyphenols (Flavanone Glycosides) from Orange (*Citrus Sinensis* L.) Peel," *Food Chem.* Vol. 119, no. 2, 2010, 851-858.

[21] Dangles, O., "The Physico-Chemical Properties of Polyphenols-How Do They Relate to Their Roles in Plants, Foods and Human Health," *Agro Food Ind. Hi-tech* Vol. 17, no. 4, 2006, 64-67.

CHAPTER IV-
IDENTIFICATION OF CANNABINOIDS IN
***CANNABIS SATIVA L.* & THEIR ENTOURAGE**
EFFECTS WITH OTHER BIOACTIVE
CONSTITUENTS

4.1. Chapter synopsis

This chapter presents the identification and qualitative assessment of the ultrasonically extracted cannabinoids and other bioactive compounds using HPLC-DAD-MS/MS and GC-MS techniques, respectively. It discusses the biosynthesis and pharmacology of the cannabinoids. It sheds light on the various advantages of using *Cannabis* extracts exhibiting entourage effects over the pure cannabinoids as well as their safety concerns.

4.2. Synthesis, pharmacological and therapeutic effects of cannabinoids

The cannabinoids are synthesized in the secretory cells inside glandular trichomes that are highly concentrated in the unfertilized female flowers prior to senescence. Geranyl pyrophosphate, which is formed as a precursor via the deoxyxylulose pathway in *Cannabis*, is a parent compound to both cannabinoids and terpenoids [1]. The acidic forms of cannabinoids are decarboxylated by the action of heat into their more familiar neutral forms [2, 3].

Cannabinoids are known to interact with the endocannabinoid system in humans leading to several pharmacological effects [3]. Anandamide and 2-arachidonoyl glycerol are the two exogenous ligands to the cannabinoid receptors, CB₁ and CB₂ that belong to the superfamily of G protein-linked receptors. The cannabinoids have shown effects on motor coordination, limbic system, cardiovascular system and have also exhibited analgesic potential [4]. THC, the main psychoactive constituent of *Cannabis*, is well-known for its euphoriant, antiemetic, antioxidant, analgesic and anti-inflammatory effects [4, 5]. CBD, a psychotropically inactive and one of the most abundant cannabinoids in *Cannabis* also has a number of medicinal properties such as antioxidant, anxiolytic, antispasmodic, anti-inflammatory, analgesic and antipsychotic [1, 4].

The cannabinoids have proven their potential in the treatment of various ailments such as glaucoma, retinitis pigmentosa, pain and inflammation [6]. They have been found effective against the diseases of the central nervous system such as Alzheimer's Parkinson's and multiple sclerosis. Cannabinoids have been explored for the cardiovascular diseases like heart failure and cardiac arrhythmias. CBD has shown attenuating effects on myocardial dysfunction, oxidative stress, inflammation, fibrosis and cell death in mice [6]. Moreover, they have anti-cancer effects and are usually well-tolerated unlike the common chemotherapeutic drugs. The therapeutic effects of *Cannabis* vary among the

different chemotypes (type I-THC predominant, type II-mixed THC:CBD and type III-CBD predominant) depending on their chemical constitutions.

4.3. Administration of cannabinoids

Cannabinoids can be administered as pure cannabinoids that have been isolated from the other phytoconstituents or as phytoextracts that have the cannabinoids of interest coexisting with some other secondary metabolites such as flavonoids and terpenoids present in the extract. To date, a number of *Cannabis*-based products have been commercialized, which mainly include *Dronabinol*, *Marinol* and *Nabilone* (synthetic analogues of THC), *Sativex* (plant extract with THC and CBD in 1:1 ratio) and *Cannador* (plant extract with THC and CBD in 2:1 ratio) [7]. Having stated that, it is still a matter of debate whether it is more beneficial to administer cannabinoids in pure/isolated form or as extract in combination with other metabolites. To that effect, it is imperative to note here that not all the pharmacological benefits of *Cannabis* reside in its THC content. Consuming cannabinoids along with other secondary metabolites as in extracts may work synergistically with the main cannabinoid (usually THC) enhancing its positive effects or reducing its side effects. In other words, the secondary cannabinoids with different pharmacological activities, although non-psychotropic in nature, may modulate the action of THC [8]. One such cannabinoid is CBD, which has demonstrated anxiolytic properties in humans and animals to reduce the THC-induced anxiety. Further, CBD may enhance the analgesic potential of THC by inverse agonism at CB₂ receptor to produce anti-inflammatory effects and inhibition of immune cell migration [9]. Additionally, it may also modulate the potential negative effects of THC by means of antagonism at CB₁ receptor [10]. Thus the cannabinoid and non-cannabinoid compounds in *Cannabis* extracts may enhance its overall therapeutic potential.

4.4. Entourage effects of cannabinoids

Cannabis extracts have demonstrated a broad range of pharmacological effects for the therapeutic treatment of a plethora of disorders such as neuropathic pain [11, 12]. Perhaps the most important applications of *Cannabis* tend to be diseases, wherein the existing medications are not fully satisfactory with potential side effects of the drugs [8]. Recently, *Cannabis* extract rich in CBD was observed to ameliorate mucosal inflammation and hypermotility in mice more effectively than pure CBD both intraperitoneally and orally, which was attributed to the presence of the other cannabinoids as well as the non-

cannabinoid constituents such as terpenoids and flavonoids in the extract [13]. An *in vivo* study on murine models reported attenuation of colon carcinogenesis and inhibition of colorectal cancer cell proliferation using CBD-rich extracts *via* CB₁ and CB₂ receptor activation [14]. A THC:CBD mixed extract showed a more promising efficacy than THC extract alone for the treatment of pain in patients with advanced cancer, which was attributed to the synergy between them [15]. It must, however, be mentioned here that most of the work done so far evaluating the efficacy of *Cannabis* extracts is largely based on *in vitro* studies or preclinical studies involving animal models. It is also important to note that the therapeutic effects of cannabinoids are drastically influenced by the route of administration, dosage as well as the duration of exposure.

The unique properties of *Cannabis* also stem from the non-cannabinoid type constituents such as such as terpenoids, hydrocarbons, nitrogen compounds, phenols, fatty acids, flavonoids, alkaloids, phytosterols and carbohydrates in addition to alcohols, aldehydes, ketones, acids, esters and lactones [4, 16]. The lipophilic nature of most of the non-cannabinoid metabolites facilitates their permeation through the lipid membranes and hence the blood-brain barrier to exert the pharmacological effects [16]. For instance, *Cannabis* terpenoids may work both individually and synergistically with the cannabinoids to exert various therapeutic effects. They also influence the binding of THC to CB₁ receptors and have been linked to the modulation of various neurotransmitters and receptors that contribute to cannabinoid-mediated analgesia effects [16, 17]. They have been attributed a wide range of pharmacological attributes including anti-inflammatory, anxiolytic, analgesia, antidepressant, anti-insomnia, cancer chemoprevention, anti-microbial, and anti-hyperglycemic effect [18]. Likewise, *Cannabis* flavonoids, which act as antioxidants in plants, have shown the ability to alter the pharmacokinetics of THC and exhibit anti-inflammatory, anti-cancer and neuroprotective effects [19]. There have been studies demonstrating correlations between the dietary phenolic intake and reduced incidence of neurodegenerative diseases, cardiovascular disorders and cancers [20].

4.5. Identification of compounds in the *Cannabis* extract

4.5.1. Identification of cannabinoids using HPLC-DAD-MS/MS

Table 4.1 lists the major cannabinoids identified in the *Cannabis* extract and **Figure 4.1** shows the HPLC chromatogram indicating the peaks of various cannabinoids based on their elution from the column at different retention times. Identification of the major

cannabinoids by their MS/MS spectra and characteristic fragments was done using literature data [21-23]. The mass spectra of the cannabinoids are shown in **Figure 4.2-4.11**.

Table 4.1 Major cannabinoids identified in the 80% methanolic *Cannabis* extract using HPLC-DAD-MS/MS (superscript a: Very weak signals obtained, superscript b,c: Not enough evidence found)

Retention time (min)	Cannabinoid	Molecular formula	Molecular weight	Ionization mode and parent ion (m/z)		Major fragments (m/z)
				Negative [M-H] ⁻	Positive [M+H] ⁺	
<i>Neutral Cannabinoids</i>						
^a 15.16	11-OH-THC	C ₂₁ H ₃₀ O ₃	330.461	-	331	313, 193
16.89	CBD	C ₂₁ H ₃₀ O ₂	314.472	-	315	259, 193, 135, 123, 93
17.36	Δ ⁹ /Δ ⁸ -THC	C ₂₁ H ₃₀ O ₂	314.472	-	315	259, 193, 135, 123, 93
<i>Acidic Cannabinoids</i>						
^b 15.96	Cannabicoumaric acid OR 4-acetoxycannabichrome	C ₂₂ H ₂₉ O ₅	373.22	-	373	355, 337, 313, 220, 219
16.85	CBDVA	C ₂₀ H ₂₆ O ₄	330.424	329	-	311, 285, 283, 243, 217, 199, 151
^c 17.04	11-OH-THCA OR 10-ethoxy-9-hydroxy-Δ ^{6a} -THC	C ₂₂ H ₃₀ O ₅	374.482	373	-	330, 312, 272, 206
17.16	CBDA	C ₂₂ H ₃₀ O ₄	358.482	357	-	339, 313, 245, 179, 158
17.29	CBGA	C ₂₂ H ₃₂ O ₄	360.498	359	-	341, 315, 298, 191
17.34	Δ ⁹ -THCA-A	C ₂₂ H ₃₀ O ₄	358.482	357	-	339, 313, 289, 271, 245, 179
17.82	Δ ⁹ -THCVA	C ₂₀ H ₂₆ O ₄	330.424	329	-	311, 285, 233, 163
17.95	CBNA	C ₂₂ H ₂₆ O ₄	354.45	353	-	309, 294, 279, 265, 238, 222, 171
18.11	CBLA	C ₂₂ H ₃₀ O ₄	358.482	357	-	339, 313, 285, 245, 229, 191, 179
18.34	CBCA	C ₂₂ H ₃₀ O ₄	358.482	357	-	339, 313, 245, 191, 179

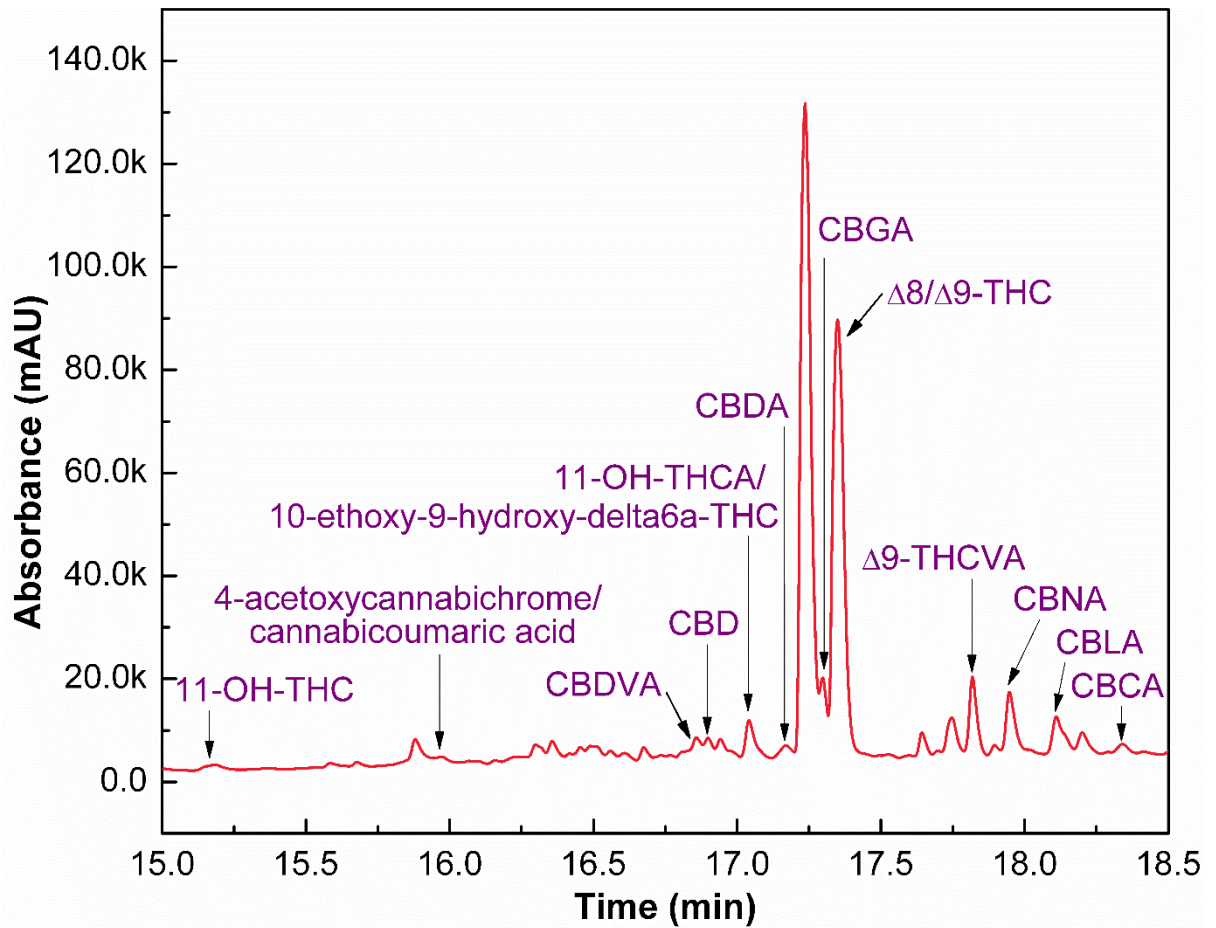


Figure 4.1 HPLC chromatogram showing various cannabinoids in the *Cannabis* extract

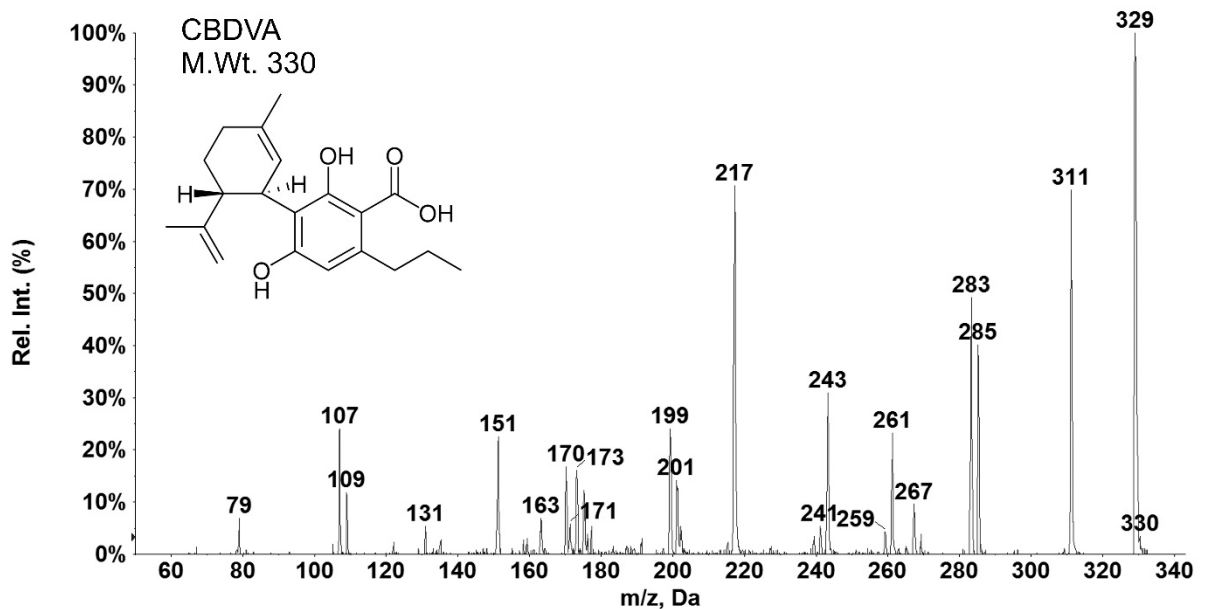


Figure 4.2 Mass spectrum of CBDVA

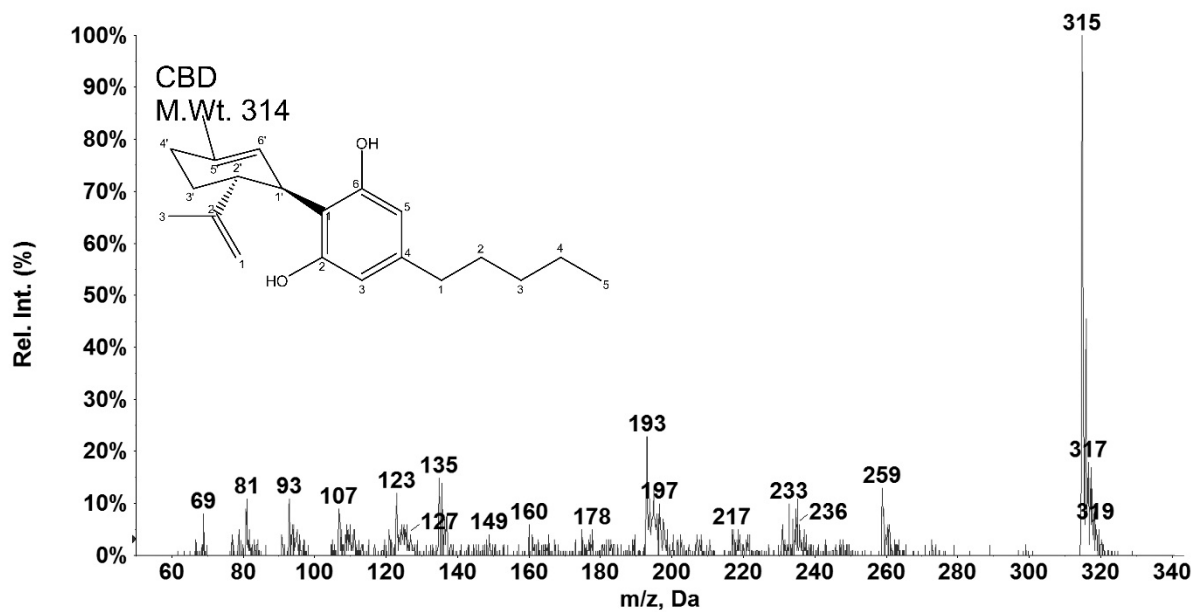


Figure 4.3 Mass spectrum of CBD

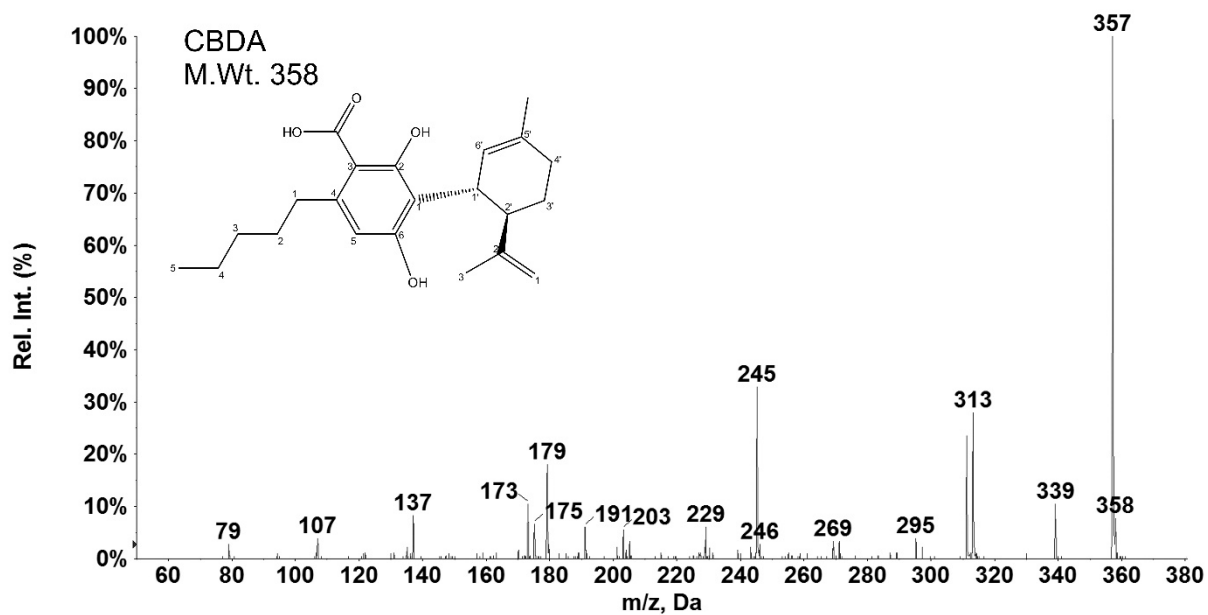


Figure 4.4 Mass spectrum of CBDA

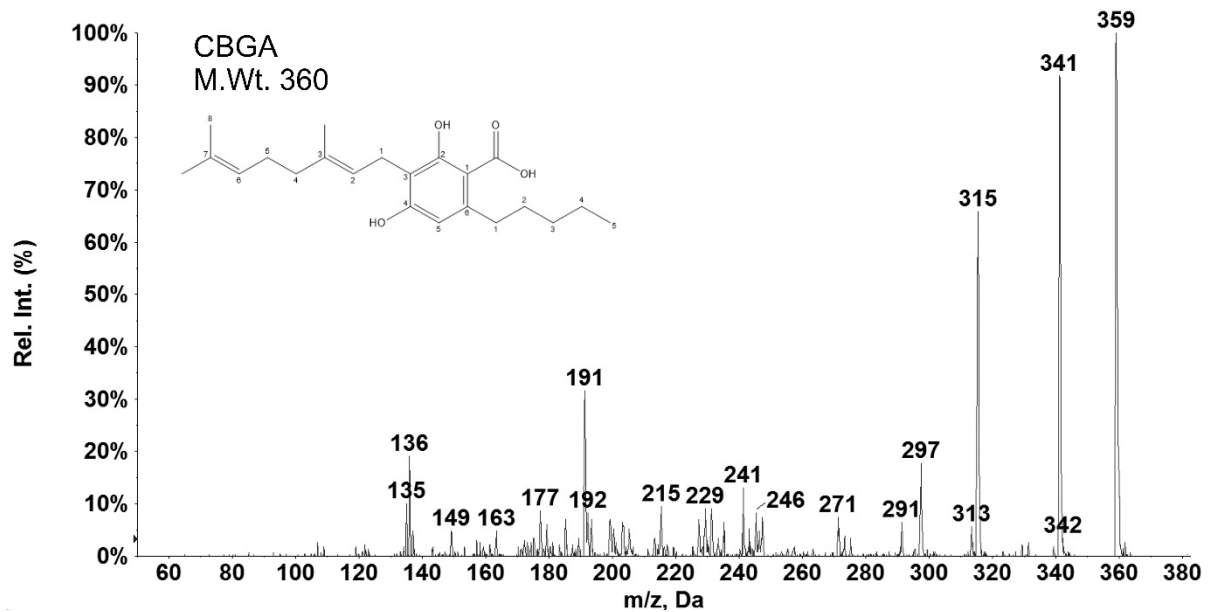


Figure 4.5 Mass spectrum of CBGA

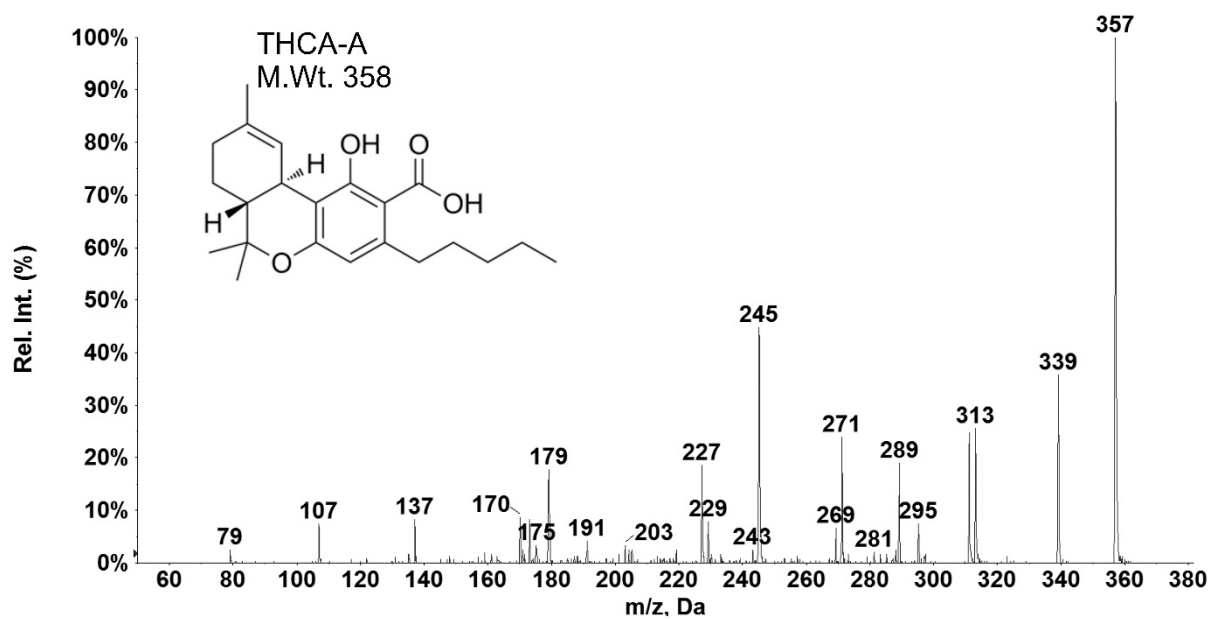


Figure 4.6 Mass spectrum of THCA-A

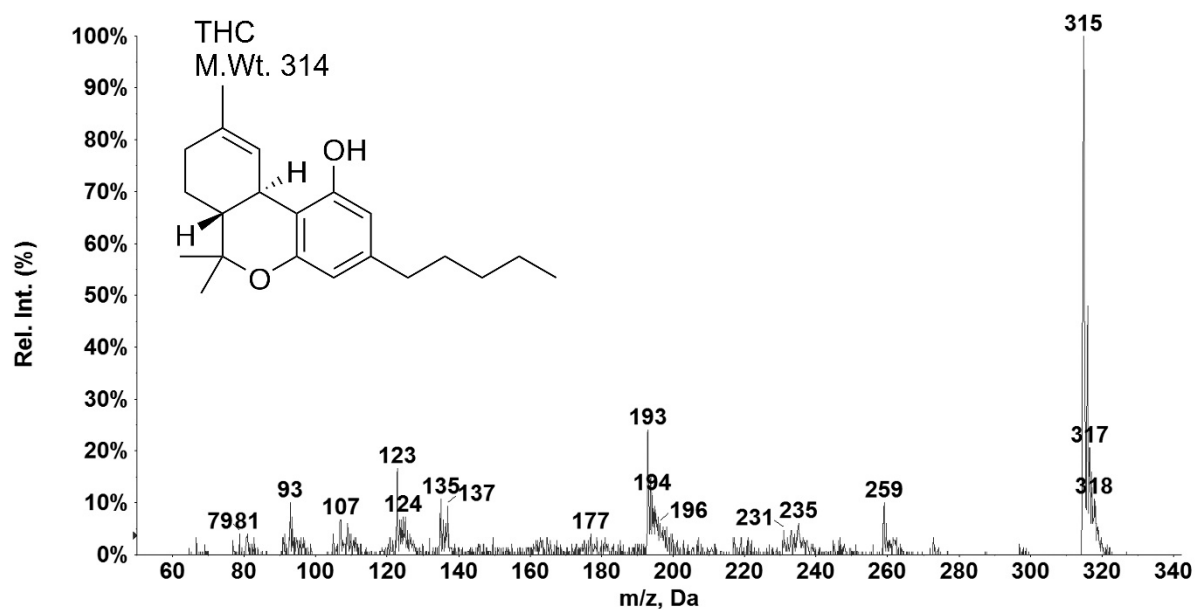


Figure 4.7 Mass spectrum of THC

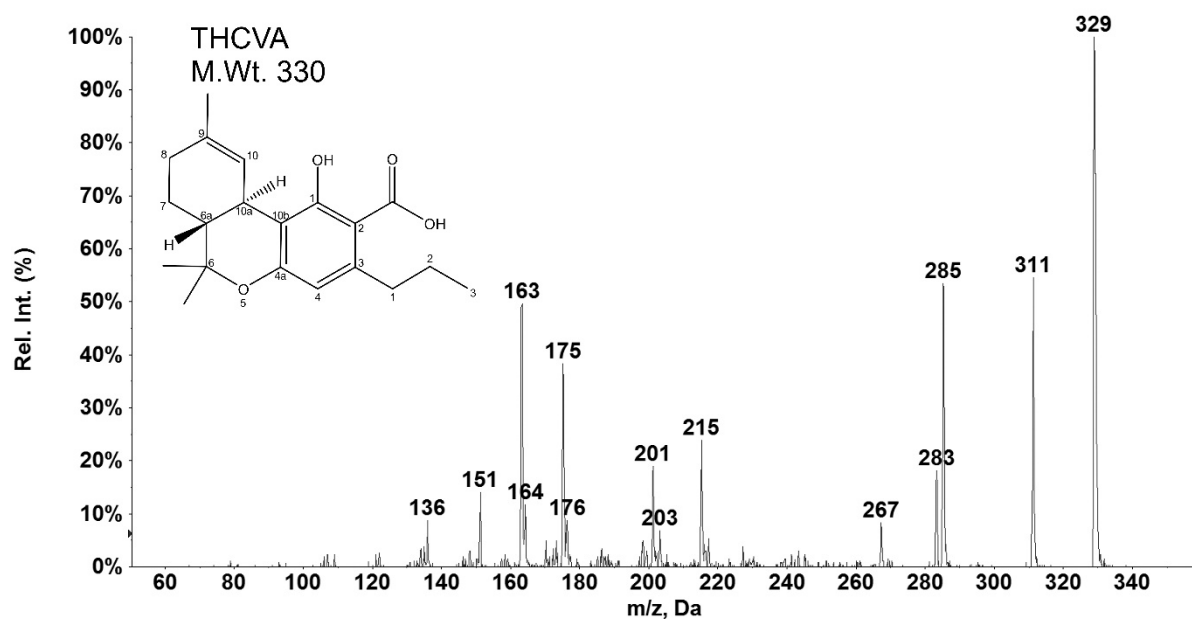


Figure 4.8 Mass spectrum of THCVA

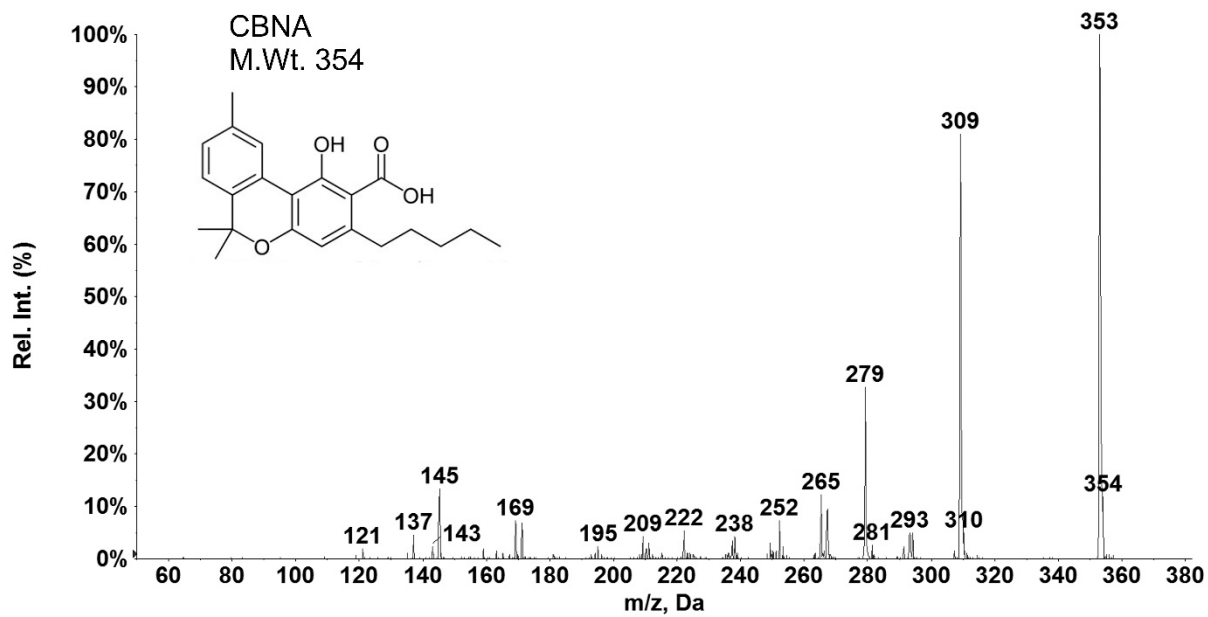


Figure 4.9 Mass spectrum of CBNA

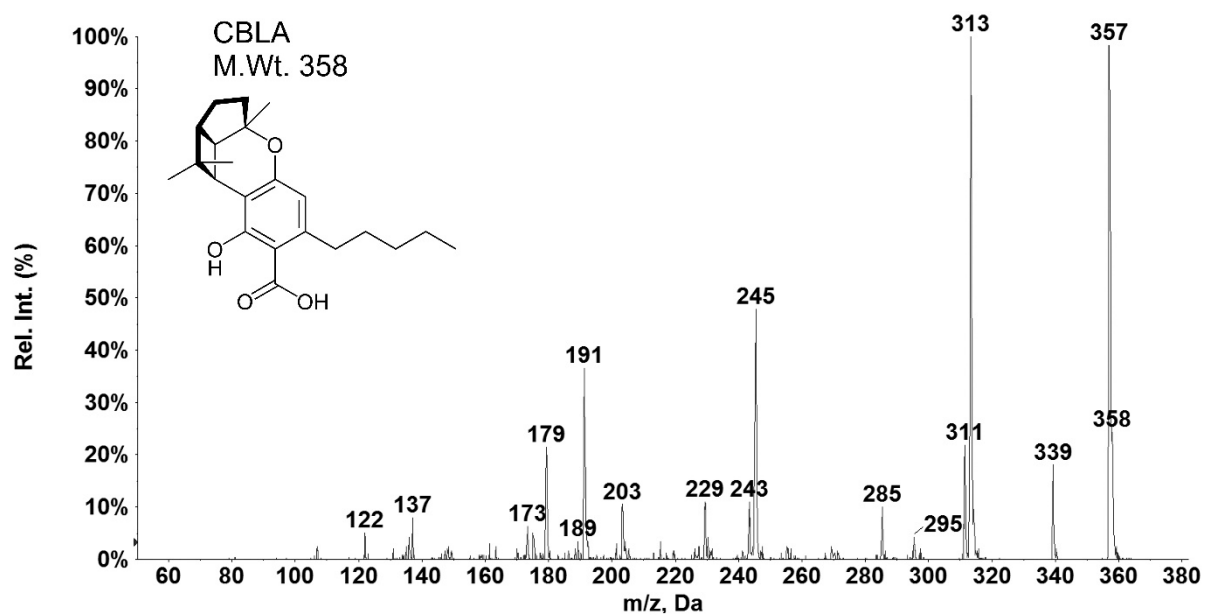


Figure 4.10 Mass spectrum of CBLA

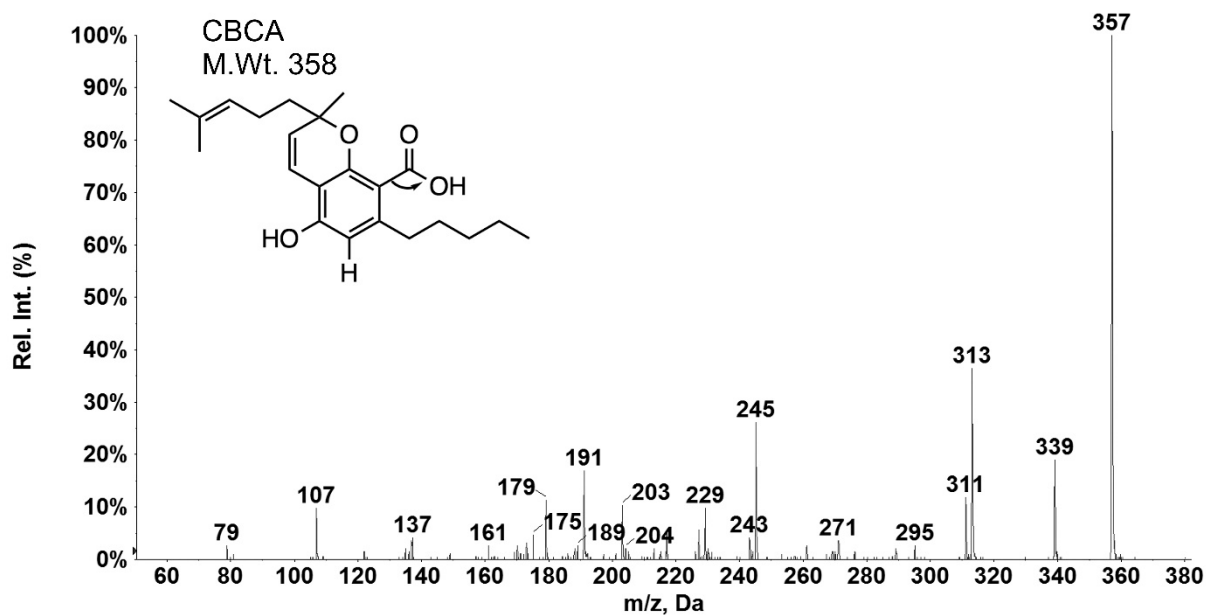


Figure 4.11 Mass spectrum of CBCA

4.5.2. Identification of other bioactive compounds using GC-MS

Apart from the cannabinoids, other bioactive compounds were identified in the methanolic *Cannabis* extract, as listed in **Table 4.2** using GC-MS technique (**Figure 4.12**). Common terpenes such as α -pinene, myrcene, β -caryophyllene and α -humulene were found to be present in the extract.

Table 4.2 Bioactive compounds identified in the methanolic *Cannabis* extract using GC-MS

Bioactive compounds in <i>Cannabis</i> extract
α -pinene
myrcene
dodecane
β -caryophyllene
α -humulene
caryophyllene oxide
tetradecanoic acid (myristic acid)
palmitic acid
phytol
resorcinol
tetratriacontane
delta-1,2-tetrahydrocannabinol
1,6-dibenzofurandiol,
cannabigerol
pentacosane
1-eicosanol

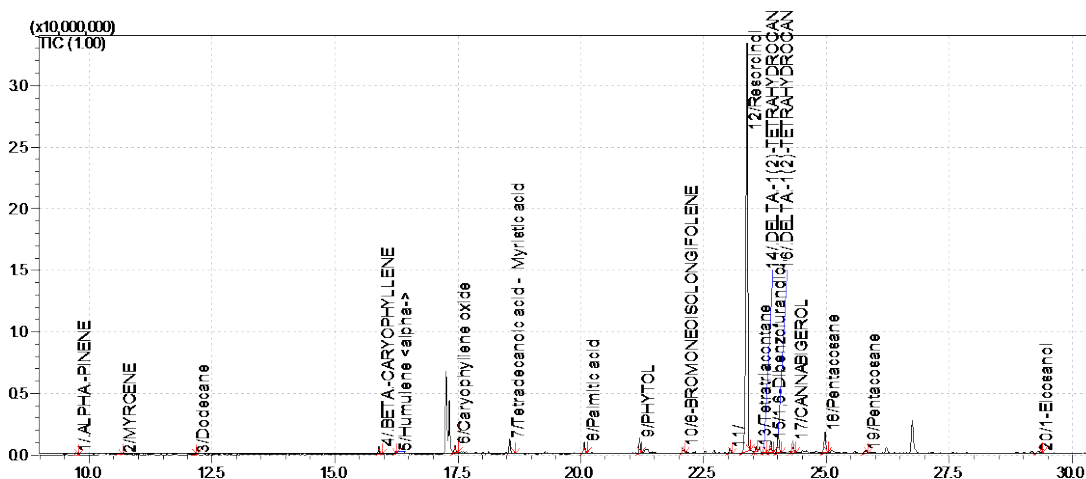


Figure 4.12 GC-MS chromatogram of non-cannabinoid bioactive compounds in the *Cannabis* extract

4.6. Adverse events and safety concerns

Despite the several benefits of *Cannabis* extracts, there have been reports of their adverse effects as well. Clinical study on epilepsy using CBD-rich extract showed signs of THC-induced intoxication followed by seizure worsening, whereas same dose of pure CBD led to improvement in intoxication signs and seizure remission [24]. This was possibly due to the combined effect of the psychopharmacological effects of THC and 11-OH-THC when the CBD-rich extract was taken orally. Thus, the relative doses of the cannabinoids of interest become significant for clinical evaluations considering that the pharmacological potency of THC is much higher than that of CBD, which implies that the amount of THC required to produce an effect will be much lower than that of CBD. Further, the pharmacokinetic interactions of THC and CBD raise safety concerns, for example, both can inhibit cytochrome P450 enzymes that affect the metabolism of the anticonvulsants commonly used with CBD [25].

4.7. Summary and inferences

Various cannabinoid and non-cannabinoid compounds extracted ultrasonically were identified in the *Cannabis* extract with the help of advanced chromatographic techniques. Several cannabinoids including THC, CBD, CBGA, CBDA, THCVA, CBLA, CBNA, CBCA, etc. were identified in the extract using HPLC-DAD-MS/MS. The other bioactive compounds identified using GC-MS included mostly the common terpenes, phytols, fatty acids, etc. The possible entourage effects between the cannabinoids and the non-cannabinoid bioactive compounds such as terpenes play a crucial role in determining

the pharmacokinetics of the main cannabinoid and thus its overall therapeutic potential. Having said that, it becomes imperative to assess the safety aspects of the cannabinoids and possible toxicity resulting from the synergistic effects. Further, the route of administration, dosage as well as the duration of exposure also influence the therapeutic value of the cannabinoids.

References

- [1] Russo, E. B., "Taming THC: Potential *Cannabis* Synergy and Phytocannabinoid-Terpenoid Entourage Effects," *Br. J. Pharmacol.* Vol. 163, no. 7, 2011, 1344-1364.
- [2] Baron, E. P., "Medicinal Properties of Cannabinoids, Terpenes, and Flavonoids in *Cannabis*, and Benefits in Migraine, Headache, and Pain: An Update on Current Evidence and *Cannabis* Science," *Headache* Vol. 58, no. 7, 2018, 1139-1186.
- [3] Andre, C. M., Hausman, J. F., and Guerriero, G., "*Cannabis Sativa*: The Plant of the Thousand and One Molecules," *Front. Plant Sci.* Vol. 7, 2016, 1-17.
- [4] ElSohly, M. A., *Marijuana and the Cannabinoids*, Humana Press Inc., New Jersey, 2007.
- [5] MacCallum, C. A., and Russo, E. B., "Practical Considerations in Medical *Cannabis* Administration and Dosing," *Eur. J. Intern. Med.* Vol. 49, 2018, 12-19.
- [6] Velmurugan, B. K., "Therapeutic Applications of Cannabinoids," *Chem. Biol. Interact.* Vol. 293, 2018, 77-88.
- [7] Kowal, M. A., Hazekamp, A., and Grotenhermen, F., "Review on Clinical Studies with *Cannabis* and Cannabinoids 2010-2014," *Mult. Scler.* Vol. 6, no. 1515, 2016, 202010-202014.
- [8] Williamson, E. M., and Evans, F. J., "Cannabinoids in Clinical Practice," *Drugs* Vol. 60, no. 6, 2000, 1303-1314.
- [9] Pertwee, R. G., "The Diverse CB₁ and CB₂ Receptor Pharmacology of Three Plant Cannabinoids: Δ^9 -Tetrahydrocannabinol, Cannabidiol and Δ^9 -Tetrahydrocannabivarin," *Br. J. Pharmacol.* Vol. 153, no. 2, 2008, 199-215.
- [10] Ripamonti, C., and Dickerson, E. D., "Strategies for the Treatment of Cancer Pain in the New Millennium," *Drugs* Vol. 61, no. 7, 2001, 955-977.

- [11] Rog, D. J., Nurmikko, T. J., Friede, T., and Young, C. A., "Randomized, Controlled Trial of *Cannabis*-Based Medicine in Central Pain in Multiple Sclerosis," *Neurology* Vol. 65, no. 6, 2005, 812-819.
- [12] Selvarajah, D., Gandhi, R., Emery, C. J., and Tesfaye, S., "Randomized Placebo-Controlled Double-Blind Clinical Trial of *Cannabis*-Based Medicinal Product (Sativex) in Painful Diabetic Neuropathy: Depression Is a Major Confounding Factor," *Diabetes care* Vol. 33, no. 1, 2010, 128-130.
- [13] Pagano, E., Capasso, R., Piscitelli, F., Romano, B., Parisi, O. A., Finizio, S., Lauritano, A., Marzo, V. D., Izzo, A. A., and Borrelli, F., "An Orally Active *Cannabis* Extract with High Content in Cannabidiol Attenuates Chemically-Induced Intestinal Inflammation and Hypermotility in the Mouse," *Front. Pharmacol.* Vol. 7, 2016, 341.
- [14] Romano, B., Borrelli, F., Pagano, E., Cascio, M. G., Pertwee, R. G., and Izzo, A. A., "Inhibition of Colon Carcinogenesis by a Standardized *Cannabis Sativa* Extract with High Content of Cannabidiol," *Phytomedicine* Vol. 21, no. 5, 2014, 631-639.
- [15] Johnson, J. R., Burnell-Nugent, M., Lossignol, D., Ganae-Motan, E. D., Potts, R., and Fallon, M. T., "Multicenter, Double-Blind, Randomized, Placebo-Controlled, Parallel-Group Study of the Efficacy, Safety, and Tolerability of THC: CBD Extract and THC Extract in Patients with Intractable Cancer-Related Pain," *J. Pain Symptom Manag.* Vol. 39, no. 2, 2010, 167-179.
- [16] Ramirez, M. R., "Potential Health Benefits of *Cannabis* Extracts: A Review," *Int. J. Chem. Biol. Sci.* Vol. 2, no. 1, 2016, 1-8.
- [17] McPartland, J. M., and Russo, E. B., "*Cannabis* and *Cannabis* Extracts: Greater Than the Sum of Their Parts?" *J. Cannabis Ther.* Vol. 1, no. 3-4, 2001, 103-132.
- [18] Paduch, R., Kandefer-Szerszeń, M., Trytek, M., and Fiedurek, J., "Terpenes: Substances Useful in Human Healthcare," *Arch. Immunol. Ther. Exp.* Vol. 55, no. 5, 2007, 315-327.
- [19] Andre, C. M., Larondelle, Y., and Evers, D., "Dietary Antioxidants and Oxidative Stress from a Human and Plant Perspective: A Review," *Curr. Nutr. Food Sci.* Vol. 6, no. 1, 2010, 2-12.
- [20] Arts, I. C. W., and Hollman, P. C. H., "Polyphenols and Disease Risk in Epidemiologic Studies," *Am. J. Clin. Nutr.* Vol. 81, no. 1, 2005, 317S-325S.

- [21] Aizpurua-Olaizola, O., Omar, J., Navarro, P., Olivares, M., Etxebarria, N., and Usobiaga, A., "Identification and Quantification of Cannabinoids in *Cannabis Sativa* L. Plants by High Performance Liquid Chromatography-Mass Spectrometry," *Anal. Bioanal. Chem.* Vol. 406, no. 29, 2014, 7549-7560.
- [22] De Backer, B., Debrus, B., Lebrun, P., Theunis, L., Dubois, N., Decock, L., Verstraete, A., Hubert, P., and Charlier, C., "Innovative Development and Validation of an HPLC/DAD Method for the Qualitative and Quantitative Determination of Major Cannabinoids in *Cannabis* Plant Material," *J. Chromatogr. B* Vol. 877, no. 32, 2009, 4115-4124.
- [23] Hazekamp, A., Peltenburg, A., Verpoorte, R., and Giroud, C., "Chromatographic and Spectroscopic Data of Cannabinoids from *Cannabis Sativa* L.," *J. Liq. Chromatogr. Relat. Technol.* Vol. 28, no. 15, 2005, 2361-2382.
- [24] Crippa, J. A., Crippa, A., Hallak, J. E., Martín-Santos, R., and Zuardi, A. W., " Δ^9 -THC Intoxication by Cannabidiol-Enriched *Cannabis* Extract in Two Children with Refractory Epilepsy: Full Remission after Switching to Purified Cannabidiol," *Front. Pharmacol.* Vol. 7, 2016, 359.
- [25] Geffrey, A. L., Pollack, S. F., Bruno, P. L., and Thiele, E. A., "Drug-Drug Interaction between Clobazam and Cannabidiol in Children with Refractory Epilepsy," *Epilepsia* Vol. 56, no. 8, 2015, 1246-1251.

CHAPTER V-
IN SITU GREEN SYNTHESIS AND
FUNCTIONALIZATION OF REDUCED
GRAPHENE OXIDE ON CELLULOSE FIBERS
BY *CANNABIS SATIVA L.* EXTRACT

5.1. Chapter synopsis

This chapter presents a discussion on the green reduction and simultaneous functionalization of graphene oxide on cellulose fibres using the aqueous extract from the inflorescences of *Cannabis*. The graphene oxide, synthesized using the modified Hummer's method, was reduced in situ on the cellulose matrix in presence of the extract without external stabilizers in order to functionalize the fibres with RGO. The characterization of RGO/cellulose composites using advanced analytical techniques and their electrical performance has been comprehensively elucidated.

5.2. Morphology and structure analysis

5.2.1. SEM analysis

The morphological analysis of the RGO/cellulose composites by SEM was done to study the surface interaction between RGO and the cellulose fibres as shown in **Figure 5.1**. The blank specimen (**Figure 5.1a**) shows the unmodified surface of the randomly oriented cellulose fibres against those modified with increasing concentrations of RGO from 0.1 to 10 m/m % (**Figure 5.1 b-f**). It was observed that the sheet-like RGO uniformly and homogeneously covered the individual cellulose fibre surface and did not alter the fibre morphology. Air voids were found to be present between the fibres even at higher RGO contents, which were seemingly a consequence of the handsheet-making technique employed for the fabrication of the composites as against other methods of fabrication such as solvent casting [1, 2], flow-directed assembly of individual nanosheets [3] and vacuum filtration through a filter paper [4]. Further, even without the use of any external stabilizers, no agglomeration of RGO layers was observed despite their tendency to aggregate arising from the strong van der Waals forces, which may be on account of (1) the rough surface of cellulose fibres, which explains their strong adhesion to the RGO sheets, and (2) the phytoconstituents present in the *Cannabis* extract, which served not only as effective reducing agents but also as stabilizing agents. It is important to note that the RGO layers have a strong binding affinity to the cellulose fibre surface on account of both hydrogen bonding and chemical bonding, which has been pointed out previously [5]. Although RGO homogeneously coated the cellulose matrix, the air voids hindered the physical contact between the RGO layers, which in turn prevented the formation of an effective conductive network contributing to the high surface resistivity of the composites even at high RGO loadings as confirmed by the measurements.

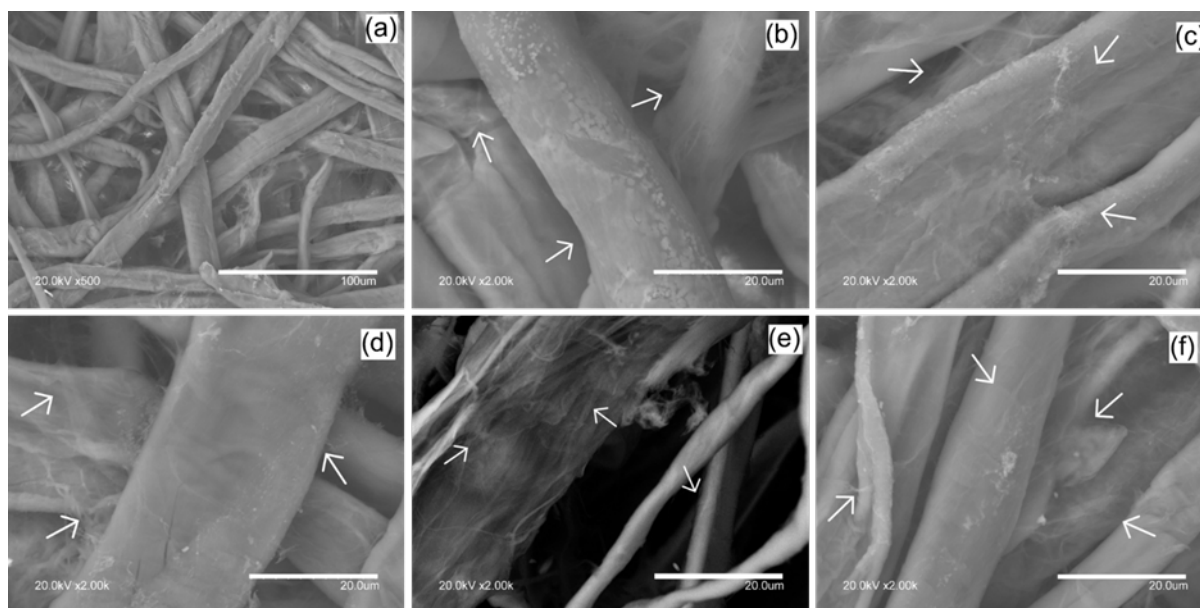


Figure 5.1 SEM images of RGO/cellulose composites at various RGO loadings: (a) 0 m/m %, (b) 0.1 m/m %, (c) 1 m/m %, (d) 2 m/m %, (e) 5 m/m % and (f) 10 m/m % (the arrows indicate the dispersion of RGO on the cellulose fibre surface)

5.2.2. FTIR analysis

The structural composition of the RGO/cellulose composites was investigated using FTIR and XRD techniques. As can be seen from **Figure 5.2a**, the FTIR spectrum of the GO powder synthesized by Hummer's method shows typical bands corresponding to the covalently bonded oxygen-containing functional moieties such as carboxyl, carbonyl, epoxy and hydroxyl. Characteristic bands were observed due to stretching vibration of hydroxyl (O-H) groups at 3300 cm^{-1} , stretching vibration of carboxyl and carbonyl (C=O) groups at 1715 cm^{-1} and stretching vibration of alkoxy (C-O) groups at 1039 cm^{-1} [6, 7]. The bands corresponding to symmetric and asymmetric stretching vibrations of epoxy (C-O-C) groups occur at 1160 cm^{-1} and 875 cm^{-1} , respectively [5]. Another band at 1620 cm^{-1} can be attributed to the skeletal vibrations (C=C) of un-oxidized graphitic regions or the stretching deformation vibration of intercalated water [8]. On the other hand, the spectrum for RGO powder synthesized via the green route clearly illustrates dramatic decrease in the band intensities of the oxygen groups indicating effective reduction of GO by the *Cannabis* extract. It is worthwhile to mention that the carbonyl, carboxyl, alkoxy and epoxy functionalities have almost disappeared after merely 3 h of reduction using the plant extract. Additionally, the C-H stretching vibration band at 2926 cm^{-1} observed for GO has vanished

for RGO indicating dehydrogenation and recovery of the C=C backbone. This confirms the ability of the extract to significantly reduce the oxygen species in GO to form RGO.

Figure 5.2b shows the FTIR spectra of cellulose functionalized with various contents of RGO synthesized in situ in presence of the extract. It is clear that the spectra of the composites are very similar to that of the blank specimen, which directly gives an evidence of the successful functionalization of RGO on the cellulose fibres. Pure cellulose shows characteristic bands for O-H stretching at 3333 cm^{-1} , C-H stretching at 2900 cm^{-1} , CH_2 symmetric bending at 1428 cm^{-1} and C-O symmetric stretching at 1316 cm^{-1} [9]. All these bands can be observed for the RGO/cellulose composites indicating that the cellulose structure remained unaltered even after the reduction with the extract and anchorage of RGO on the fibres. Furthermore, the presence of electron-rich hydroxyl and ether groups in cellulose makes it a suitable reducing agent [10, 11]. Thus, the presence of *Cannabis* extract and cellulose created a synergistic effect for the simultaneous reduction and functionalization of RGO on the surface of the cellulose fibres.

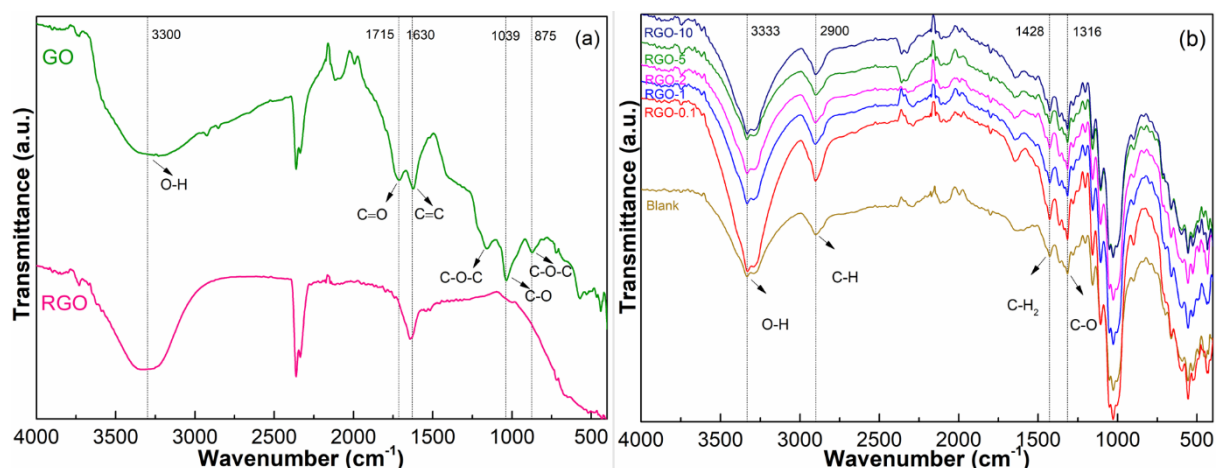


Figure 5.2 FTIR spectra of (a) GO & RGO powders and (b) RGO/cellulose composites with various RGO loadings

5.3. X-ray diffraction and photoelectron spectroscopy analysis

5.3.1. XRD analysis

The XRD patterns for GO and RGO are shown in **Figure 5.3a**. The spectrum for GO shows distinct diffraction peaks at 2θ values of 8.1° and 30.1° , which are assigned to the (002) and (100) planes of GO, respectively [12]. Additionally, the peak at 52.9° can be ascribed to the (004) plane of residual graphite [13]. The peak broadening for the (002) reflection in GO arises due to lattice distortion in the stacking order of the graphite lattice

due to its oxidation [14]. The intensity of these peaks decreased dramatically after reduction with *Cannabis* extract due to removal of the oxygen-containing functional groups. As a result, the interlayer distance between graphene sheets decreased due to restacking, thus shifting the peak to a higher 2θ value of 13.5° , which indicates the formation of graphene nanosheets having a thickness of a few layers in case of RGO [15]. It suggests that the conjugated graphene network of sp^2 -hybridized carbon was restored during the reduction process. It should also be noted here that the degree of exfoliation of RGO is controlled by the interactions between the functional groups in the adjacent sheets along with the lateral interactions due to terminal carboxyl groups [12]. The peaks appearing at 30.1° in GO and around 31° in RGO, indicate a short-range order in stacked graphene layers [13]. Furthermore, a sharp peak appearing at $2\theta = 4.3^\circ$ in RGO may be due to the organic components of the plant extract, which has also been found in other reports [15-17].

The diffraction spectra for the RGO/cellulose composites are very similar to that of the blank specimen (**Figure 5.3b**). All the composites show well-defined major peaks at 10.7° , 11.9° , 14.7° , 16.2° and 24.6° along with some other smaller peaks, which correspond to the I β form of crystalline cellulose [18], indicating homogeneous dispersion of RGO on cellulose. It should also be noted that the peak at 2θ value of 8.1° corresponding to GO (**Figure 5.3a**) disappeared in the XRD spectra of the RGO/cellulose composites (**Figure 5.3b**), which confirmed significant reduction of GO and the exfoliation of layered GO in the cellulose matrix [3]. Moreover, it did not have a significant effect on the crystallinity of cellulose, which remained intact even after reduction with *Cannabis* extract.

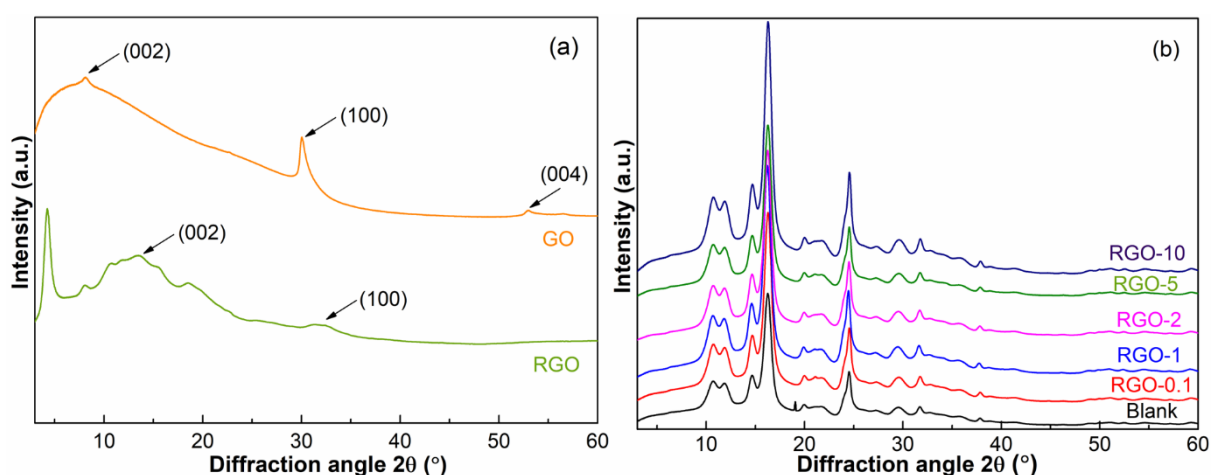


Figure 5.3 XRD spectra of (a) GO & RGO powders and (b) RGO/cellulose composites with various RGO loadings

5.3.2. XPS analysis

The chemical composition of GO and RGO was further confirmed by high-resolution XPS spectra as shown in **Figure 5.4**. In order to reveal the various carbon–oxygen groups, the spectra were fitted using the Gaussian–Lorentzian function to individual components with the reported binding energy values of C 1s and O 1s photoelectrons characteristic for the particular groups [19–21]. It should also be noted here that the binding energy depends on the synthesis of GO as well as on the reaction parameters during the reduction process [22, 23].

The C 1s region spectrum for GO shows six different signals present, two of which can be assigned to the carbon skeleton bonding of the sp^2 (284.5 eV) and sp^3 (285.2 eV)-hybridized states of the graphitic structure (**Figure 5.4a**) [13]. The other four signals correspond to the various oxygen-containing functional groups on the surface of the GO due to the oxidation of graphite- hydroxyl (286.4 eV), epoxy/alkoxy (287.1 eV), carbonyl (288 eV) and carboxyl (289.2 eV) [13]. Although similar signals were observed at almost the same positions for RGO, a considerable increase in the C sp^2 peak intensity along with an appreciable decrease in the peak intensities of the oxygen-bearing carbon groups, especially the epoxy/alkoxy group, confirms the removal of most of the oxygen-containing functionalities after reduction with *Cannabis* extract (**Figure 5.4b**).

In the O 1s region spectrum for GO (**Figure 5.4c**), the signals were observed for hydroxyl (532.2 eV), epoxy (533.1 eV), carbonyl (531.2 eV), carboxyl C=O (531.8 eV), carboxyl C-O (534.1 eV) and water (535.0 eV), which were within the typical range of their binding energy values [21]. After reduction, the peak intensities of epoxy and carbonyl groups dropped, which is clear from the O 1s spectrum of RGO (**Figure 5.4d**). However, the carboxyl and hydroxyl groups exhibited a rise in their peak intensities, which could be possibly due to the release of water from the water-oxygen groups during the reduction of GO [13]. Thus, it is evident that the number of oxidizing groups on the surface of GO decreased significantly post-reduction with *Cannabis* extract.

The mechanism of reduction of GO by phytoextracts has been documented earlier [24]. The plant extracts contain various classes of chemical compounds with a potential to be easily oxidized including phenols, simple sugars, polysaccharides, amino acids, fatty acids, vitamins, minerals and enzymes. The carboxyl, hydroxyl and epoxy groups in GO

undergo condensation reactions with the reduced forms in the extract causing ring cleavage, which facilitates the reduction of GO.

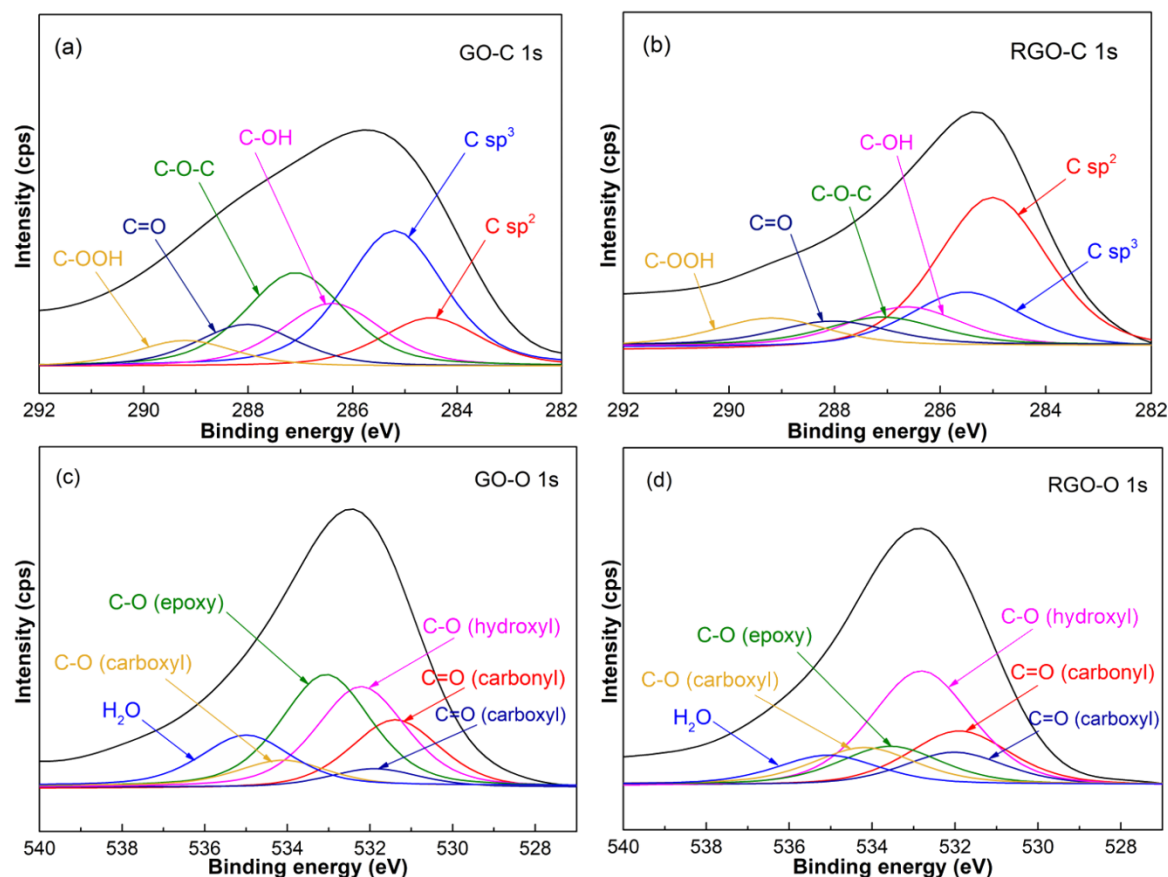


Figure 5.4 XPS spectra of GO and RGO powders (a, b) C 1s region and (c, d) O 1s region

5.4. Electrical performance study

The surface resistivity of the RGO/cellulose composites as a function of RGO loading measured at 40 V is plotted in **Figure 5.5**. Clearly, the surface resistivity of the composites considerably decreased with increasing RGO content, showing a polynomial fit with R^2 value of 0.98. With just 0.1 m/m % RGO loading, the surface resistivity at 40 V showed a marked drop by over a 100 orders of magnitude compared to that of the blank specimen ($420 \times 10^{11} \Omega$). The lower surface resistivity values for the composites against the blank specimen resulted from the functionalization of the cellulose fibres with RGO. By increasing the RGO loading of the composites from 0.1 m/m % to 10 m/m %, the surface resistivity showed an over tenfold drop from 1.81×10^{11} to $0.15 \times 10^{11} \Omega$, which resulted from the incorporation of RGO within the fibre matrix. It should also be noted that although the magnitude of the surface resistivity increased by increasing the applied voltage, the trend remained more or less similar. The considerably high values of surface resistivity can

be attributed to the presence of air voids within the cellulose fibre matrix, which became less dominant due to the filling of voids between the fibres with increase in RGO content. It confirms that the air voids acted as an obstacle to prevent the formation of an effective conductive network of RGO layers, as observed in the morphological study. The electrostatic interaction between the functional groups on the cellulose fibres and RGO sheets resulted in the strong binding of RGO over the fibre surface, thus leaving the voids. Therefore, the RGO itself contributed only a minor fraction towards decreasing the surface resistivity of the RGO/cellulose composites, which were comparable to that of air and pure cellulose ($3000 \times 10^{11} \Omega$) [25]. It also explains why the surface resistivity values obtained for the composites are several orders of magnitude higher than the previously reported ones for the same RGO content [2]. It is worth mentioning that the voids existed even at higher RGO loading, which indicates that the cellulose matrix was porous enough with a potential to hold more RGO. Further, the green-synthesized RGO coating on cellulose fibre surface did not decrease the surface resistivity below $10^{10} \Omega$, which would be a desirable feature for many applications in order to avoid static electrical problems.

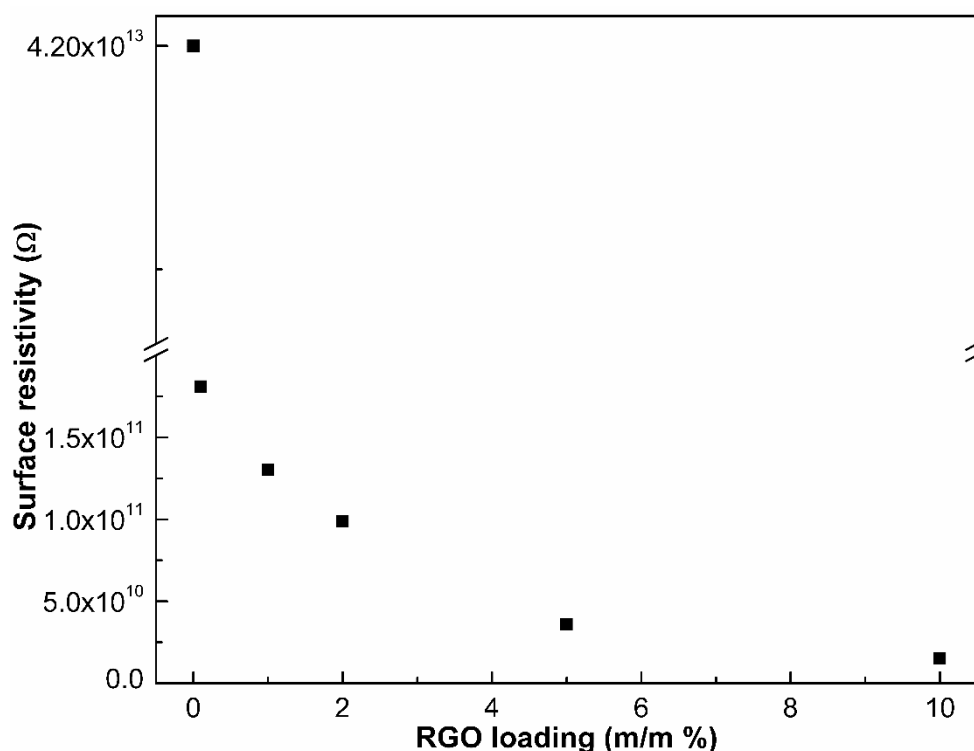


Figure 5.5 Surface resistivity of RGO/cellulose composites with increasing RGO loading from 0-10 m/m % at 40 V

The surface charging capacity of the RGO/cellulose composites with increasing RGO loading in Δ mAh at 40 V is summarized in *Table 5.1*. It was recorded by calculating

the averages of the differences in the surface charging after each 60 s interval to give $\Delta nC/60$ s. At a given voltage, the surface charging capacity was found to decrease markedly as the RGO content increased. A sharp drop in the surface charging capacity can be seen after increasing the RGO loading from 0.1 to 1 m/m %. This indicates that more charging time was required to achieve the same amount of charging as the RGO content in the cellulose matrix increased, which is also consistent with the previous observations [26]. It was observed that the surface charging values were not saturated after 1 hour of DC charging and their magnitude increased with the voltage. It should be noted, however, that the trend of the surface charging capacities for the composites remained the same at all the measured voltages.

Table 5.1 Surface charging capacity of RGO/cellulose composites with different RGO loadings at 40 V

Surface charging capacity	RGO loading (m/m %)					
	0	0.1	1	2	5	10
$\Delta nC/60$ s at 40V	7.03	269.75	173.87	107.17	58.23	54.89
ΔmAh at 40V	8.24×10^{-7}	1.21×10^{-3}	5.04×10^{-4}	1.91×10^{-4}	5.65×10^{-5}	5.02×10^{-5}

Figure 5.6 shows the logarithmic plot of RGO loading *versus* the surface charging capacity in ΔmAh at 40 V, demonstrated by a polynomial fitting with R^2 value of 0.99. It is evident that the surface charging capacity dropped by two orders of magnitude from 1.21×10^{-3} ΔmAh to 5.02×10^{-5} ΔmAh as the RGO loading was increased from 0.1 m/m % to 10 m/m %. The drop in surface charging capacity confirms the rise in conductivity with increasing RGO loading, which has also been reported by other studies [5, 27]. The very high surface charging capacity at 0.1 m/m % RGO content shows that there was very little physical contact between the conducting layers of RGO. The drastic fall of the surface charging capacity when the RGO loading was increased from 0.1 to 1 m/m % indicated that the contact between the RGO-functionalized fibres had come into being within the cellulose matrix. However, even after doubling the RGO content from 5 to 10 m/m % there was only a marginal drop in the surface charging capacity due to the air pockets between the fibres, which hampered the formation of an effective conducting network, as is clear from the $\Delta nC/60$ s values in **Table 5.1**. It is also worthwhile to note here that the measured

properties are significantly influenced by the degree of reduction of RGO, which can be readily tuned by altering the reaction parameters such as the time, temperature and amount of the reducing agent.

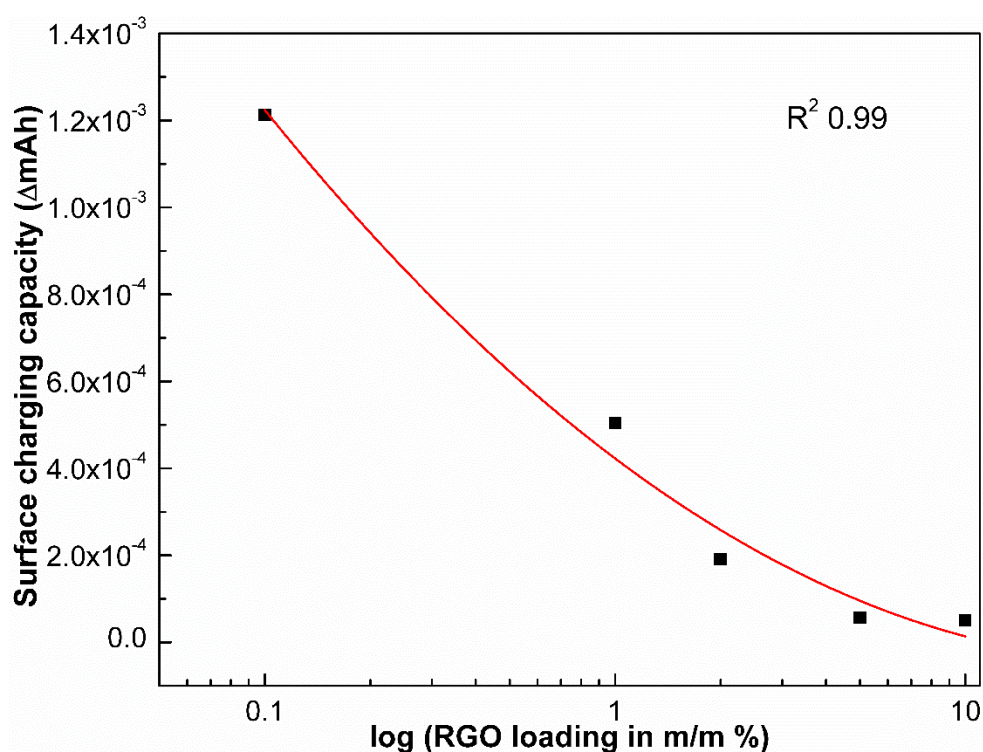


Figure 5.6 Surface charging capacity of RGO/cellulose composites with increasing RGO loading from 0.1-10 m/m % on log scale at 40 V

5.5. Summary and inferences

An in-depth analysis for the green and facile reduction with simultaneous functionalization of GO carried out in situ on the cellulose fibres using the aqueous extract from the inflorescences of *Cannabis* has been presented. The composites were fabricated with different contents of RGO ranging from 0.1 to 10 m/m %. The cellulose fibres served a dual role of a supporting matrix with excellent anchorage to RGO resulting from strong electrostatic surface interactions as well as a reductant due to the presence of free hydroxyl and ether groups. Morphological analysis revealed a homogeneous coating of RGO over the fibre surface with uniform dispersion throughout the porous cellulose matrix thus eliminating the need for additional stabilizing agents. The spectroscopic and diffraction techniques confirmed successful removal of oxygen-containing functional groups and in situ reduction of GO on the cellulose fibres. The RGO/cellulose composites exhibited a drop in surface resistivity with increasing RGO content from to $1.81 \times 10^{11} \Omega$ for 0.1 m/m

% RGO to $0.15 \times 10^{11} \Omega$ for 10 m/m % RGO loading at 40 V. Similarly, the surface charging capacity of the composites at 40 V dropped from $1.21 \times 10^{-3} \Delta\text{mAh}$ for 0.1 m/m % RGO to $0.05 \times 10^{-3} \Delta\text{mAh}$ for 10 m/m % RGO content, which can be exploited for many electrical applications. The presence of air voids within the cellulose fibre matrix hindered the physical contact between the RGO layers and significantly affected the electrical properties. The porosity of the cellulose fibre matrix and the strong interaction between RGO and cellulose played an instrumental role in determining the performance of the composites. Thus, employing *Cannabis* extract for the green reduction of GO seems to be an appealing choice as compared to the conventional reducing agents.

References

- [1] Kafy, A., Sadasivuni, K. K., Kim, H. C., Akther, A., and Kim, J., "Designing Flexible Energy and Memory Storage Materials Using Cellulose Modified Graphene Oxide Nanocomposites," *Phys. Chem. Chem. Phys.* Vol. 17, no. 8, 2015, 5923-5931.
- [2] Mianehrow, H., Sabury, S., Bazargan, A. M., Sharif, F., and Mazinani, S., "A Flexible Electrode Based on Recycled Paper Pulp and Reduced Graphene Oxide Composite," *J. Mater. Sci. Mater. Electron.* Vol. 28, no. 6, 2016, 4990-4996.
- [3] Peng, H., Meng, L., Niu, L., and Lu, Q., "Simultaneous Reduction and Surface Functionalization of Graphene Oxide by Natural Cellulose with the Assistance of the Ionic Liquid," *J. Phys. Chem. C* Vol. 116, no. 30, 2012, 16294-16299.
- [4] Weng, Z., Su, Y., Wang, D.-W., Li, F., Du, J., and Cheng, H.-M., "Graphene-Cellulose Paper Flexible Supercapacitors," *Adv. Energy Mater.* Vol. 1, no. 5, 2011, 917-922.
- [5] Luong, N. D., Pahimanolis, N., Hippi, U., Korhonen, J. T., Ruokolainen, J., Johansson, L.-S., Nam, J.-D., and Seppälä, J., "Graphene/Cellulose Nanocomposite Paper with High Electrical and Mechanical Performances," *J. Mater. Chem.* Vol. 21, no. 36, 2011, 13991-13998.
- [6] Chen, J., Yao, B., Li, C., and Shi, G., "An Improved Hummers Method for Eco-Friendly Synthesis of Graphene Oxide," *Carbon* Vol. 64, 2013, 225-229.
- [7] Zhang, J., Yang, H., Shen, G., Cheng, P., Zhang, J., and Guo, S., "Reduction of Graphene Oxide Via L-Ascorbic Acid," *Chem. Commun. (Camb.)* Vol. 46, no. 7, 2010, 1112-1114.

- [8] Feng, H., Cheng, R., Zhao, X., Duan, X., and Li, J., "A Low-Temperature Method to Produce Highly Reduced Graphene Oxide," *Nat. Commun.* Vol. 4, 2013, 1539-1546.
- [9] Wan, C., Jiao, Y., and Li, J., "Flexible, Highly Conductive, and Free-Standing Reduced Graphene Oxide/Polypyrrole/Cellulose Hybrid Papers for Supercapacitor Electrodes," *J. Mater. Chem. A* Vol. 5, no. 8, 2017, 3819-3831.
- [10] Li, Z., Friedrich, A., and Taubert, A., "Gold Microcrystal Synthesis Via Reduction of HAuCl₄ by Cellulose in the Ionic Liquid 1-Butyl-3-Methyl Imidazolium Chloride," *J. Mater. Chem.* Vol. 18, no. 9, 2008, 1008-1014.
- [11] Xiong, R., Lu, C., Wang, Y., Zhou, Z., and Zhang, X., "Nanofibrillated Cellulose as the Support and Reductant for the Facile Synthesis of Fe₃O₄/Ag Nanocomposites with Catalytic and Antibacterial Activity," *J. Mater. Chem. A* Vol. 1, no. 47, 2013, 14910-14918.
- [12] Guerrero-Contreras, J., and Caballero-Briones, F., "Graphene Oxide Powders with Different Oxidation Degree, Prepared by Synthesis Variations of the Hummers Method," *Mater. Chem. Phys.* Vol. 153, 2015, 209-220.
- [13] Stobinski, L., Lesiak, B., Malolepszy, A., Mazurkiewicz, M., Mierzwa, B., Zemek, J., Jiricek, P., and Bieloshapka, I., "Graphene Oxide and Reduced Graphene Oxide Studied by the XRD, TEM and Electron Spectroscopy Methods," *J. Electron Spectrosc.* Vol. 195, 2014, 145-154.
- [14] Krishnamoorthy, K., Veerapandian, M., Yun, K., and Kim, S. J., "The Chemical and Structural Analysis of Graphene Oxide with Different Degrees of Oxidation," *Carbon* Vol. 53, 2013, 38-49.
- [15] Khan, M., Al-Marri, A. H., Khan, M., Mohri, N., Adil, S. F., Al-Warthan, A., Siddiqui, M. R. H., Alkathlan, H. Z., Berger, R., Tremel, W., and Tahir, M. N., "*Pulicaria Glutinosa* Plant Extract: A Green and Eco-Friendly Reducing Agent for the Preparation of Highly Reduced Graphene Oxide," *RSC Adv.* Vol. 4, no. 46, 2014, 24119-24125.
- [16] Khan, M., Al-Marri, A. H., Khan, M., Shaik, M. R., Mohri, N., Adil, S. F., Kuniyil, M., Alkathlan, H. Z., Al-Warthan, A., Tremel, W., Tahir, M. N., and Siddiqui, M. R., "Green Approach for the Effective Reduction of Graphene Oxide Using *Salvadora Persica* L. Root (Miswak) Extract," *Nanoscale Res. Lett.* Vol. 10, no. 1, 2015, 281-289.
- [17] Thakur, S., and Karak, N., "Green Reduction of Graphene Oxide by Aqueous Phytoextracts," *Carbon* Vol. 50, no. 14, 2012, 5331-5339.

- [18] Ye, Y.-S., Zeng, H.-X., Wu, J., Dong, L.-Y., Zhu, J.-T., Xue, Z.-G., Zhou, X.-P., Xie, X.-L., and Mai, Y.-W., "Biocompatible Reduced Graphene Oxide Sheets with Superior Water Dispersibility Stabilized by Cellulose Nanocrystals and Their Polyethylene Oxide Composites," *Green Chem.* Vol. 18, no. 6, 2016, 1674-1683.
- [19] Yang, D., Velamakanni, A., Bozoklu, G., Park, S., Stoller, M., Piner, R. D., Stankovich, S., Jung, I., Field, D. A., Ventrice, C. A., and Ruoff, R. S., "Chemical Analysis of Graphene Oxide Films after Heat and Chemical Treatments by X-Ray Photoelectron and Micro-Raman Spectroscopy," *Carbon* Vol. 47, no. 1, 2009, 145-152.
- [20] Fan, L.-Z., Liu, J.-L., Ud-Din, R., Yan, X., and Qu, X., "The Effect of Reduction Time on the Surface Functional Groups and Supercapacitive Performance of Graphene Nanosheets," *Carbon* Vol. 50, no. 10, 2012, 3724-3730.
- [21] Shim, S. H., Kim, K. T., Lee, J. U., and Jo, W. H., "Facile Method to Functionalize Graphene Oxide and Its Application to Poly(Ethylene Terephthalate)/Graphene Composite," *ACS Appl. Mater. Interfaces* Vol. 4, no. 8, 2012, 4184-4191.
- [22] Chen, J., Li, Y., Huang, L., Li, C., and Shi, G., "High-Yield Preparation of Graphene Oxide from Small Graphite Flakes Via an Improved Hummers Method with a Simple Purification Process," *Carbon* Vol. 81, 2015, 826-834.
- [23] Pei, S., and Cheng, H.-M., "The Reduction of Graphene Oxide," *Carbon* Vol. 50, no. 9, 2012, 3210-3228.
- [24] Bhattacharya, G., Sas, S., Wadhwa, S., Mathur, A., McLaughlin, J., and Roy, S. S., "Aloe Vera Assisted Facile Green Synthesis of Reduced Graphene Oxide for Electrochemical and Dye Removal Applications," *RSC Adv.* Vol. 7, no. 43, 2017, 26680-26688.
- [25] Lekpittaya, P., Yanumet, N., Grady, B. P., and O'Rear, E. A., "Resistivity of Conductive Polymer-Coated Fabric," *J. Appl. Polym. Sci.* Vol. 92, no. 4, 2004, 2629-2636.
- [26] Kafy, A., Akther, A., Zhai, L., Kim, H. C., and Kim, J., "Porous Cellulose/Graphene Oxide Nanocomposite as Flexible and Renewable Electrode Material for Supercapacitor," *Synth. Met.* Vol. 223, 2017, 94-100.
- [27] Yang, W., Zhao, Z., Wu, K., Huang, R., Liu, T., Jiang, H., Chen, F., and Fu, Q., "Ultrathin Flexible Reduced Graphene Oxide/Cellulose Nanofibre Composite Films with

Strongly Anisotropic Thermal Conductivity and Efficient Electromagnetic Interference Shielding," *J. Mater. Chem. C* Vol. 5, no. 15, 2017, 3748-3756.

CHAPTER VI-
CONCLUSIONS & FUTURE OUTLOOK

6.1. Chapter synopsis

This chapter proposes the main conclusions from the present research work, followed by the directions for further research. The conclusions have been derived based on the studied extraction method, the variation of the extraction parameters and their optimization, the identification of the compounds using advanced chromatographic tools as well as the use of the extract for the in situ green reduction on a fibre matrix. The underlying basis of the research work is the development and optimization of the extraction principle for the extraction of phytoconstituents and demonstrate the proof-of-concept for their usage to achieve eco-friendly reduction of materials.

6.2. Main conclusions and achievements of the research

The research work has been summarized in the following bullet points that indicate the achievements as well as implications.

- Extraction of bioactive compounds such as terpenes, flavonoids and cannabinoids was successfully accomplished using the technique of ultrasonication from the inflorescences of *Cannabis*. The extraction was done by varying the ultrasonic parameters of time, power and solvent. **(CA-JA1)**
- The optimization of the extraction parameters was done using a 3-factor central composite design approach. The responses were analysed by fitting a second order polynomial; the TPC was well described by the factor interaction model while linear models described the TF, FRAP and yield. The regression and graphical analysis revealed the solvent composition and time to be the most predominant factors influencing the extraction process, except in case of the FRAP assay. **(CA-JA1)**
- The time had a positive effect on the responses. More methanol content in the solvent favoured the TPC while it negatively affected TF and the extraction yield. The ultrasonic power, on the other hand, did not have any significant impact on any of the responses investigated. **(CA-JA1)**
- Considerably higher values of all the responses were obtained for the ultrasonic extraction than the control one. Ultrasonication also considerably enhanced the extraction of cannabinoids, which was confirmed by HPLC chromatograms. Several cannabinoids including THC, CBD, CBGA, CBDA, THCVA, CBLA, CBNA, CBCA, etc. were identified in the extract using HPLC-DAD-MS/MS. **(CA-JA1, CA-JA3)**

- In situ green reduction of GO with simultaneous functionalization on the cellulose fibres using the aqueous extract from the inflorescences of *Cannabis* was achieved. The successful removal of oxygen-containing functional groups and anchorage to the cellulose fibres was confirmed by spectroscopic and diffraction techniques. **(CA-JA4)**
- The cellulose fibres served a dual role of a supporting matrix with excellent anchorage to RGO resulting from strong electrostatic surface interactions as well as a reductant due to the presence of free hydroxyl and ether groups. **(CA-JA4)**
- The surface resistivity of the composites dropped markedly (by over a 100 orders of magnitude) by incorporation of the conducting RGO in the cellulose fibres. However, it was found to be significantly affected by the presence of air voids, which acted as an obstacle preventing the formation of an effective conductive network of RGO layers within the cellulose matrix. The porosity of the cellulose fibre matrix and the strong interaction between RGO and cellulose played an instrumental role in determining the performance of the composites. **(CA-JA4)**

6.3. Scope for further research

The present research work demonstrated successful extraction of bioactive compounds from *Cannabis* using facile ultrasonication, as confirmed by advanced chromatographic techniques. The extract exhibited a promising potential for the eco-friendly reduction of graphene oxide on cellulose fibres, as established by different analytical techniques. This methodology could be extended in various sectors as follows:

- The extraction method can be applied for the extraction of bioactive compounds from various parts of other plants including roots, stem, flowers, leaves, fruits.
- Different solvents can be experimented with for the extraction of phytoconstituents depending on the desired class of compounds to be extracted.
- The extract can be used for the green reduction of nanomaterials such as metal and metal oxide nanoparticles for targeted applications, wherein cellulose can serve as an ideal platform for the anchorage of the synthesized nanomaterials.

LIST OF PUBLICATIONS

Journal Articles:

CA-JA4: Charu Agarwal, M. N. Singh, R. K. Sharma, Archana Sagdeo, Levente Csóka, “In Situ Green Synthesis and Functionalization of Reduced Graphene Oxide on Cellulose Fibers by *Cannabis sativa* L. Extract” *Materials Performance and Characterization* doi: 10.1520/MPC20180149, **2019**

CA-JA3: Charu Agarwal, Tamás Hofmann, Levente Csóka, “Ultrasonically-Extracted Phytocannabinoids from a Hungarian Chemovar of *Cannabis sativa* L.: Possible Entourage Effects?”, *Food and Function* (submitted)

CA-JA2: Charu Agarwal, Levente Csóka, “Functionalization of Wood/Plant-Based Natural Cellulose Fibers with Nanomaterials: A Review”, *TAPPI Journal* 17 (2), 92-111, **2018**

CA-JA1: Charu Agarwal, Katalin Máthé, Tamás Hofmann, Levente Csóka, “Ultrasound-Assisted Extraction of Cannabinoids from *Cannabis sativa* L. Optimized by Response Surface Methodology”, *Journal of Food Science* 83 (3), 700-710, **2018**

Book Chapters:

CA-BC3: Charu Agarwal, Levente Csóka “Recent Developments in Biogenic Synthesis of Nanomaterials for Different Applications: A Pre-Eminent Approach Towards Green Technology” in Inamuddin (ed.) *Green Composites: Materials and Applications*. Materials Research Forum, USA (submitted)

CA-BC2: Charu Agarwal, Levente Csóka (**2019**) “Surface Modified Cellulose in Biomedical Engineering” in Grumezescu A. M., Grumezescu V. (eds.) *Bioactive Materials, Properties and Applications*. Elsevier (In press)

CA-BC1: Charu Agarwal, Levente Csóka (**2019**) “Recent Advances in Paper-Based Analytical Devices: A Pivotal Step Forward in Building Next-Generation Sensor Technology” in Inamuddin, Thomas S., Kumar Mishra R., Asiri A. (eds.) *Sustainable Polymer Composites and Nanocomposites*. Springer, Cham, pp. 479-517

Conference Proceedings:

CA-CP6: Charu Agarwal, Levente Csóka, (2019, May 6-10). Cellulose as a substrate for modification with functional materials. Published in the proceedings of *International Project Week and Scientific Conference on Sustainable Raw Materials* (p. 29), University of Szeged, Szeged, Hungary (Oral)

CA-CP5: Charu Agarwal, Tamás Hofmann, Levente Csóka, (2018, October 14-16). Ultrasound-assisted extraction of cannabinoids from *Cannabis sativa* L. Published in the proceedings of *3rd International Medical Cannabis Conference* (p. 61), Tel-Aviv, Israel (Oral)

CA-CP4: Charu Agarwal, Levente Csóka, (2018, May 17-19). Biogenic synthesis of iron oxide nanostructures for targeted applications. Published in the proceedings of *7th Interdisciplinary Doctoral Conference* (p. 23), University of Pécs, Pécs, Hungary (Oral)

CA-CP3: Charu Agarwal, Levente Csóka, (2017, October 9). Bioextraction of pharmaceutical compounds from *Cannabis sativa* L. Presented as Speaker in *International Conference on Advances in Agriculture & Crop Science*, New Delhi, India (Oral)

CA-CP2: Charu Agarwal, Katalin Máthé, Tamás Hofmann, Levente Csóka, (2017, September 14-16). Ultrasonic extraction of bioactive compounds from *Cannabis sativa* L. and response surface optimization of extraction conditions. Published in the proceedings of *3rd Asia-Oceania Sonochemical Society Conference*, SRM University (p. 105), Chennai, India (Poster)

CA-CP1: Charu Agarwal, Levente Csóka, (2017, July 2-4). Green synthesis of iron oxide nanostructures for biomedical applications: Mimicking bacterial magnetosomes. Published in the proceedings of *National Symposium on Nano Science and Technology* (p. 9), IISc Bengaluru, India (Poster)

Doctoral complex exam 2018:

CA-CE: Charu Agarwal, “Plant extract-mediated synthesis of nanomaterials for targeted applications”, University of Sopron (Hungary), June 2018

Doctoral conference 2017:

CA-DC: Charu Agarwal, “Extraction of bioactive compounds”, University of Sopron (Hungary), May **2017**